IMPROVEMENT OF AN URBAN TURBULENCE PARAMETRIZATION FOR METEOROLOGICAL OPERATIONAL FORECAST AND AIR QUALITY MODELING

THÈSE N^{O} 3766 (2007)

PRÉSENTÉE LE 27 AVRIL 2007

À LA FACULTÉ DE L'ENVIRONNEMENT NATUREL, ARCHITECTURAL ET CONSTRUIT

Laboratoire de pollution atmosphérique et du sol

SECTION DES SCIENCES ET INGÉNIERIE DE L'ENVIRONNEMENT

ÉCOLE POLYTECHNIQUE FÉDÉRALE DE LAUSANNE

POUR L'OBTENTION DU GRADE DE DOCTEUR ÈS SCIENCES

PAR

Clive MULLER

ingénieur du génie rural diplômé EPF
de nationalité suisse et originaire de Yens (VD)

acceptée sur proposition du jury:

Dr A. Clappier , directeur de thèse
Prof. I. Bey, rapporteur
Dr A. Martilli, rapporteur
Dr Ph. Thunis, rapporteur

ÉCOLE POLYTECHNIQUE
FÉDÉRALE DE LAUSANNE

Lausanne, EPFL
2007

Abstract

During the last century, urban pollution has increased with the growth of cities. Urban air quality has become a high priority as it is directly linked to concerns such as human exposure and health. The present work is dedicated to urban air quality modeling with focus on urban meteorology. The main goal is to improve meteorological and air quality simulations in urban areas.
Based on measurements and numerical air quality simulations, Chapter 3 describes the meteorological situation and tests an emission inventory for an ozone pollution episode in Mexico City (2 March 1997), in order to determine the principal factors to be accounted in an air quality study. The Mexico City case shows the great influence of meteorological conditions and pollutant emissions on air quality. A thorough understanding of the phenomena governing the meteorological conditions, like small scale convergence, and an accurate emission inventory validated by VOC measurements in the city, are sensitive elements in an air quality study.
In Chapter 4, the presence of an Urban Heat Island (UHI) is underlined over the city of Basel (Switzerland) with the BUBBLE measurements. Further on, the ability of aLMo (the operational weather prediction model of MeteoSwiss) to reproduce the effect of a city on the boundary layer atmospheric flow fields is investigated. Results show that aLMo is not able to reproduce the UHI and hence that its surface scheme based on the Monin-Obukhov Similarity Theory (MOST) is not adapted for the urban areas. Therefore, the Buildings Effects Parametrization (BEP) which has been developed by Martilli et al.(2002) especially for urban areas, is implemented in aLMo. Results show that alMo is now able to reproduce the main behavior of the urban boundary layer as the UHI and BEP has hence a real enhancement potential for aLMo.
Chapter 5 shows the sensitivity of aLMo with respect to its vertical resolution. In order to limit the sensitivity of aLMo to the grid resolution, BEP is modified. The mesoscale model furnishes the upper boundary conditions for the inner calculation of BEP. That is, BEP recalculates independently the vertical profiles of wind, temperature and energy based on the surface fluxes of momentum, heat and turbulent kinetic energy. The results obtained show a decrease in the sensitivity to the resolution and a better agreement with the measurements. Furthermore, the modified version of BEP gives additional meteorological fields (temperature, wind and TKE) in the urban canopy. The computed temperature in the urban canopy shows a good agreement with measurements in a Basel street canyon.
This work shows that it is not necessary to have a high resolution for taking into account modification of the atmospheric flow fields induced by a city.

Keywords : urban surface exchange parametrization, Mexico City, air quality modeling, numerical weather forecast, BUBBLE, measurement-model comparison, urban boundary layer, urban climatology.

Résumé

Le vingtième siècle a été le témoin d'un incroyable développement des villes qui a conduit à une densification des populations y résidant. L'ensemble des activités anthropogéniques a engendré une forte pression sur l'environnement, en particulier sur la qualité de l'air qui s'est dégradée dans la majorité des villes du globe. Les processus gouvernant la dispersion et les transformations chimiques des polluants sont complexes et fortement non linéaires. La meilleure approche, actuellement disponible, pour comprendre et prédire la pollution atmosphérique, est l'utilisation de modèles numériques. Ce travail se concentre sur la modélisation de la qualité de l'air et plus particulièrement sur la modélisation de la météorologie en milieu urbain, l'objectif premier étant d'améliorer les simulations sur les villes.

La première partrie de ce travail décrit la situation météorologique, à l'aide de mesures et de simulations numériques, et teste un cadastre d'émissions pour un épisode de pollution de l'air sur la ville de Mexico afin de déterminer les paramètres prédominants dans une telle étude. Les résultats obtenus montrent l'importance de la météorologie et des émissions sur les concentrations de polluants dans l'atmosphère. La compréhension et la représentation détaillées des conditions météorologiques, ainsi qu'un cadastre d'émissions validé, sont des éléments clés dans une étude de qualité de l'air.

La seconde partie de ce travail se concentre sur les effets induits par la présence d'une ville sur les champs météorologiques, et met l'accent sur la paramétrisation BEP développée spécialement pour les surfaces urbaines par Martilli et al. (2002). Le modèle aLMo (modèle opérationnel de prévision météorologique de Météo-Suisse) a été utilisé sur la ville de Bâle. En observant les mesures effectuées lors d'une campagne intensive (BUBBLE), un îlot de chaleur urbain (UHI) a été mis en évidence sur Bâle. Les simulations réalisées avec aLMo n'ont pas reproduit ce UHI. Le schéma de surface basé sur la théorie de similitude de Monin-Obukhov (MOST) n'est pas adapté aux zones urbaines. BEP a donc été implémenté dans aLMo. Avec cette paramétrisation, les simulations reproduisent les principaux phénomènes induis par la ville sur les champs météorologiques dont le UHI.

Dans la troisième partie, il est montré que les simulations aLMo sont dépendantes de la résolution verticale du modèle. BEP a été modifié afin de diminuer la sensibilité du modèle à la résolution verticale et d'améliorer le résultat des simulations. De plus, les modifications apportées à BEP permettent de simuler des champs météorologiques à l'intérieur de la canopée urbaine dont les résultats ont été validés par des mesures effectuées dans une rue de Bâle.

En conclusion, ce travail améliore les simulations météorologiques sur les zones urbaines et montre qu'il n'est pas nécessaire d'utiliser de hautes résolutions pour tenir compte de la présence des villes dans les modèles numériques.

Mots clés : Paramétrisation urbaine, Mexico City, modélisation de la qualité de l'air, climatologie urbaine, BUBBLE, modèle de prévision météorologique.

Acknowledgements

First, I would like to thank Dr. Alain Clappier, my PhD adviser, who gave me the opportunity to do this thesis. I would like to further thank the members of the jury, Prof. Isabelle Bey, Dr. Philippe Thunis, Dr. Alberto Martilli (without him this work would never been possible) and the president of the jury Dr. César Pulgarin. I also thank Prof. Hubert Van den Berg for hosting me in the Air and Soil Pollution Laboratory.

The Swiss National Science Foundation provided the funding of this study (Project *No.* 200020-101811).

Remerciements

Je tiens à remercier et saluer toutes les personnes qui m'ont aidé, soutenu ou accompagné durant ces dernières années. Tout d'abord, je remercie mes parents, Eric et Fernande, pour leur soutien, leur amour et leur présence tout au long du chemin qui m'a amené ici, ainsi que ma soeur, Audrey, mon beau-frère Laurent et leurs trois merveilleuses filles, Camille, Romane et Clara.

Un immense merci à Pascal, Kathleen et Chanelle Helfer ainsi que à Alain et Melissa Haertel pour votre sincère amitié et tous les moments passés en votre compagnie. Je veux également remercier deux personnes sans qui je ne me serais probablement pas engagé dans ce travail de thèse; mes amis et anciens collègues, Martin Junier et Yves-Alain Roulet qui m'ont aidé et accompagné dès mes premiers jours au $LPAS$. Longue vie aux soirées "Fondue, Meringues et double crème".

Je remercie encore Oliver Fuhrer pour sa participation à ce travail, mais également pour son enthousiasme, son dynamisme et tout ce qu'il a apporté à notre bureau. J'ai également une pensée spéciale pour Erika Zárrate avec qui j'ai arpenté le long chemin du thésard et qui m'a initié à la culture colombienne. Merci à Gil Fontannaz (my partner in crime) pour son travail, mais surtout pour son amitié et sa complicité. Je salue ici aussi mes collègues avec qui cela a toujours été un plaisir d'aller boire le câfé; Andrea Krpo et Luis Carlos Belalcázar Ceron. Je remercie aussi David Meylan pour avoir résolu tant de problèmes informatiques et Véronique Bauler pour sa disponibilité.

Je termine ces remerciements par saluer quelques amis, Big up à vous: Alexandre Caboussat, Carole Noverraz, David Vladyka, Ludivine Helfer Gleyre, Marco Matter, Raphael Timms et Stéphane Nicod.

Contents

List of Figures

List of Tables

List of Abbreviations

AGL	Above Ground Level
ASL	Above See Level
aLMo	aLpine Model
AVER	Aerosol and Visibility Research
BEP	Buildings Effects Parametrization
BUBBLE	Basel UrBan Boundary Layer Experiment
CAM	Comision Ambiental Metropolitan
CFD	Computational Fluid Dynamics
CH_4	Methane
CO	Carbon oxide
COSMO	COnsortium for Small-Scale MOdeling
CPU	Central Processing Unit
CSCS	Swiss National Supercomputing Center
DAO	Data Assimilation Office
DWD	National Weather Service of Germany

E	Turbulent Kinetic Energy
ECMWF	European Center for Medium-Range Weather Forecasts
EPA	U.S. Environmental Protection Agency
EPFL	Ecole Polytechnique Fédérale de Lausanne
FDDA	Four-Dimensional Data Assimilation
FVM	Finite Volume Model
GEOS	Goddard Earth Observing System
GMT	Greenwich Mean Time
$HCHO$	Formaldehyde
HNO_3	Nitric acid
H_2O_2	Hydrogen peroxide
hPa	Hectopascal
IMADA	Investigacion sobre Materia Particulada y Deterioro Atmosferico
IOP	Intensive Observation Period
ISO	Isoprene
KABA	Climate Analysis of the Region of Basel
LES	Large Eddy Simulations
LM	Local Model
LT	Local Time
MCMA	Mexico City Metropolitan Area

MOST	Monin-Obukhov Similarity Theory
NASA	National Aeronautics and Space Administration
NCAR	National Center for Atmospheric Research
NCEP	National Centers for Environmental Prediction
NMVOC	Non-Methane Volatile Organic Compounds
NO	Nitric oxide
NO_2	Nitrogen dioxide
N_2O_5	Dinitrogen pentoxide
NO_X	Nitrogen oxides
NWP	Numerical Weather Prediction
O_3	Ozone
PAH	Poly-Aromatic Hydrocarbons
PBL	Planetary Boundary Layer
PM	Particulate Matter
ppb	Parts per billion
PPM	Piecewise Parabolic Method
RACM	Regional Atmospheric Chemistry Model
RANS	Reynolds-Averaged Navier-Stokes
SO_2	Sulphur dioxide
TAPOM	Transport and Air POllution Model

TI	Ticino
TKE	Turbulent Kinetic Energy
TUV	Tropospheric Ultraviolet-Visible Model
UBL	Urban Boundary Layer
UCL	Urban Canopy Layer
UCM	Urban Canopy Model
UHI	Urban Heat Island
UK	United Kingdom
UN	United Nations
UNEP	United Nations Environment Programme
U.S.	United States
VOC	Volatile Organic Compounds
WHO	World Health Organization

Chapter 1

Introduction

The twentieth century has seen a rapid urbanization of the World's population. The global proportion of urban population increased from 13 % in 1900 to 49 % in 2005. These overall trends have intensified and according to the United Nations population projections (UN, 2004), 4.9 billion people, representing 60 % of the World's population, are expected to live in cities by 2030.

This urbanization has caused the emergence of 20 mega-cities[1]. Never before such large populations had been concentrated in cities. Such concentration of the population leads to a better access to health services, technologies (especially for cities in developing countries), trades and cultural activities. The concentration often produces economies of scale and leads to social and economic benefits. Furthermore, the cities are at the forefront of political, economic, social and cultural changes. Cities are a major attraction point for our society.

Unfortunately, most of today's cities are not healthy to live. The populations and activities accumulation produces a high concentration of food, water and energy, and leads to the spoiling of urban environment (Brown, 2006). Manage wastes, treat sewage, reduce noise or control air quality have become a challenge for planners and administrations at all levels.

Establishing policies and strategies in order to limit the negative urban impacts on the environment produces heavy costs and governments have to take into account numerous economic, social and environmental factors. Thus, some recommendations and decision-support tools based on scientific knowledge are necessary in order to help the decision-maker (Molina et al., 2002).

As an example, more than 2 million premature deaths each year can be attributed to the effects of indoor-outdoor urban air pollution (WHO, 2005). The process leading to air pollution are diversified, complex and non-linear. Extended knowledge on type, quantity, residence time and sources of the pollutants emitted in the

[1] Cities with 10 million residents or more.

urban atmosphere are necessary, in order to reduce the human health effects. Air quality and meteorology measurements and emissions studies are conducted in order to give an overview of the cities situation. Associating these data to modeling tools makes it possible to provide decision-support and forecast tools to planners and governments in order to design pollutants emissions abatement strategies.

Understanding and forecasting the air quality in urban areas have emerged as an active field of research with clear socio-economics demands. The present thesis is focused on modeling tools and more particularly on meteorological modeling in urban areas.

Firstly, some urban atmosphere features such as the structure of the atmosphere above the city, urban impact on weather and urban air quality problems are presented in chapter 2. Methods to take into account the presence of cities in meteorological models are also described.

Then the core of this thesis is structured into three chapters.

Chapter 3 intends to determine the principal factors to be accounted for in an air quality study and to illustrate the complexity of such studies. Based on measurements and numerical air quality simulations, the Mexico City case is presented for a two day episode. Mexico City is the second largest mega-city in the world with around 20 million inhabitants and one of the most polluted cities (Baldasano et al., 2003) where pollutant concentrations have reached highest levels during the 90's.

Chapters 4 and 5 investigate the capacity of a mesoscale meteorological model to take into account the modification of the atmosphere in an urban area. Hence, the detailed urban parametrization (BEP), which was developed by Martilli et al. (2002), is modified and implemented in the operational numerical weather prediction model of the Swiss Office of Meteorology and Climatology (MeteoSwiss). The

aim of both chapters is to improve meteorological simulations in urban areas by implementing the urban parametrization and testing it in an operational forecast model. It is hoped that this thesis will improve the urban air quality simulations and our knowledge on the interaction between the urban local scale and the mesoscale.

The conclusion sums up the main results obtained and gives some outlooks, and perspectives on future works.

Bibliography

Baldasano, J.M., Valera, E., Jiménez, P.: 2003, 'Air quality data from large cities', *Sci. Total Environ.*, **307**, 141-165.

Brown, L. R.: 2006, *Plan B 2.0: Rescuing a Planet Under Stress and a Civilization in Trouble*, W.W. Norton & Co., New York, 343 pp.

Martilli, A., Clappier, A., Rotach, M. W.: 2002, 'An urban surfaces exchange parameterisation for mesoscale models', *Bound.-Layer Meteor.*, **104**, 261-304.

Molina, L.T., Molina, M.J.: 2002, *Air Quality in the Mexico Megacity: an Integrated Assessment*, (Eds.) Kluwer Acad., Norwell, Mass., 384 pp.

United Nations: 2006, 'World Urbanization Prospects. The 2005 Revision', *Departement of Economic and Social Affairs, Population Division*, New York.

World Health Organization: 2005, 'WHO, Air qualtity guidelines for particulate matter, ozone, nitrogen dioxide and sulfur dioxide', *WHO Press*, Geneva.

Chapter 2

The Urban Atmosphere

Some features of the urban atmosphere such as the urban impact on meteorological flow fields, the urban air quality problem and the way to take into account an urban area into meteorological models are presented in this chapter. Firstly, the vertical structure of the urban atmosphere is briefly introduced.

2.1 VERTICAL STRUCTURE OF THE TROPOSPHERE

The Earth's atmosphere is commonly divided into four layers, starting from the ground: the troposphere, the stratosphere, the mesosphere and the thermosphere. The troposphere is the lowest portion of the Earth's atmosphere and is around 10 km thick (16 km at the Equator and 7 km at the Poles) (Seinfeld and Pandis, 1998). In this study, we focus on the troposphere. The use of mesoscale models to tackle the problematic of urban air quality requires knowledge on this layer, where all interactions between the Earth's surface and the atmosphere take place.
The troposphere is the densest layer of the atmosphere and contains approximately 80% of the atmosphere mass and almost all the water vapor. The Earth's gravity leads to an exponential increase of pressure from the tropopause to the Earth's surface. Thus, temperature in the troposphere decreases with height.
The Earth's surface temperature is directly influenced by radiative processes. The air temperature near the ground is not determined by solar radiation direct forcing (23 % of total incoming solar radiation is absorbed by the atmosphere) but by sensible and latent heat flux from the ground, where 46 % of the incoming solar radiation is absorbed.

Thus, air temperature depends on sensible and latent heat fluxes, which are directly correlated with solar radiation reaching the Earth's surface and soil thermal

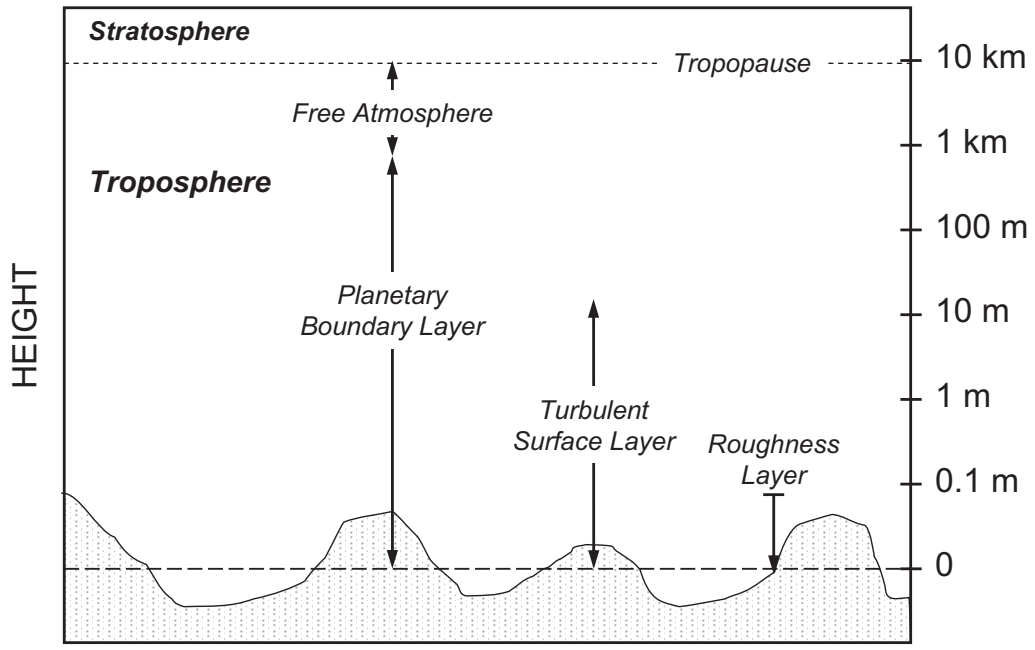

Figure 2.1: The vertical structure of the troposphere (modified after Oke (1987))

properties and moisture.

It is possible to divide the troposphere into two distinct layers; The Planetary Boundary Layer (PBL) from the ground to about 1 km and the Free Atmosphere from 1km above the ground to the tropopause (Fig. 2.1). According to Stull (1988), the PBL can be defined as '*that part of the troposphere that is directly influenced by the presence of the earth's surface, and responds to surface forcings with a timescale of about an hour or less. These forcing include frictional drag, evaporation and transpiration, heat transfer, pollutant emission, and terrain induced flow modification*'.

The PBL itself can be divided into two different layers (Fig. 2.1).

The *turbulent surface layer* is characterized by intense small-scale turbulence gen-

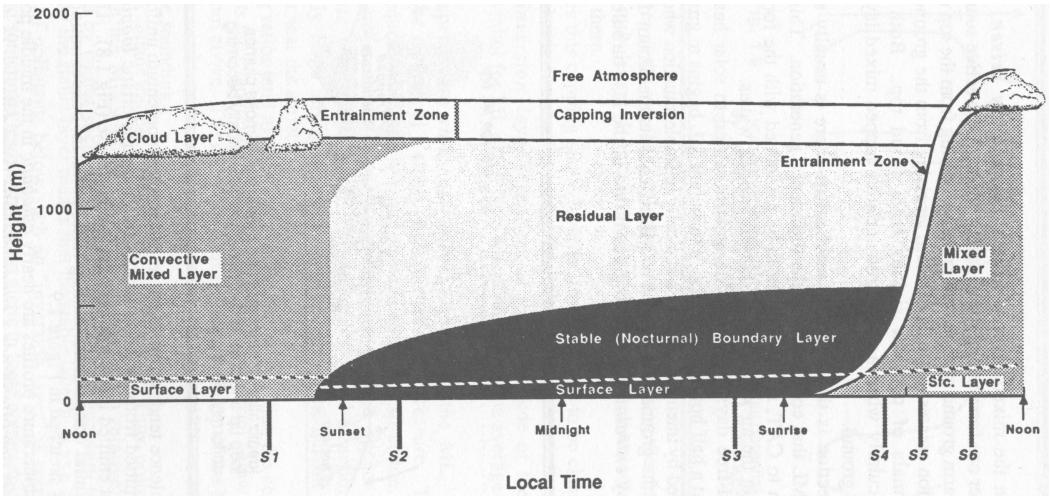

Figure 2.2: Diurnal development of the Planetary Boundary Layer thickness. The daytime convective mixed layer, with a very homogenous vertical distribution (temperature, air pollutants, etc.), is replaced by a stable boundary layer near the ground and a residual layer containing the remainder of daytime turbulence and trapping the air pollutants (Stull, 1988).

erated by the surface roughness and convection. Despite its short term variability, the surface layer can be considered as horizontally homogenous for periods longer than 10 minutes (Oke, 1987).

The *roughness layer* is related to the height of the roughness elements and its height varies from some millimeters to some meters (Seinfeld and Pandis, 1998). In the roughness layer, the flow is highly irregular being strongly affected by the nature of the individual roughness elements. It is generally considered that wind speed is equal to zero and air temperature is equal to the surface temperature into the roughness layer (Holton, 1979).

As Figure 2.2 shows, the PBL structure evolves during daytime as a function of the air stability. Thus, PBL thickness is mainly dependant on solar activity at the Earth's surface.

Representing the PBL with successive layers is a model which allows to have a

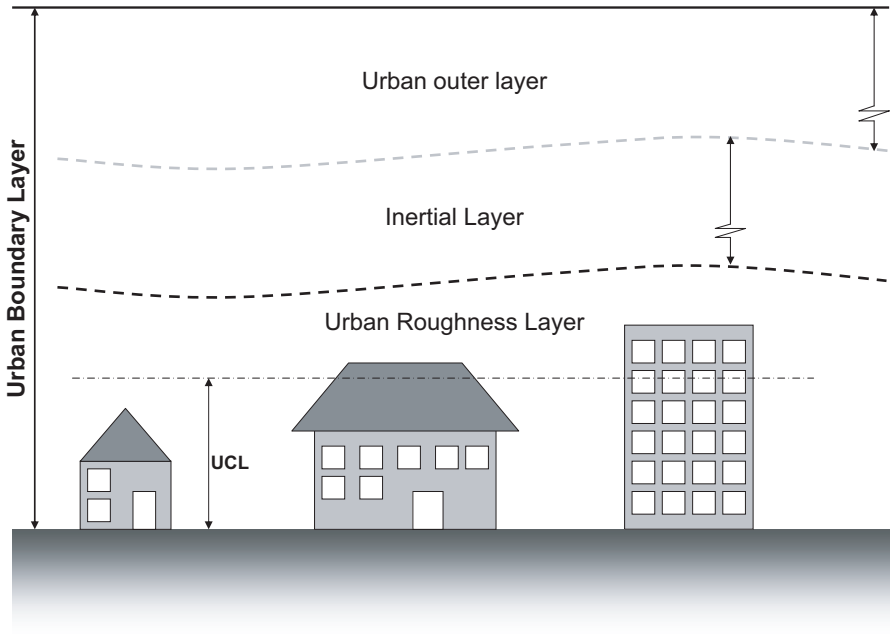

Figure 2.3: The Urban Boundary Layer structure composed of an urban roughness layer including the Urban Canopy Layer, an inertial layer and an urban outer layer (modified after Rotach et al. (2005)).

better representation and understanding of the atmosphere. But these layers do not appear very clearly in a real atmosphere. As an example, the presence of buildings deeply modifies the PBL structure over urban areas. The Urban Boundary Layer (UBL) shows therefore a more detailed vertical structure, as presented in Figure 2.3.

The urban roughness layer depends on buildings height and density, but for simplicity often expressed as $z* = a\overline{z_H}$ (Raupach et al., 1991) where a ranges between 1.3 and 3. (Roth, 2000) and $\overline{z_H}$ is the averaged buildings height, denoting the Urban Canopy Layer (UCL).

Above the roughness layer, an inertial layer forms which can be compared to a surface layer over ideal surfaces (Tennekes and Lumley, 1972). The outer urban layer corresponds to the convective mixed layer or to the residual layer under stable stratification as described by Stull (1988).

2.2 URBAN IMPACTS ON WEATHER

Modifications in the vertical structure of the atmosphere induced by urban areas are driven by mechanical and thermal factors.

The *mechanical effects* are mainly governed by the high roughness of cities. Buildings increase surface drag and wake turbulence, and decrease wind speed (Roth, 2000). By strong winds and low solar radiation condition, the mechanical effects can be more important than the thermal effects (Fast et al., 2005).

The *thermal effects* characterize generally the modifications in the energy balance induced by the presence of a city. The structure and material heterogeneity of an urban area modifies the radiative and energy budget. Furthermore, a city is a relatively dry environment compared to a rural area and latent heat fluxes are hence lower. A city is also an important anthropogenic heat source. As consequence of these characteristics, urban areas are often warmer than the surroundings areas. This phenomenon is called the Urban Heat Island (UHI).

In 1833, Luke Howard provided evidence that air temperatures are often higher in the city of London than in its surroundings countryside. Since then, the UHI have been largely studied and observed in numerous cities of various latitudes, sizes, densities, etc. Some generalizations can be done about the UHI (Arnfield, 2003; Oke, 1982):

- UHI intensity decreases with increasing wind speed or cloud cover.
- UHI intensity is more important under stable atmospheric conditions (anti-

cyclonic conditions or nighttime).

- UHI intensity is best developed in summer or warm half of the year.

- UHI intensity tends to increase with increasing city size and/or population density.

UHI intensity can vary between 0 to 7 °C (Chow and Roth, 2006) depending on season, solar radiation and city characteristics. The increase of temperature in urban areas leads to a less stable atmosphere and an increase of the mixing in the lowest part of the atmosphere. Thus, UHI can be observed up to 0.5 to 1.5 km above ground level (Oke, 1982), depending upon the strength of the surface sensible heat flux, the air stability and the wind speed. Furthermore, the heat island can be entrained on many kilometers downwind an urban area. The UHI modifies also the air flow in and around the city. The increase of temperature in an urban area can lead to the formation of a wind convergence above the city and an increase of wind speed opposed to the decrease induced by the mechanical effects. By impacting the regional atmospheric circulation, urban areas modify also the precipitation distribution. Many studies have shown that rainfall patterns, amount and distribution in and downwind of cities can be modified (Collier, 2006). An increase of convective rainfalls during warm-season have been observed over and downwind of major urban areas (Bornstein and Lin, 2000).
As a conclusion, the anthropogenic forcing [1] induced by the presence of cities modifies radiative, energy and water budget and hence the whole urban climate.

[1] Forcing due to human activities.

2.3 URBAN AIR QUALITY

Today, urban air quality is directly linked to the energy consumption. The principal source of energy is provided by burning fossil fuels for transports and industries. In spite of technology improvement and plans for reducing the urban air pollution, air quality is degraded in most of the cities. The increase of city sizes and the associated fast growing number of cars leads to an increase of the pollutant emissions.

The major pollutants (Fenger, 1999) in the urban atmosphere are:

Sulphur dioxide (SO_2) is the classical air pollutant associated with sulphur in fossil fuels. It is at the origin of acid rain. The sulphur dioxide concentration have been successfully reduced in most of the industrialized country, but it remains a major pollutant in many cities. Health effects caused by exposure to high levels of SO_2 include breathing problems, respiratory illness, changes in the lung's defences, and worsening respiratory and cardiovascular disease (EPA, 1991).

Nitrogen oxides (NO_x) are formed by oxidation of atmospheric nitrogen during combustion. The main part, especially from cars, is emitted in the form of the non-toxic nitric oxide (NO), which subsequently oxidized in the atmosphere to the secondary pollutant NO_2. Nitrogen dioxide acts mainly as an irritant affecting the mucosa of the eyes, nose, throat, and respiratory tract (EPA, 1991).

Carbon monoxide (CO) is the result of incomplete combustion in motor vehicles. Health effects caused by exposure to CO are cardiovascular disease and decreased exercise performance (Allred et al., 1989).

Volatile organic compounds (VOC) are the results of incomplete combustion in motor vehicles. Some industrial processes and the use of solvent results in the emission of VOC. Trees are also an important biological source of VOC. It can be divided into two separate categories; methane (CH_4) and non-methane ($NMVOC$s). Methane is an extremely efficient greenhouse gas. The most important compounds in urban atmosphere are benzene and poly-aromatic hydrocarbons (PAH) which are suspected carcinogens.

Ozone (O_3) is not emitted directly by car engines or by industrial operations. It is a secondary pollutant which is formed by photochemical reactions. The majority of tropospheric ozone formation occurs when NO_x, CO and VOCs react in the atmosphere in the presence of sunlight (Seinfeld and Pandis, 1998). NO_x and VOCs are called ozone precursors. The maximum of ozone concentration are generally observed many kilometers (10 to 100 km) downwind the cities. In city center, the predominant reaction is a reduction of ozone by NO. As a result, ozone levels are generally low near NO sources. O_3 is a greenhouse gas. Health effects caused by exposure to O_3 are irritation of the respiratory system, reduction of lung function and aggravation of asthma.

Particulate matter (PM) are referred to aerosols and fine particles suspended in the air. The major part of PM are naturally emitted by volcanoes, and forest fires. Particles emission of anthropogenic origin results from combustion. PM can affect the climate by changing the way radiation is transmitted through the atmosphere (radiative forcing). They have significant health effects, including premature death, aggravated asthma, chronic bronchitis and decreased lung function (EPA, 1991).

An important variety of pollutants are concentrated in urban areas and people are exposed to toxic air pollutants in many ways, such as by breathing contaminated air, eating contaminated food, drinking contaminated water or being in contact with contaminated soil, dust, or water. Health risk is particularly important in urban areas.
The concentration of pollutants in the urban atmosphere depends upon quantity and type of emissions, chemistry reactions between the pollutants and prevailing weather conditions.
Pollutants transport, chemistry reaction rates and diffusion depend on the meteorological phenomenons. As an example;

- A strong wind situation leads to a rapid dispersion of the pollutants outside the city, far from sources.

- A very stable atmosphere (nighttime or wintertime situation) leads to high pollutants concentrations within the city

- A strong solar radiation activates the photochemical reaction, which increased the ozone concentration, and decreases the pollutant concentration by increasing the mixing.

Numerous parameters and their evolution in space and time as well as type and quantity of emissions, background concentrations, chemical transformations, meteorological conditions and dry and humid deposition have to be taken into account in order to determine the urban air quality.

2.4 URBAN PARAMETRIZATION

Urban air quality is driven by different complex physical and chemical processes, which encompass a wide range of spatio-temporal scales. Consequently, numerical air quality models, which constitute a robust approach to forecast air pollution, require an integrated approach to simulate both the local urban scale and the city surroundings mesoscale. As it is shown above, urban areas deeply modify the meteorological conditions in and around the cities. It is necessary to take them into account in the simulation tools.

Presently, two modeling approaches are possible:

- The **street canyon models** provide spatially detailed results, but are restricted to a small area (one to a few streets) and generally decoupled from the larger scale circulation (which limits their accuracy to short time intervals). They are not able to simulate the secondary pollutant maximum concentrations, which appear outside the simulation domain.
- The **mesoscale models** cover a relatively large area (domains of the order of 100-200 km), but their resolution (typically 1 to 10 km horizontally and a few tens of meters in the vertical) does not allow to reproduce the detailed structure of the urban areas. Consequently, sub-grids surface fluxes and turbulence parametrizations are necessary in order to take into account the significant perturbations induced by the cities.

Street canyon models are adapted to study the air quality in the streets but cannot be used to simulate the development of the urban plume. Because an integrated approach both at the local and regional level is necessary, a full coupling of the two approaches (insertion within each mesoscale grid cell of a street canyon model) seems to be an ideal approach. But it is a lengthy and computationally extremely

expensive process due to the computation and data preparation. For this reason, the method consisting of taking into account the effects of buildings and streets in a mesoscale model through turbulence parametrizations represents a better compromise.

Based on a study of Masson (2006), different parametrizations can be applied:

The *Empirical Models* are based on observations of the urban surface energy balance (Grimmond and Oke, 1999). The aim is to reproduce the energetics of the canopy using statistical relations derived from observations. Those models use extremely simple schemes, but they need many measurements data and are limited to the range of those data conditions (city, land cover, climate, season, etc...).

The *adapted vegetation schemes* are the most common way to simulate the urban surface energy balance. This approach is based on the adaptation of the thermic and mechanic properties of a rural area in a soil vegetation transfer scheme which is generally based on the Monin-Obukhov Similarity Theory (MOST).
The dynamical effects are generally reproduced by increasing the surface roughness (and displacement heights) (Grimmond et al., 1998) or by deriving a drag force from a forest canopy model.
For radiative effects and the energy balance, surface albedo is generally decreased, ground is "dried", soil heat capacity is modified and anthropogenic fluxes are sometimes prescribed as additional energy source (Makar et al., 2006).
This approach is not able to take into account the geometry of the buildings and does not reproduce the radiative interactions between the different urban surfaces. Furthermore, MOST is not able to reproduce the urban canopy (Rotach, 1993a,b).

The *urban canopy parametrizations* aim to solve the urban surface energy balance for a realistic $3D$ urban canopy. These models are based on a simplified geometry representation of the urban area, which is reasonably close to the reality. Thus, they are able to compute energy budget for different surfaces of the city (wall, roof, road), taking explicitly into account the interaction between these surfaces, as well as the impact of the solar radiation.
Two approaches are possible with those models. The *single-layer* approach interacts only with the first mesoscale layer (Masson, 2000), whereas the *multi-layer* approach is able to impact on all mesoscale layer directly influenced by the buildings (Vu et al., 1999; Martilli et al., 2002; Kondo et al., 2005).

In this study, we use the Buildings Effect Parametrization (BEP) developed by Martilli et al. (2002) which is a multi-layer urban canopy parametrizations.

Bibliography

Allred, E. N., Bleecker, E. R., Chaitman, B.R., Dahms, T.E., Gottlieb, S.O., Hackney, J.D., Hayes, D., Pagano, M., Selvester, R.H., Walden, S.M., Warren, J.: 1989, 'Shortterm Effects of Carbon Monoxide Exposure on the Exercise Performance of subjects with Coronary Artery Disease', *N. Engl. J. Med.*, **321**, 1426-1432.

Arnfield, A. J.: 2003, 'Two decades of urban climate research: A review of turbulence, exchange of energy and water, and the urban heat island', *Int. J. Climatol.*, **23**, 1-26.

Bornstein, R., Lin, Q.: 2000, 'Urban heat island and summertime convective thunderstorms in Atlanta: three cases studies', *Atmos. Environ.*, **34**, 507-516.

Chow, W. T. L., Roth, M.: 2006, 'Temporal dynamics of the urban heat island of singapore', *Int. J. Climatol.*, **26**, 2243-2260.

Collier, C. G.: 2006, 'The impact of urban areas on weather', *Q. J. R. Meteorol. Soc.*, **132**, 1-25.

EPA: 1991, 'Air Pollution and Health Risk', U.S. Environmental Protection Agency, EPA 450/3-90-022.

Fast, F. D., Torcolini, J. C., Redman, R.: 2005, 'Pseudo verticale temperature pro-

files and the urban heat island measured by a temperature data logger network in Phoenix, Arizona', *J. Appl. Meteorol.*, **44**, 3-13.

Fenger, J.: 1999, 'Urban air quality', *Atmos. Environ.*, **33**, 4877-4900.

Grimmond, C. S. B, King, T. S., Roth, M., Oke, T. R.: 1998, 'Aerodynamic roughness of urban areas derived from wind observations', *Bound.-Layer Meteor.*, **89**, 1-24.

Grimmond, C. S. B, Oke, T. R.: 1999, 'Heat storage in urban areas: local-scale observations and evalutation of a simple model', *J. Appl. Meteor.*, **38**, 922-940.

Holton, J. R.: 1979, 'An Introduction to Dynamic Meteorological, Second Edition', *Academic Press inc.*, San Diego, 391 pp.

Kondo, H., Genchi, Y., Kikegawa, Y., Ohashi, Y., Yoshikado, H., Komiyama, H.: 2005, 'Development of a Multi-Layer Urban Canopy Model for the Analysis of Energy Consumption in a Big City: Structure of the Urban Canopy Model and its Basic Performance', *Bound.-Layer Meteor.*, **116**, 395-421.

Makar, P.A., Gravel, S., Chirkov, V., Strawbridge, K.B., Froude, F., Arnold, J., Brook, J.: 2006, 'Heat flux, urban properties, and regional weather', *Atmos. Environ.*, **40**, 2750-2766.

Martilli, A., Clappier, A., Rotach, M. W.: 2002, 'An urban surfaces exchange parameterisation for mesoscale models', *Bound.-Layer Meteor.*, **104**, 261-304.

Masson, V.: 2006, 'Urban surface modeling and the meso-scale impact of cities', *Theor. Appl. Climatol.*, **84**, 35-45.

Oke, T. R.: 1982, 'The energetic basis of the urban heat island', *Q. J. R. Meteorol. Soc.*, **108**, 1-24.

Oke, T. R.: 1987, 'Boundary Layer Climates', 2nd edn. London: Methuen, 435 pp.

Raupach, M. R., Antonia, R. A., Rajagopalan, S.: 1991, 'Roughwall turbulent boundary layers', *Appl. Mech. Rev.*, **44**, 1-25.

Rotach, M. W., Vogt, R., Bernhofer, C., Batchvarova, E., Christen, A., Clappier, A., Feddersen, B., Gryning, S.-E., Martucci, G., Mayer, H., Mitev, V., Oke, T. R., Parlow, E., Richner, H., Roth, M., Roulet, Y.-A., Ruffieux, D., Salmond, J. A., Schatzmann M., Voogt, J. A.: 2005, 'BUBBLE - an Urban Boundary Layer Meteorology Project', *Theor. Appl. Climatol.*, **81**, 231-261.

Rotach, M. W.: 1993, 'Turbulence close to a rough urban surface. Part I: Reynolds stress', *Bound.-Layer Meteor.*, **65**, 1-28.

Rotach, M. W.: 1993, 'Turbulence close to a rough urban surface Part II: variances and gradients', *Bound.-Layer Meteor.*, **66**, 75-92.

Roth, M.: 2000, 'Review of atmospheric turbulence over cities', *Q. J. R. Meteorol. Soc.*, **126**, 941-990.

Seinfeld, J. H., Pandis, S. N.: 1998, 'Atmospheric Chemistry and Physics', *Wiley Interscience publication*, New-York, 1326 pp.

Stull, R.B.: 1988, 'An Introduction to Boundary Layer Meteorology', *Kluwer Academic Publisher*, Dordrecht, 670 pp.

Tennekes, H., Lumley, J.: 1972, 'A first course in turbulence', *MIT Press*, Cambridge, 300 pp.

Vu, T. C., Asaeda, T., Ashie, Y.: 1999, 'Developpement of a numerical model for the evaluation of the urban thermal environment', *J. Wind Enginneering*, **81**, 181-196.

Chapter 3

Air quality simulation over Mexico City: Impacts of the specific meteorological conditions and VOC/NOx emission variations

Abstract

Based on measurements and numerical air quality simulations, this study describes the meteorology and tests an emission inventory for a high ozone pollution episode in Mexico City on 2 March 1997.

Numerical simulations reproduce well the main meteorological features. Only at very fine resolutions of the mesoscale model, the meteorological conditions in this complex topography can be reproduced satisfactorily. The meteorological conditions are dominated by thermally driven flows which take place on continental, regional and local scale and lead to the creation of a wind convergence in the Mexico City Basin. The air quality simulations reveal that the movement of the ozone plume for the episode studied is determined by this wind convergence.

The NO_x concentrations are reproduced well by the simulations but the O_3 concentrations are underestimated. These findings can be explained by an underestimation of VOCs in the emission inventory. In increasing the emitted VOCs a better fit between the simulated ozone concentrations and the measured data is found. However in this case, the O_3 production regime changes over the Mexico City Basin, passing from a strong VOC-sensitive regime to a mixed regime with VOC-sensitive and NO_x-sensitive region.

This study shows the great influence of meteorological conditions and pollutant emissions on air quality. An understanding of details of the meteorological conditions, like small scale convergence in this case, and an accurate emission inventory validated by VOC measurements in the city, are sensitive elements in a complete air quality study.

3.1 INTRODUCTION

The Mexico City Metropolitan Area (MCMA) is one of the largest mega-cities in the world with more than 19 million inhabitants and an average population density of 12 200 per km^2 in 2000 (Molina et al., 2002). There are more than 35 thousand industries, 12 thousand service facilities and 3.5 million motor vehicles (buses, minibuses, taxis, trucks and private cars) which burn about 20 million liters of gasoline daily (Bravo et al., 2002).

The city covers 1500 km^2 and is located in the Transverse Neovolcanic Belt at an altitude of 2240 mASL in the Mexico Basin. The basin is surrounded on three sides (east, south and west) by mountain ridges with a broad opening to the north and a narrow gap to the southwest. The west and south mountain ridges culminate around 3500 mASL and at the east, we found the Popocatepetl volcano, the second highest peak in Mexico (5452 mASL).

The high concentration of human activities in the basin involves important emissions of atmospheric pollutants and the topographical situation, most of time does not allow good ventilation of the basin. Furthermore, the subtropical latitude ($\sim$ 19.40N) and the high altitude of the MCMA are conducive to ozone production all year long. The combination of these elements makes Mexico City one of the most polluted cities in the world (UNEP/WHO, 1992) and the city with the world's largest photochemical 'smog' problem (Baldasano et al., 2003).

Among the parameters which are particularly important for air quality are first, the pollutant emissions which are characterized by their type, amount, time and space repartition, and second, the atmospheric flow fields, which determine dispersion and mixing of air pollutants. The complex and nonlinear nature of the processes involved implies the use of numerical meteorological and photochemical models for studying, understanding and forecasting the air quality. Numerical simulations help to identify the mechanisms leading to high air pollution and enable

to evaluate emission reductions strategies.

In 1997, a boundary layer field experiment in the Mexico City basin with intensive measurements was conducted during the period 24 February - 22 March. The experiment was a part of a research program entitled Investigacion sobre Materia Particulada y Deterioro Atmosferico-Aerosol and Visibility Research (IMADA-AVER). It is the first time that a southeasterly wind entering the basin was observed. Doran et al. (1998) have pointed out that this meteorological situation regularly occurs and possibly has significant effects on air quality. This article will be focused on one high ozone episode of IMADA where this meteorological situation occurs. We choose March 2nd which it is a clear day with observed ozone values of more than 230 ppb. We stress again that the focus of this article is not to make emission reductions scenarios but to describe and to understand the meteorological pattern, to reproduce it with the model and to evaluate the emission inventory and its impact for this specific episode. Two Eulerian mesoscale models are used. The first one is a meteorological model which uses an urban parametrization to simulate the impact of a city on the planetary boundary layer structure. The second one is a photochemical model which solves the equations governing transport, diffusion and chemical reaction of the pollutants.

Using both measurement data and numerical simulations the following three main goals are addressed in this paper:

- Describe the wind pattern and its influence on the ozone plume (intensity and position) for a two day episode during the IMADA measurement campaign of March 1997 (Doran et al., 1998).

- Reproduce the meteorological conditions and the air pollution episode with the numerical meteorological and air quality simulations.

- Testing the sensitivity of the ozone (O_3) concentration to the emissions of volatile organic compounds (VOCs) and nitrogen oxides (NO_x).

3.2 MODEL DESCRIPTION

3.2.1 METEOROLOGICAL MODEL

The applied mesoscale numerical model FVM (Martilli et al., 2002) has been developed at the Swiss Federal Institute of Technology (EPFL). It is a three dimensional, Eulerian, anelastic model with a terrain following mesh. The mean transport is computed with a third-order piecewise parabolic method (PPM, Collella et al., 1984) corrected for multidimensional applications (Clappier, 1998). In the transition layer, turbulent exchange coefficients are derived from turbulent kinetic energy (TKE, computed prognostically) and mixing length, following the formulation of Bougeault and Lacarrere (1989). In rural areas, the surface fluxes are parametrized using the formulation of Louis (1979). In urban areas, FVM allows the use of an advanced parametrization (Martilli et al., 2002) for near surface fluxes, entitled the Buildings Effect Parametrization (BEP). This parametrization takes into account the impact of buildings on the mean airflow, on the modification on turbulent length scales, as well as the effect of radiation trapping and of shading in street canyons. The latent heat fluxes in the urban area are taken into account only by a fraction of rural area (parks and gardens) using the Louis formulation. The model boundaries are forced with large scale meteorological data (wind and temperature) using four-dimensional data assimilation (FDDA, Stauffer et al., 1994). FVM has already been used for calculating meteorological fields in several cities among which Athens (Martilli et al., 2003), Bogotà (Zárate et al., 2006), Basel (Roulet, 2004), Geneva, Ho Chi Minh City, Madrid and Milan.

3.2.2 AIR QUALITY MODEL

A three-dimensional air quality model to simulate photochemical air pollution is used. This transport and photochemistry Eulerian model (TAPOM, Junier et al. (2005)) calculates gas phase chemistry, transport, diffusion, solar radiation and dry deposition in a terrain-following mesh using a finite volume discretisation. It is based on the resolution of the mass balance equation for several atmospheric substances. TAPOM includes the RACM lumped species mechanism (Stockwell et al., 1997), the Gong and Cho chemical solver (Gong et al., 1993), an improved Piecewise Parabolic Method (PPM) for the advection (Collella et al., 1984; Clappier, 1998) and the solar radiation module TUV (Madronich, 1998) to calculate the photolysis rate constants. It uses meteorological fields (wind speed, wind direction, temperature, humidity, pressure, air density, turbulent mixing coefficients) provided by the meteorological model FVM described above.

3.2.3 MODEL SETUP

METEOROLOGICAL MODELING

Tests (not shown) have been made with one to three days for the initialization. It showes that one day is enough and the day before does not have any influence on the results. In consequence, a two day period is simulated from 1 March to 2 March 1997 and results of the first day are not considered due to spin-up effects. A system of four nested grids (Fig. 3.1) is used for the meteorological simulation, covering an area of 810 000 km^2 for the largest domain and 11 000 km^2 for the smallest. The horizontal grid sizes and resolutions are shown in Table 3.1.

The largest domain (G1) extends from the Pacific Ocean in the West to the Gulf of Mexico and the Caribbean See in the East. Thus, the domain takes into

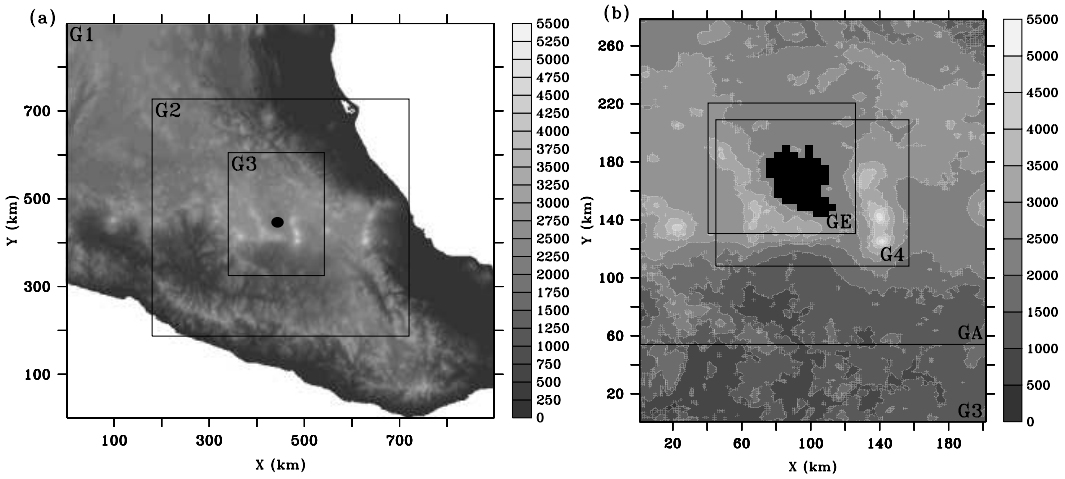

Figure 3.1: (a) Topography of Mexico with the Pacific Ocean in the South, the Gulf of Mexico in the North-East and Mexico City symbolized by a dot. Shown are the simulation domains for the meteorological simulations using a horizontal resolution of 60 (G1), 15 (G2) and 4.5 km (G3). (b) Topography of the Mexico City Basin showing the Mexico City urban area (black) and the simulation domains: Meteorological domain with a horizontal resolution of 2.25 km (G4); Air quality simulation domain with a horizontal resolution of 4.5 km (GA); Emission inventory grid with a horizontal resolution of 4.5 km (GE).

Table 3.1: Grid spacings (Δx, Δy), number of cells (nx, ny) and the lower-left cell coordinates of the simulation grids used in this study.

Grid	Δx [km]	Δy [km]	nx	ny	lon [°]	lat[°]
G1	60.	60.	15	15	-103.25	15.11
G2	15.	15.	36	36	-101.57	16.73
G3	4.5	4.5	45	62	-99.97	17.90
G4	2.25	2.25	50	45	-99.54	18.90
GA	4.5	4.5	45	50	-99.97	18.41
GE	4.5	4.5	19	20	-99.57	19.06

account the Mexico situation as well as the large mountain ranges which traverse the country from North-East to South-West.
The domains G2 and G3 are intermediate domains used in the nesting process in order to respect the optimal spatial resolution decrease (Fast, 1995). The domain G3 with a resolution of 4.5 km encompasses the large mountain slopes to the south and the mountain ranges surrounding the Mexico City Basin, thus allowing the development of slope winds which can strongly impact the air circulation in the basin.
Finally, a fourth domain (G4) with a high resolution of 2.25 km is used to reproduce accurately:

- The modification introduced to wind, temperature and mixing height in the planetary boundary layer (Rotach, 1993a, b) by the presence of a large urban area like Mexico City.
- Impacts of the complex topography inside and around the basin including scales ranging from the small volcanoes in the south-east part of the city to the large slopes surrounding the basin (Fig. 3.2).

A 2.25 km resolution was chosen as an optimal compromise between computational speed and a high resolution. At this resolution both the impact of the city and the local topography on the atmospheric flow fields are reasonably well resolved for the present purposes.
In the vertical direction, a stretched terrain-following grid is used for each domain with vertical layers of a thickness of 10 m near the earth's surface (50 m for the larger domain G1) and 1000 m at the top of the domain at an elevation of 14 000 mASL.
At the boundaries of the larger domain (G1), temperature and wind values are

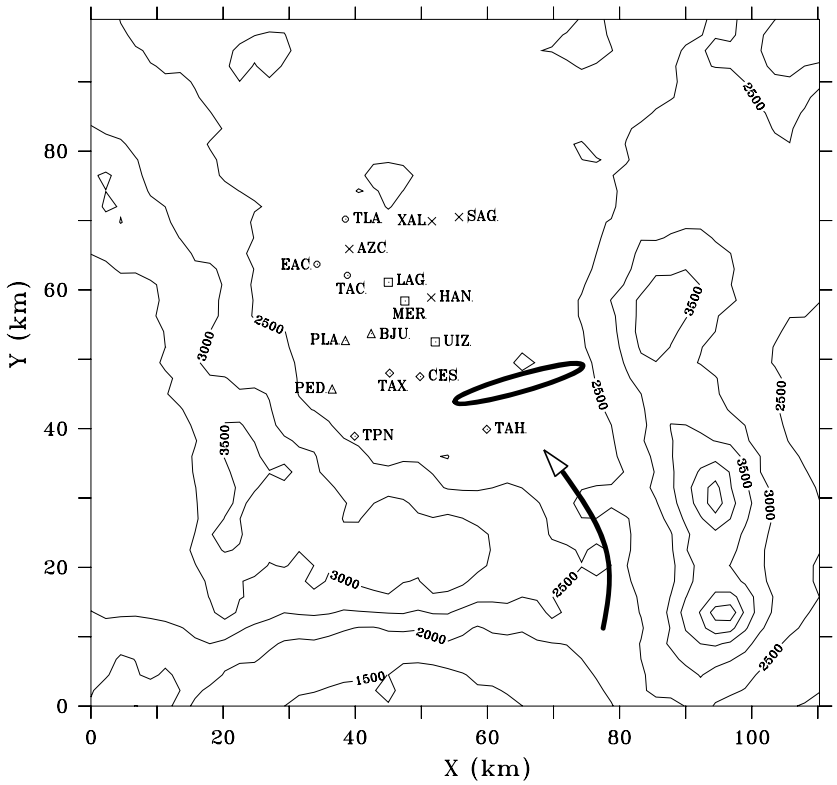

Figure 3.2: Location of the 17 measurement stations within the domain G4 with the mountains (contours) surrounding the basin. Different symbols are used to distinguish stations into five groups: North-West (circles), North-East (crosses), Central (squares), South-West (triangles) and South-East (diamonds). The arrow shows the gap in the South-East of the Mexico City Basin and the black ellipse shows the range of small volcanos located in the South-Eastern part of the basin.

initialized and forced using the NCEP/NCAR Reanalysis data applying the four-dimensional data-assimilation.

The urban area within the small domain (G4) occupies 256 horizontal grid points (1230 km^2) representing 11% of the total simulated area. The remaining surface is considered as rural with sandy-clay-loam soil characteristics (Tremback et al., 1985). The initial volumetric soil moisture content is set to 0.21. In agreement with reported data and literature (Oke et al., 1992, 1999; Masson et al., 2002), the city is represented by a single urban class with an average building height of 12 m and 10% of rural area (parks and gardens) within the city. The street and building width were set to 15 m and 30 m, respectively.

AIR QUALITY MODELING

The emission inventory has been provided by West and Zavala from the Massachusetts Institute of Technology, who have estimated the spatial and temporal distribution of the 1998 official emission inventory for the Mexico City Metropolitan Area (CAM, 2001). This emission inventory is based on a horizontal grid (GE) of 19 by 20 cells with a 4.5 km resolution and with a one hour time resolution. The emission inventory is largely describe in West et al. (2004). The domain for air-quality (GA) modeling (Figure 3.1b) is chosen to contain the emission domain (GE) as a subdomain and exactly match its resolution. In order to follow the ozone plume development and to take into account possible recirculation, the air quality modeling domain is extended to a size of 45 by 50 cells.

For the air quality simulations, a vertical stretched terrain-following grid is used with 12 vertical layers ranging in thickness from 30 m near the surface to 2000 m at the top of the domain at an elevation of 7500 mASL. This resolution allows to follow the vertical variation of the mixing height while requiring a reasonable

Table 3.2: Time and space-averaged boundary conditions for the concentrations of some main pollutants considered by the photochemical model used in this study (ISO = Isoprene).

Chemical species	Mixing ratio [ppb]
NO	0.5
O_3	31.5
HNO_3	0.3
H_2O_2	1.4
HCHO	0.4
CO	71.1
N_2O_5	$5.5 \cdot 10^{-4}$
ISO	$6.0 \cdot 10^{-2}$

computing time.

The initial and boundary conditions for the pollutant concentrations are provided by GEOS-CHEM (Bey et al., 2001). GEOS-CHEM is a three-dimensional global model for tropospheric chemistry driven by assimilated meteorological observations from the Goddard Earth Observing System (GEOS) of the NASA Data Assimilation Office (DAO). Table 3.2 shows the average concentrations used as boundary conditions of the air-quality modeling domain.

The meteorological fields used as input for the photochemical model are provided by the meteorological simulation and are interpolated from the meteorological grid G3 and G4 onto the photochemical grid GA.

3.3 MEASUREMENT ANALYSIS AND METEOROLOGICAL DESCRIPTION

Ozone measurement inside and around an urban area can be used to locate the pollution plume emitted by a city, *e.g.* studies over Milan by Martilli (2002), and over Athens by Clappier et al. (2000). It is often possible to differentiate three categories of measurement stations depending on their ozone levels:

- Measurement stations which are representative for the background pollution coming from outside the city, where the ozone data show almost no daily variation. Ozone levels remain relatively high during night-time and do not significantly increase during daytime.
- Measurement stations located inside the city and near pollutant sources, where the ozone level is very low during night-time and reaches the background level during daytime.
- Stations located in the city plume but away from pollutant sources, where ozone measurements show relatively high concentrations, i.e. background concentrations, during night-time and the highest ozone concentrations in the afternoon.

Compared to this classical situation, the episode of 2 March 1997 in Mexico City exhibited some special features. The low levels of ozone measured during night-time at all observation sites would place them into the second category defined above, *i.e.* inside the city. On the other hand, some of these stations[1] recorded a high and sharp ozone peak during the afternoon, and hence indicate that the city plume remained inside the city. The large spread of the urban area and specific features of the meteorological circulation lead indeed to this complexe

[1] A complete list of stations and abbreviations is found in appendix .1

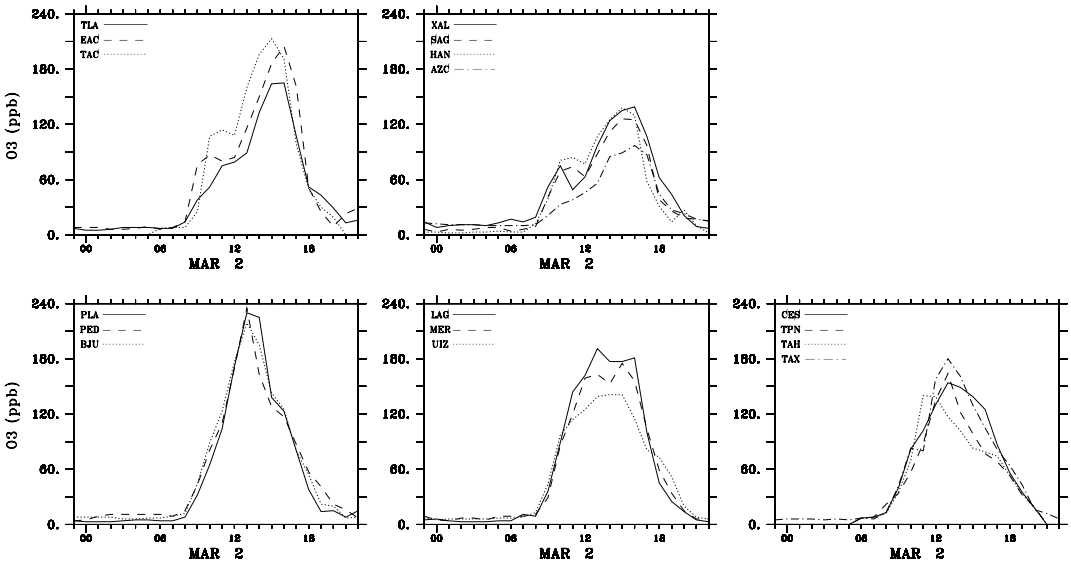

Figure 3.3: Ozone data recorded from 00 LT 2 March to 23 LT 2 March 1997, and arranged in five distinct groups of measurements stations differing in peak intensity and time.

situation which is not able to classified with criteria used in previous studies. The location of the measurement sites is shown in Figure 3.2.

The ozone concentrations start to increase at 09 LT (Local Time) in every station (Fig. 3.3). The maxima are reached at 13 LT in those stations located southward of the city center (PED, PLA, BJU, and CES, TPN, TAH, TAX). For the stations located in the northern part of the city (TAC, EAC, TLA, and SAG, XAL, HAN, AZC) the ozone maximum occurs around 16 LT. Additionally, higher ozone levels are also recorded at the stations in the western part of the basin (PED, PLA, BJU, and TAC, EAC, TLA).

Using two criteria, the ozone maximum concentration and the time of occurrence of the ozone peak, five groups of stations can be distinguished (Fig. 3.3):

- The South-West side, where the ozone maximums occur in early afternoon (around 13 LT) and reach 230 to 240 ppb. The measurement stations in this

group are PED, PLA and BJU.

- The South-East side where the ozone maximum occurs again in early afternoon but shows lower ozone concentrations between 140 and 180 ppb; CES, TPN, TAH and TAX.

- The North-West side, where the ozone peak takes place later in the afternoon (around 16 LT) and reaches from 160 to 210 ppb; TAC, EAC and TLA.

- The North-East side, where the ozone peak occurs later in the afternoon (around 16 LT) and reaches from 100 to 140 ppb; SAG, XAL, HAN and AZC.

- The city center, where no distinct or sharp ozone peak was recorded. Ozone levels range between 130 and 200 ppb; LAG, MER and UIZ.

The classification presented above shows that at 13 LT, the urban plume is located along a line from PLA in the eastern part of the basin to TAH in the western part of the basin, and moves towards the northern part of the domain during the afternoon (line from EAC to SAG at 17 LT).
This plume behavior can be explained by considering the meteorological situation. On 2 March, the circulation is dominated by topography induced, thermally driven flow (Bossert, 1997). In such a situation, the synoptic scale winds are low and the winds induced thermally by the topography are predominant. The ground radiative cooling occurring at night-time induces downslope winds from the surrounding mountains which converge into a complex circulation within the basin. Over the city area the winds are very weak (around 1 ms^{-1}). Upslope easterly and northerly winds are generated from 9 LT to 13 LT (Fig. 3.4) due to differential heating of the ground in the western and southern part of the domain (close to EAC, TAC, PLA, and PED).

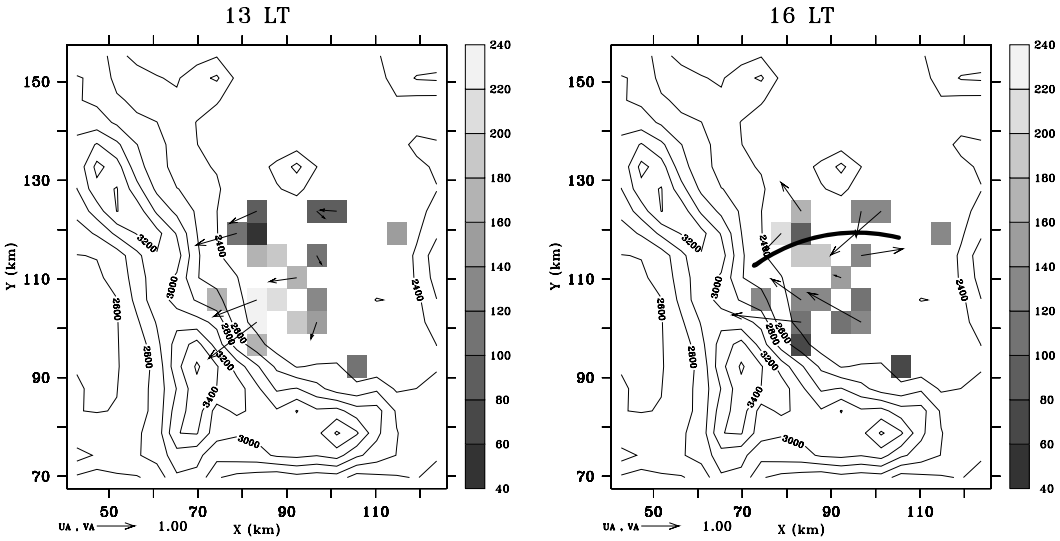

Figure 3.4: Wind vector and measured O_3 concentration (shaded) on 2 march 1997 at 13 LT (left) and 16 LT (right). It shows a O_3 peak of 230 ppb at the Pedregal measurement site South-Western part of the basin at 13 LT. Afterwards, the O_3 peak moves northwards and reaches 205 ppb at 16 LT to ENEP Acatlán (EAC) measurement site. The line shows the wind convergence at 16 LT on which the O_3 plume is located.

Between 13 LT and 14 LT, a south-easterly wind starts to blow into the basin and a wind convergence line is formed south of the city. This convergence then moves progressively northwards, since the southerly wind is stronger than the northerly wind in the basin. A large part of the pollutants are advected and trapped by the convergence where they are concentrated. Thus the pollution plume emitted by the city is located in the wind convergence (Fig. 3.4) and the maximum levels of ozone coincide with the convergence line.

The presence of a wind convergence has already been observed by de Foy et al. (2006) and Jazcilevich et al. (2005) for different episodes in 1996, 2001 and 2003. Those numerous episodes generally lead to high levels of pollution. Thus it is particulary important to study this meteorological pattern in Mexico City.

3.4 METEOROLOGICAL MODELING RESULTS

In this section, the quadruply nested simulations are described one by one at each modeling scale and the simulated meteorological fields are compared with data from several observation sites within Mexico City.
On 2 March the synoptic conditions are given by a high pressure system over central Mexico with weak upper-level winds (Doran et al., 1998). Under these synoptic conditions, the air flows in the boundary layer are mainly driven by radiative heating and cooling effects. Thus the wind is downslope during the first hours of the morning and the simulation in domain G1 exhibits a divergence along the mountain ridge from the North-West to the South-East. During the rest of the morning a thermal regime is installed, driven by the slope of the mountain range and reinforced by the presence of the Pacific Ocean in the West and by the Gulf of Mexico and the Caribbean Sea in the East. Thus, a convergence zone forms during the afternoon along the mountain ridge (Fig. 3.5).

The simulation on domain G3 exhibits a wind blowing downslope (not shown). These slope winds bring clean upper level air into the Mexico City Basin during the night and early the morning. When the sun rises, the flow reverses and a thermal upslope wind is installed (Fig. 3.6 at 11 LT). This pattern generates a particularly strong southerly wind on the south slope of the mountain range located at south of the basin. During the afternoon, this wind from south is stronger than the winds inside the basin, and it enters the basin via the pass (Fig. 3.2) in the South-East of the City and produces rapid winds in the Eastern part of the basin (Fig. 3.6 at

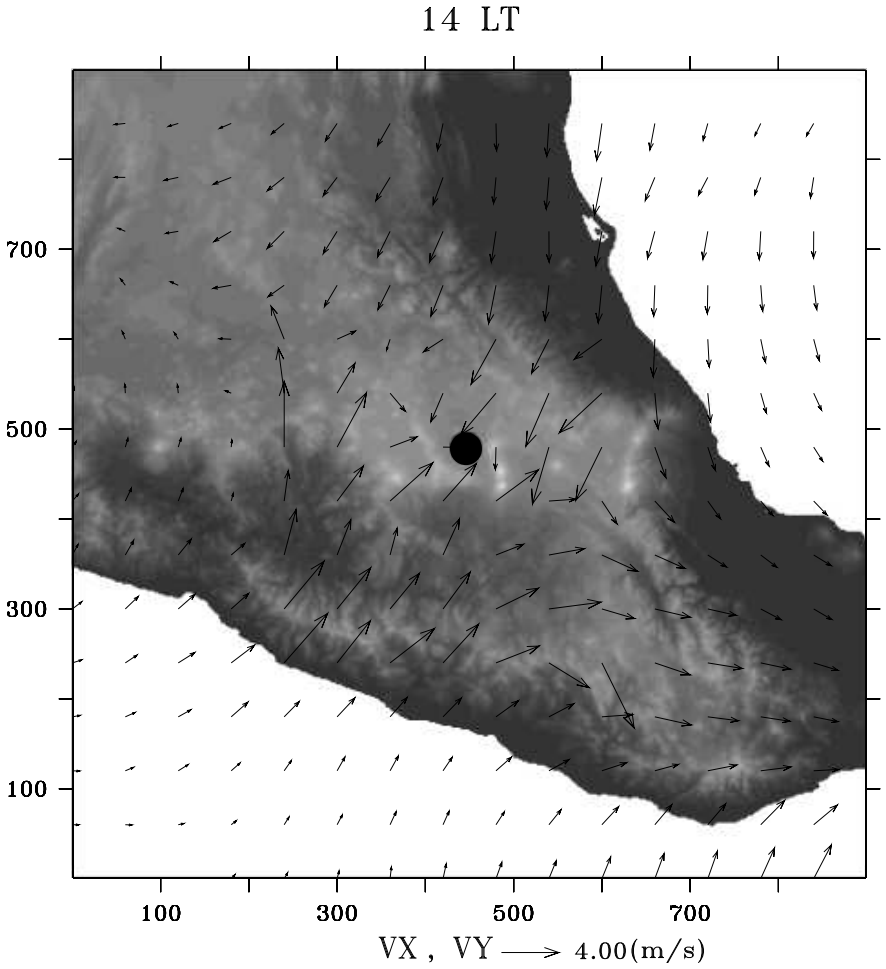

Figure 3.5: Wind fields close to the ground modeled by FVM at 14 LT 2 March 1997 on the largest domain G1. Mexico City is symbolized by a dot. A wind convergence is formed along the mountain ridge from South-East to North-East

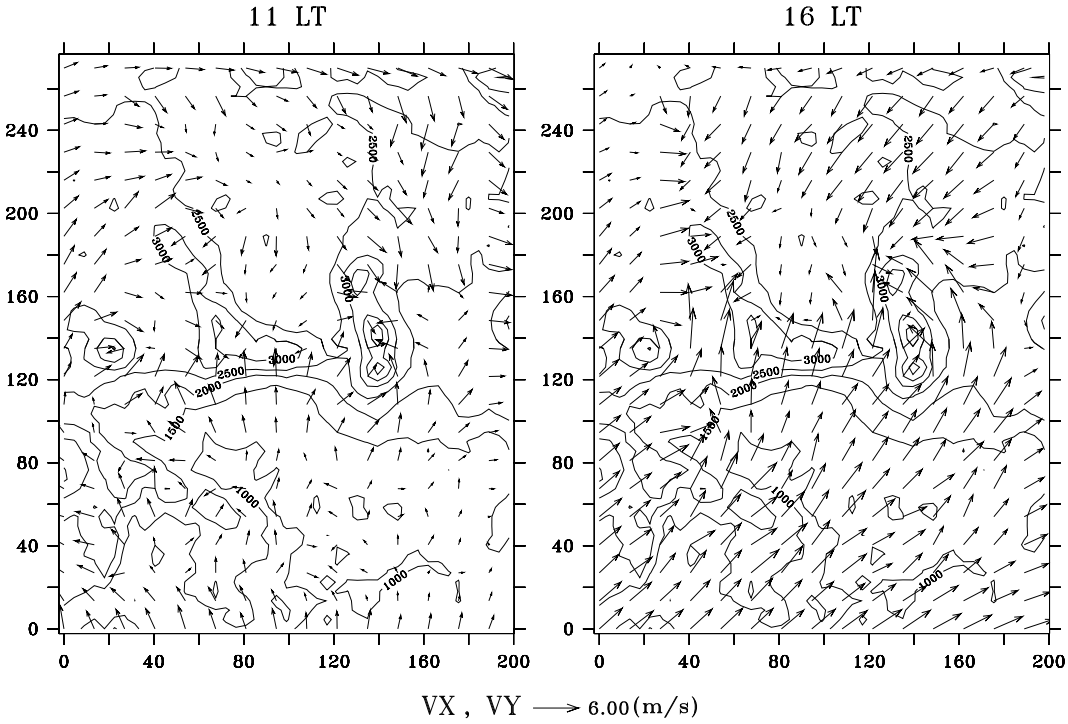

Figure 3.6: Wind fields close to the ground modeled by FVM at 11 LT (left) and at 16 LT (right) 2 March 1997 on domain G3. The simulation on domain G3 shows a strong southerly wind in the south slope. But the convergence observed in the measurements into the basin is not captured and the simulated southerly winds at 16 LT are too strong in the East part of the basin and flush the air from the basin.

16 LT). At the end of the afternoon, the southerly wind passes over the top of the mountain range and blows into the basin.

In other words, the simulation on domain G3 captures the timing of the thermal slope wind quite well. However, the convergence observed in the measurements (Fig. 3.4), and of great importance for the pollution plume in the basin, is not captured. The simulated southerly winds in the afternoon are too strong as compared to the real situation, especially in the Eastern part of the basin, and tend to flush the air from the basin.

Until 11 LT, the simulation in domain G4 shows the same general development of

wind pattern as domain G3. Winds are downslope during night-time until early morning (Fig. 3.7 at 07 LT). A few hours later, the wind direction reverses to upslope and a weak wind blows over Mexico City (Fig. 3.7 at 11 LT). From noon, southerly winds dominate and reach the basin blowing to the North-West by the hills situated in the south-eastern part of the city. These winds from the south, at the beginning come through the pass and a few hours later tend to flow over the crests at the southern end of the basin. This leads to the formation of a convergence over Mexico City (Fig. 3.7 at 15 LT). This convergence is generated in the southern part of the basin at 14 LT, and it moves northwards and disappears at 19 LT at the northern end of the basin (Fig. 3.7 at 19 LT).

These meteorological simulations are validated using the measurements of the IMADA campaign. Five measurement stations are selected here for the ground level comparisons, each station is representative of its own group presented in the measurement description, TLA for North-West, XAL for North-East, PED for South-West, MER for city center and CES for South-East. Figure 3.8 shows the air temperature evolution above the ground. A good agreement between the measurements and the simulation is achieved, nevertheless the simulation has a tendency to cool faster after 18 LT. As a consequence, model results underestimate the observations by 1 to 3 °C during the night. However the maxima and the minima of temperature are well represented in amplitude and time.

In figure 3.9, the wind speed at the ground level is compared between model predictions and measurements. The simulated wind is overestimated by 0.5 to 1 m/s in TLA (North-West) and PED (South-West) during the night. But for the rest of time and stations, the model results are shown to be in good agreement with the measurements, especially in the late afternoon (around 18 LT) when an increase

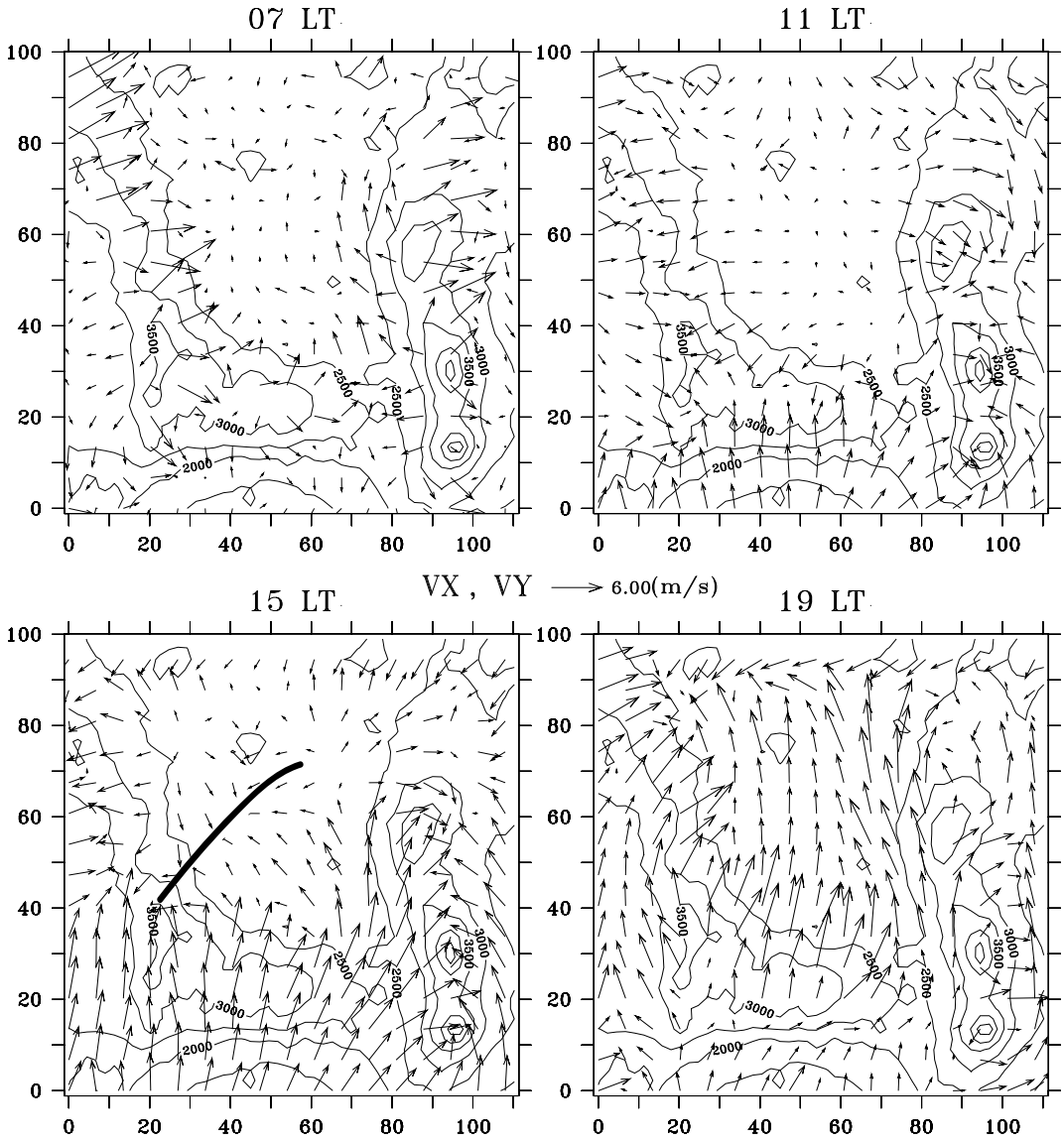

Figure 3.7: Modeled wind fields close to the ground at 7 LT (top left), 11 LT (top right), 15 LT (bottom left) and 19 LT (bottom right) 2 March 1997 on domain G4. It shows the evolution of the wind circulation which leads during the afternoon to the formation of a wind convergence (line) over Mexico City.

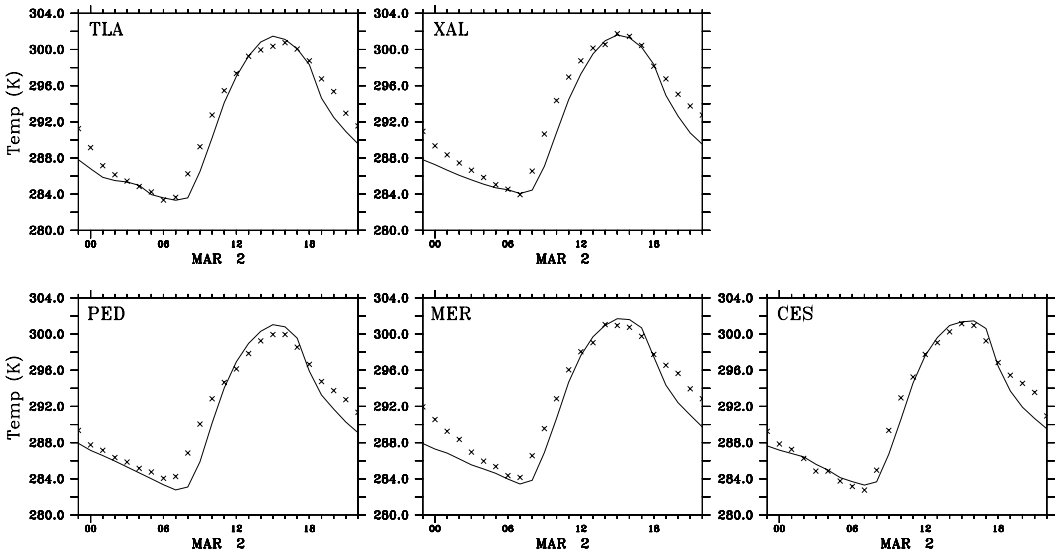

Figure 3.8: Temperature evolution close to the ground as a function of time from 23 LT 1 March to 22 LT 2 March 1997. Simulation with FVM (solid line) and measurement (crosses) for five measurement sites (cf. Fig. 3.2), representing the five defined groups (cf. Fig. 3.3).

of wind speed is observed. This increase, corresponding to the establishment of the southerly wind, is well represented by the simulation and of great importance for the air quality simulation. In summary, the simulation with the finest resolution shows the importance of the detailed topography inside and around the basin. The urban parametrization is of great importance in order to reproduce the wind circulation taking into account a more realistic resistance (Fig. 3.9). The more detailed urban parametrization also leads to a more appropriate air temperature near the ground by considering urban heat storage during nighttime (Fig. 3.8).

Overall, it is fair to state that the comparison between the simulations and the measurements shows that the main meteorological features are well reproduced in the simulation.

It may thus be concluded that in the present case of low synoptic winds, the meteorological situation over the Mexico City metropolitan area depends on continental,

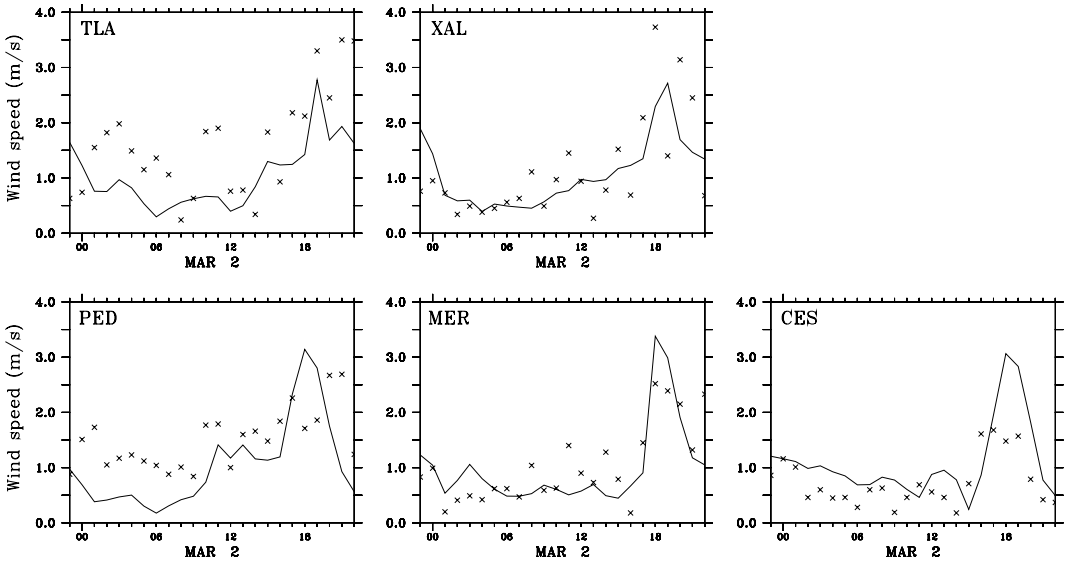

Figure 3.9: Wind speed close to the ground as a function of time from 23 LT 1 March to 22 LT 2 March 1997. Simulation with FVM (solid line) and measurement (crosses) for five measurement sites (cf. Fig. 3.2), representing the five defined groups (cf. Fig. 3.3).

regional and local factors, in particular:

- The *Continental influence* on the air circulation in MCMA is due to the high plateau in the center of Mexico, the Pacific Ocean and the Gulf of Mexico which lead to the creation of a large scale thermal flow regime.

- The *Regional influence* is due to the mountains surrounding the Mexico City Basin and the large slope extending to the south which is steeper and longer (from 3000 down to 1000 mASL) on the south side than the slope on the Mexico Basin side (from 3000 to 2000 mASL). This difference generates a dominant southerly wind entering the basin.

- The *Local influence* is caused by the topography inside the basin and by the presence of the city itself which modifies the basins thermal budget and the surface roughness properties.

To capture all these factors in a reasonably realistic and effective way, the quadruple nesting procedure is necessary, especially in the case of the final simulation in domain G4 with a high resolution of 2.25 km. It is only at this resolution that all meteorological phenomena leading to the wind convergence, which is fundamental to observed air pollution measurements, are well represented in the numerical model.

3.5 AIR QUALITY MODELING RESULTS

3.5.1 PRIMARY POLLUTANTS AND OZONE

The nitrogen dioxide (NO_2) measurements show maximum levels in the morning, with values between 60 to 160 ppb. They drop to 10 ppb in the afternoon (12 LT to 16 LT), and then increase to 50 ppb at the end of the day. Figure 3.10 shows that this general behavior and the levels of NO_2 are well reproduced by the model in every part of the domain. Except during nighttime for TLA and PED where the model overestimated the NO_2. As it is shown in previous section, the wind is underestimated at this moment for these stations and the NO_2 overestimation is due to a lack of advection. So the NO_x emissions and the dispersion (advection, diffusion and mixing height) seem generally in good agreement with measurements.

Simulated ozone shows spatial and temporal patterns that agrees well with measurements (Fig. 3.11). As indicated by the measurements discussed in the previous chapter, ozone formation starts in the North-East side of the basin at 9 LT. The ozone plume afterwards moves to the South with increasing ozone concentrations. At 12 LT the plume moves to South-West until reaching a maximum at 14 LT. Afterwards, it is trapped in the wind convergence and it moves to the North following the mountain range on the West side of the city.

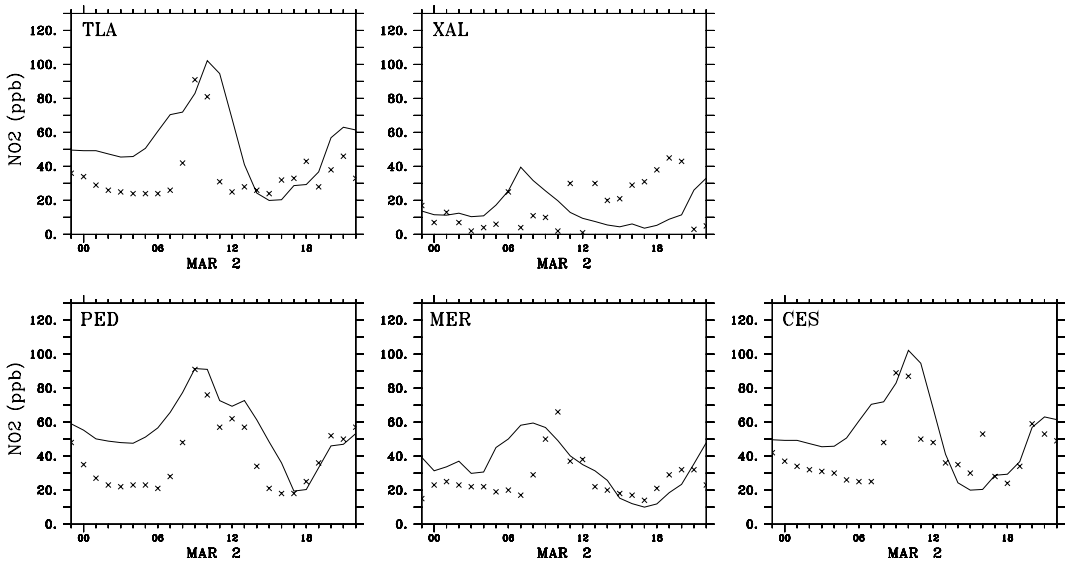

Figure 3.10: NO_2 concentration in ppb close to the ground as a function of time from 23 LT 1 March to 22 LT 2 March 1997. Simulation with TAPOM (solid line) and measurement (crosses) for five measurement sites (cf. Fig. 3.2), representing the five defined groups (cf. Fig. 3.3).

The good agreement between the measurements and the model results for the meteorological data as the NO_2 concentrations and the coherence between the ozone observed behavior and the model response, give confidence in the measurements interpretation and in the capacity to the model to well reproduce the main phenomena as the advection, the mixing height and the dry deposition. But if we look the ozone concentration at the Pedregal measurement site (PED), the maximum observed ozone concentration reaches 235 ppb at 14 LT, while the maximum levels at the other measurement stations vary between 140 ppb and 180 ppb. In contrast, the modeled ozone concentrations do not exceed 121 ppb (Fig. 3.12) and are generally too low.

Previous studies, one conducted on measurements of VOC between 1992 and 2001 (Arriaga-Colina et al., 2004) and another one modeling the air quality in Mexico City (West et al., 2004) show that the official emission inventory is accu-

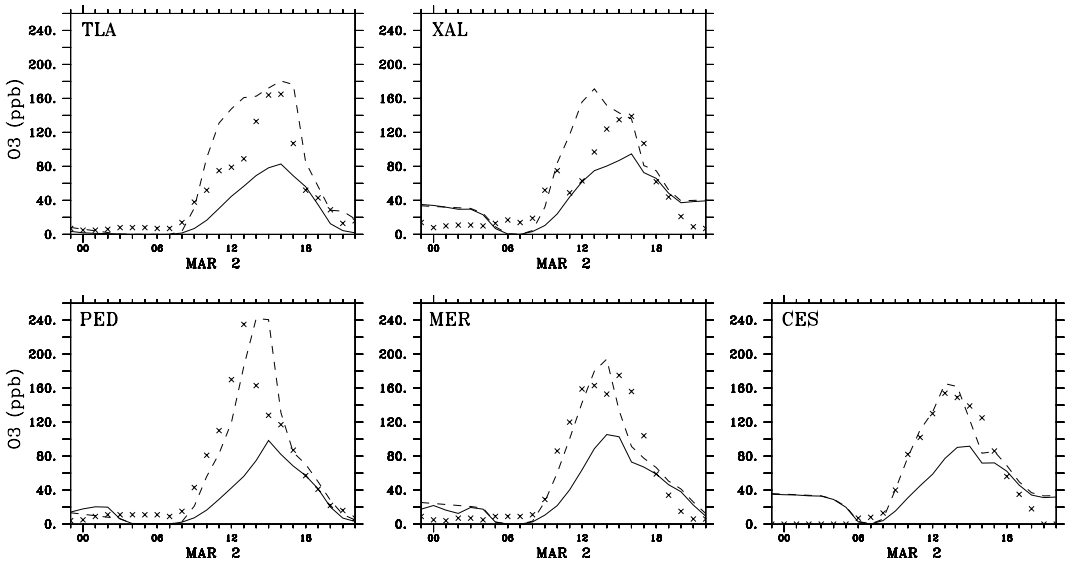

Figure 3.11: O_3 concentrations in ppb close to the ground as a function of time from 23 LT 1 March to 22 LT 2 March 1997. TAPOM simulations with the regular emissions (solid lines), with VOC emissions multiplied by a factor 2.2 (dashed lines) and according to the measurements (crosses) for five measurement sites (cf. Fig. 3.2), representing the five defined groups (cf. Fig. 3.3).

rate enough for NO_x but underestimated by a factor of two to three the VOCs emissions. Since the emission inventory used in this study is based on the official inventory for 1998 (CAM, 2001), we will test it in order to look if it is possible to simulate the right level of ozone by increasing the ozone precursor emissions and how it affects the ozone production regime.

3.5.2 EVALUATION OF THE EMISSION INVENTORY

In order to investigate the possibility to simulate right level of ozone and to evaluate the factor of underestimation of VOC emissions, a series of simulations are conducted by varying the total NO_x emissions from 0% to 200% and the total

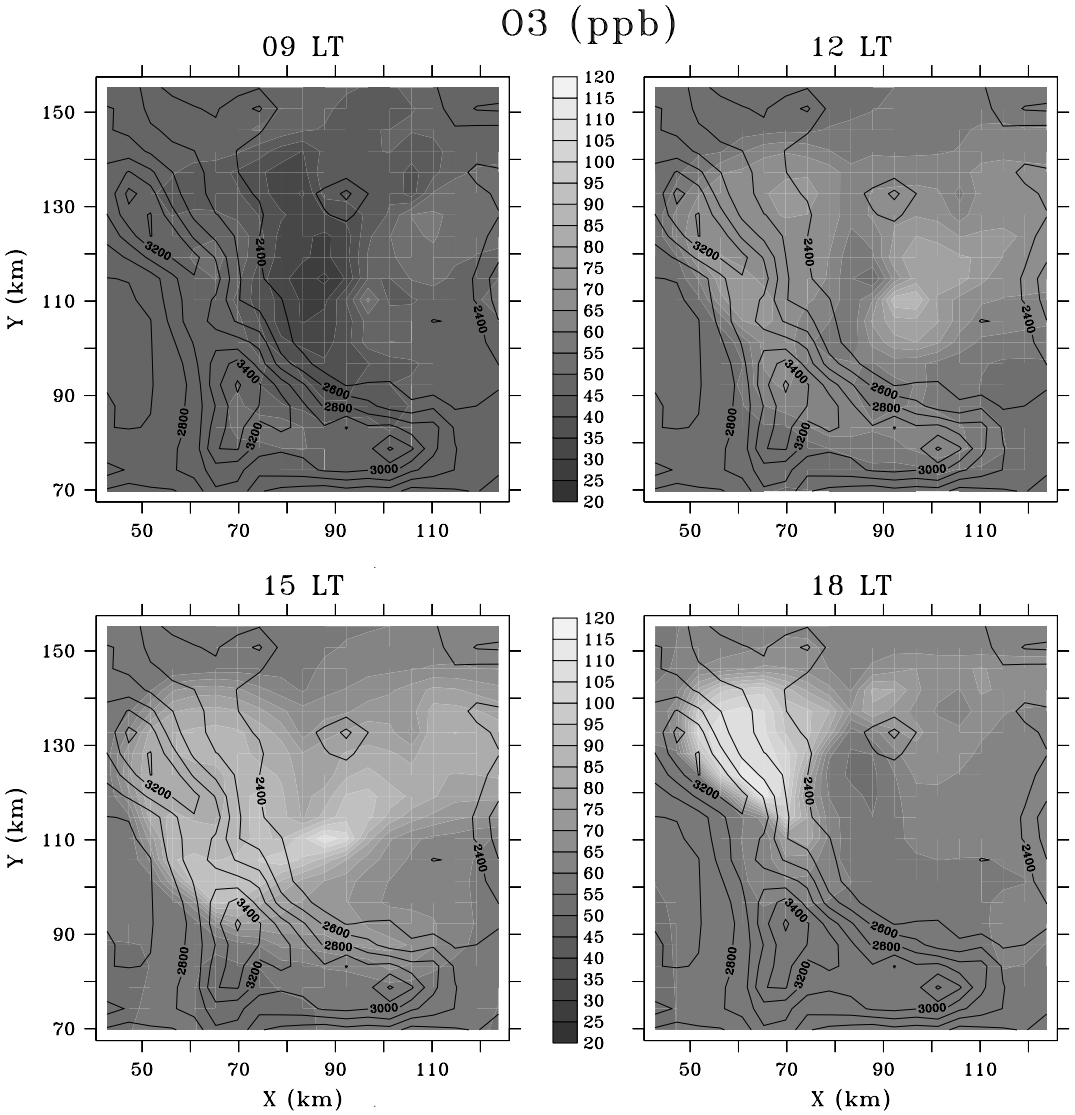

Figure 3.12: Simulated O_3 concentration in ppb close to the ground in the Mexico City Area at 09 LT (top left), 12 LT (top right), 15 LT (bottom left) and 18 LT (bottom right) on 2 March 1997 according to a TAPOM simulation.

VOC emissions from 20% to 300% as compared to the base case. The variation of NO_x emissions decreases the agreement between simulation and measurement of NO_2. The best fit of NO_2 concentration between simulation and measurement is with unchanged NO_x emissions as compared to the base case. This is in agreement with the results in the previous section (Fig. 3.10). The best fit between simulation and measurement for the ozone concentrations is found when the total VOC emissions are increased by a factor of 2.2 (Fig. 3.11, dashed lines). This increase is in agreement with earlier studies Arriaga-Colina et al. (2004) and West et al. (2004). Therefore it is now possible taking into account the corrected VOC emissions to reproduce the right level of ozone with a good spatial and temporal distribution.

By increasing the VOC emissions, it's important to specify the sensitivity of ozone to a variation of NO_x and VOC emissions in order to evaluate how this modification affects the ozone production regime, *i.e.* NO_x *vs.* VOC limitation. In order to quantify the sensitivity of ozone, two simulations are performed: a first simulation with a 35% reduction of NO_x emission, and a second simulation with a 35% reduction of VOC emissions. The results of these simulations are presented as graphs of the difference in ozone concentrations between the run with a VOC reduction and a run with a NO_x reduction, respectively, *i.e.* $\Delta O_3 = O_3(65\%\ \text{VOC}) - O_3(65\%\ NO_x)$. Two regions can be distinguished in these plots: if ΔO_3 is positive, a reduction of NO_x emissions is more efficient to reduce ozone concentrations and the region is called NO_x-sensitive. If a VOC emission reduction is more efficient, ΔO_3 is negative and the area is named VOC-sensitive.

In the base case, without increasing the emissions, the Mexico City basin is clearly VOC-sensitive in the morning, while in the afternoon, the VOC-sensitive region is reduced and is limited to a zone corresponding to ozone concentration greater than 65 ppb (Fig. 3.13 a). Nevertheless, the MCMA remains always VOC-sensitive but

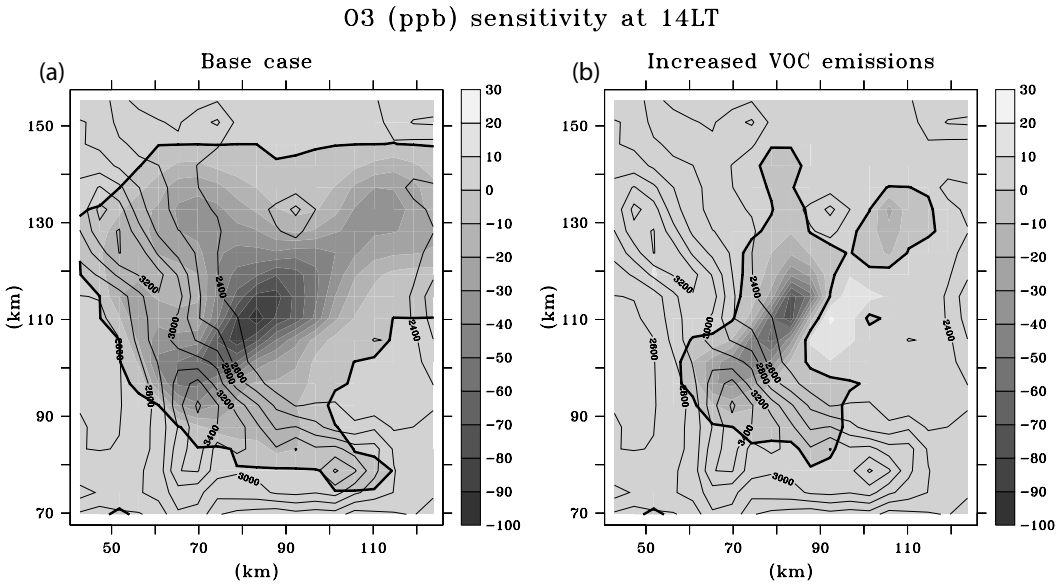

Figure 3.13: (a) Difference of O_3 concentration between a run with a 35% reduction of the VOC emissions and a run with a 35% reduction of the NO_x emissions on 2 March 1997 at 14 LT. The negative areas (dark grays) are VOC sensitive, the positive areas (light grays) are NO_x sensitive. A thick line separates the two regions. (b) Same as (a) with the VOC emission multiplied by a factor 2.2. It shows that the basin is passing from a strong VOC-sensitive regime all over Mexico City for the base case to a mixed regime with weaker VOC-sensitive region and a NO_x-sensitive region for the case with the increased VOC emissions.

a reduction of the VOC emissions is more efficient to reduce ozone than in the morning.

When VOC emissions are increased by the above-mentioned factor of 2.2, the VOC-sensitive region is smaller than in the base case and a reduction of VOC emissions is less efficient to achieve a reduction of ozone. There is even a significant NO_x-sensitive region which appears in city center with the ozone peak at 14 LT (Fig. 3.13 b). Nevertheless the ozone peak essentially remains VOC-sensitive. Later in the afternoon, at 17 LT, most of the basin is NO_x-sensitive at the location of the ozone peak (not shown).

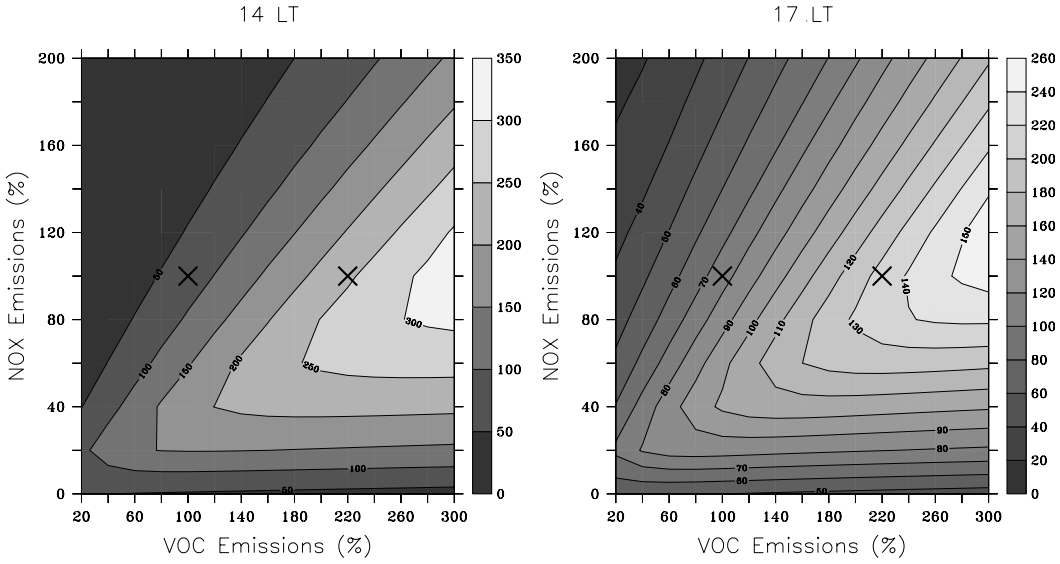

Figure 3.14: Ozone concentration isopleths [ppb] as a function of NO_x and VOC emissions percentage. Plots are evaluated at the grid point where maximum ozone concentrations occur in the base case simulation at 14 LT (left) at 17 LT (right). The crosses represent the base case and the case with the increased VOC emissions. It shows a strong dependency of the ozone variation and concentration to the VOC and NO_x emission.

Figure 3.14 shows ozone concentration isopleths as a function of VOC and NO_x concentrations simulated at the grid point where the hourly maximum ozone concentration appears at 14 LT and 17 LT respectively. It points out a strong dependency of the ozone variation and concentration on the VOC and NO_x emissions. This ozone variation may also depend on time and space. In this case, if we would made reduction scenarios, the response would be different in the base case and the case with the increasing VOC emissions. So the emission inventory for the VOCs would not be correct to forecast the effect of ozone reduction strategies over Mexico City with reasonable accuracy for the studied episode. In consequence, it is probably not at all optimal to try to make ozone reduction strategies with the emission inventory used in the base case presented in this paper.

3.6 CONCLUSION

The meteorological conditions over the Mexico City Metropolitan Area depend on phenomena taking place on a wide range of geographical scales. From the continental scale of the general synoptic conditions to the local scale of the slope wind systems in the Mexico City Basin. Even the city itself influences the atmospheric flow fields by slowing down the wind and by maintaining relatively high temperatures during night-time. The wind circulation over the MCMA is dominated by radiative heating especially in the case of low synoptic wind speeds. Thus, topography is particularly important in the development of the meteorological conditions and a fine resolution (2.25 km) is necessary in order to properly take into account the complex morphology of the Mexico City Basin. The specific meteorological situation already observed often involves the creation of a convergence line over the city which keeps the ozone plume over the city during daytime. Even if this meteorological pattern is not representative of all the meteorological situation in MCMA, it occurs frequently enough (Jazcilevich et al., 2005; de Foy et al., 2006) for being study especially since it leads to high ozone pollution episodes.

Numerical simulations using a mesoscale model are shown to reproduce these meteorological conditions well, leading, in this case, to a strong pollution episode. This gives hope for further research that aims at a better understanding of the meteorological conditions over MCMA that are conducive for high ozone pollution episodes.

In the second part of this study an emission inventory together with output from the meteorological model have been used to conduct air quality simulations. These simulations reproduce the nitrogen oxide concentrations reasonably well, hence indicating a good accuracy of the NO_x in the emission inventory. The general behavior of the ozone plume is well represented by the model as compared the measurements. But the ozone concentrations are underestimated.

Based on previous studies that show an underestimation by factor 2 to 3 of VOC emissions in the official emission inventory, we decide to change the ozone precursor emissions. By increasing VOCs in the inventory, a better fit between the simulated ozone concentrations and the measurements is found, but the O_3 production behavior changes completely over the basin, passing from a strong VOC-sensitive regime all over Mexico City to a mixed regime with a weak VOC-sensitive region combined with a NO_x-sensitive region. Since the response to the emission variations is significantly different between the base case and the case with increased VOC emissions, care is indicated if we use this emission inventory and we are not able to make realistic O_3 reduction scenarios with it.

This study describes the case of a specific meteorological pattern. For a more complete study and for being able to develop emission abatement strategies, a sizable set of day are required for having a representative sample of different patterns which occur in Mexico City. For future studies, it will be of great interest to study many episodes with different patterns, to have VOC measurements and a more accurate emission inventory in order to be able to use simulations as a tool to test reduction scenarios. VOC measurements in the city are of great importance to evaluate the inventory. Also, primary pollutants and ozone measurements are missing outside the metropolitan area. These are essential for a validation of the background concentrations which characterize the air swept into the MCMA.

Acknowledgements

This study would not have been possible without Prof M. J. Molina, Dr L. T. Molina, Dr. J. J. West and M. A. Zavala from the Department of Earth, Atmospheric and Planetary Sciences of the Massachusetts Institute of Technology who have provided the emission inventory.
I would like to thank:

- Dr. F. Kirchner for his expertness with RACM.
- Dr. Y.-A. Roulet, P. Helfer and Dr. M. Junier for their collaboration.
- Professor I. Bey (Atmospheric Chemistry Modeling Laboratory, EPFL) for providing GEOS-CHEM data and B. Hohl for his work on the boundary conditions.
- Professor B. de Foy (Department of Earth and Atmospheric Sience,Saint Louis University, USA) for welcoming us in Boston and for valuable discussions and scientific exchanges.

Bibliography

Arriaga-Colina, J.L., West, J.J., Sosa, G., Escalona, S.S., Ordúñez, R.M., Cervantes, A.D.M.: 2004, 'Measurements of VOCs in Mexico City (1992-2001) and evaluation of VOCs and CO in the emissions inventory', *Atmos. Environ.*, **38** (16), 2523-2533.

Baldasano, J.M., Valera, E., Jiménez, P.: 2003, 'Air quality data from large cities', *Sci. Total Environ.*, **307**, 141-165.

Bey I., Jacob, D. J., Yantosca, R. M., Logan, J. A., Field, B., Fiore, A. M., Li, Q., Liu, H., Mickley, L. J., and Schultz, M.: 2001, 'Global modeling of tropospheric chemistry with assimilated meteorology: Model description and evaluation', *J. Geophys. Res.*, **106**, 23073-23096.

Bossert, J. E.: 1997, 'An investigation of flow regimes affecting the Mexico city region', *J. Appl. Meteor.*, **36**, 119-140.

Bougeault, P. and Lacarrere, P.: 1989, 'Parameterisation of orography-induced turbulence in a mesobeta-scale model', *Mon. Wea. Rev.*, **117**, 1872-1890.

Bravo, H., Sosa, R., Sánchez, P., Bueno, E., González, L.: 2002, 'Concentrations of benzene and toluene in the atmosphere of the southwestern area at the Mexico City Metropolitan Zone', *Atmos. Environ.*, **36**, 3843-3849.

CAM (Comisión Ambiental Metropolitana): 2001, 'Inventario de emisiones a la atmósfera, Zona Metropolitana de Valle México, 1998'

Clappier, A.: 1998, 'A correction method for use in multidimensional time splitting advection algorithms: application to two- and three-dimensional transport', *Mon. Wea. Rev.*, **126**, 232-242.

Clappier, A., Martilli, A., Grossi, P., Thunis, P., Pasi, F., Krueger, B. C., Calpini, B., Graziani, P., and van den Bergh, H.: 2000, 'Effect of sea breeze on air pollution in the Greater Athens Area. Part I: Numerical simulations and field observations', *J. Appl. Meteor.*, **39**, 546-562.

Collella, P. and Woodward, P.: 1984, 'The Piecewise Parabolic Method (PPM) for gas dynamical simulations', *J. Comput. Phys.*, **54**, 174-201.

de Foy, B., A. Clappier, T. Molina and M. J. Molina: 2006, 'Distinct wind convergence patterns in the Mexico City basin due to the interaction of the gap winds with the synoptic flow', *Atmos. Chem. Phys.*, **6**, 1249-1265.

Doran, J. C., Abbott, S., Archuleta, J., Bian, X., Chow, J., Coulter, R. L., de Wekker, S. F. J., Edgerton, S., Elliott, S., Fernandez, A., Fast, J. D., Hubbe, J. M., King, C., Langley, D., Leach, J., Lee, J. T., Martin, T. J., Martinez, D., Martinez, J. L., Mercado, G., Mora, V., Mulhearn, M., Pena, J. L., Petty, R., Porch, W., Russell, C., Salas, R., Shannon, J. D., Shaw, W. J., Sosa, G., Tellier, L., Templeman, B., Watson, J. G., White, R., Whiteman, C. D., and Wolfe, D.: 1998, 'The IMADA-AVER boundary layer experiment in the Mexico City area', *Bull. Amer. Meteor. Soc.*, **79**, 2497-2508.

Fast, J. D.: 1995, 'Mesoscale Modeling and Four-Dimensional Data Assimilation in Areas of Highly Complex Terrain', *J. Appl. Meteor.*, **34**, 2762-2782.

Gong, W., Cho, H.-R.: 1993, 'A numerical scheme for the integration of the gas-phase chemical rate equations in three-dimensional atmospheric models', *Atmos. Environ.*, **27**A (14), 2147-2160.

Jazcilevich, A. D., Garciá, A. R., Caetano, E.: 2005, 'Locally induced surface air confluence by complex terrain and its effects on air pollution in the valley of Mexico', *Atmos. Environ.*, **39** (30), 5481-5489.

Junier, M., Kirchner, F., Clappier A. and van den Bergh, H.: 2005, 'The chemical mechanism generation program CHEMATA, part II: Comparison of four chemical mechanism in a three-dimensional mesoscale simulation', *Atmos. Environ.*, **39**, 1161-1171.

Louis, J.-F.: 1979, 'A parametric model of vertical eddy fluxes in the atmosphere', *Bound.-Layer Meteor.*, **17**, 187-202.

Madronich, S.: 1998, 'TUV Tropospheric Ultraviolet and Visible radiation model', URL *http://acd.ucar.edu/models/open/tuv/tuv.html*

Mage, D., Ozolins, G., Peterson, P., Webster, A., Orthofer, R., Vandeweerd, V., Gwynne, M.: 1996, 'Urban air pollution in Megacities of the world', *Atmos. Environ.*, **30**, 681-686.

Martilli, Alberto: 2001, *Development of an urban turbulence parameterisation for mesoscale atmospheric models*, PhD Thesis N^o **2445**. Federal Institute of Technology (EPFL), Lausanne, Switzerland.

Martilli, A., Neftel, A., Favaro, G., Kirchner, F., Sillman, S., Clappier, A.: 2002, 'Simulation of the ozone formation in the northern part of the Po Valley', *J. Geophys. Res.*, **107**, 8195.

Martilli, A., Clappier, A., Rotach, M. W.: 2002, 'An urban surfaces exchange parameterisation for mesoscale models', *Bound.-Layer Meteor.*, **104**, 261-304.

Martilli, A., Roulet, Y.-A., Junier, M., Kirchner, F., Rotach, M., Clappier, A.: 2003, 'On the impact of urban surface exchange parameterisations on air quality simulations: the Athens case', *Atmos. Environ.*, **37**, 4217-4231.

Masson, V., Grimmond, C. S. B., and Oke, T. R.: 2002, 'Evaluation of the Town Energy Balance (TEB) scheme with direct measurements from dry districts in two cities', *J. Appl. Meteor.*, **41**, 1011-1026

Mayer, Helmut: 1999, 'Air pollution in cities', *Atmos. Environ.*, **33**, 4029-4037.

Molina, L.T., Molina, M.J.: 2002, *Air Quality in the Mexico Megacity: an Integrated Assessment*, (Eds.) Kluwer Acad., Norwell, Mass., 384 pp.

Oke, T. R., Spronken-Smith, R. A., Jáuregui, E., and Grimmond, C. S. B.: 1999, 'The energy balance of central Mexico City during dry season', *Atmos. Environ.*, **33**, 3919-3930.

Oke, T. R., Zeuner, G., and Jauregui, E.: 1992, 'The surface energy balance in Mexico City', *Atmos. Environ.*, **26**B, 433-444.

Rotach, M., W.: 1993, 'Turbulence close to a rough urban surface. Part I: Reynolds stress', *Bound.-Layer Meteor.*, **65**, 1-28.

Rotach, M., W.: 1993, 'Turbulence close to a rough urban surface Part II: variances and gradients', *Bound.-Layer Meteor.*, **66**, 75-92.

Roulet, Y.-A.: 2004, *Validation and Application of an urban turbulence parameterisation scheme for mesoscale atmospheric models*, PhD Thesis N^o. **3032**, Swiss Federal Institute of Technology, Lausanne.

Stauffer, D.R. , Seaman, N.L.: 1994, 'Multiscale four-dimensional data assimilation', *J. Appl. Meteor.*, **33**, 416-434.

Stockwell, W. R., Kirchner, F., Kuhn, M., Seefled, A.: 1997, 'A new mechanism for regional atmospheric chemistry modeling', *J. Geophys. Res.*, **102** (D22), 25847-25879.

Tremback, C. J., and Kessler, R.: 1985, 'A surface temperature and moisture parameterisation for use in mesoscale numerical models', in Proceedings of 7th Conference on Numerical Weather Prediction, June 17-20, Montreal, Quebec, Canada.

United Nations Environmental Program/World Health Organisation: 1992, *Urban Air Pollution in Megacities of the World*, Blackwell Publisher, Oxford.

West, J.J., Zavala, M.A., Molina, L.T., Molina, M.J., San Martini, F., McRae, G.J., Sosa-Iglesias, G., Arriaga-Colina, J.L: 2004, 'Modeling ozone photochemistry and evaluation of hydrocarbon emissions in the Mexico City metropolitan area', *J. Geophys. Res.*, **109** (19), D19312 1-15.

Zárate, E., Clappier, A., Belalcázar, L. C.: 2006, 'A study of the photochemical plume formed in Bogota (Colombia) using numerical simulations', *submitted to J. Environ. Manage.*

Appendices

.1 ABBREVIATIONS OF MEASURING STATIONS

Station Name	Abbreviation
Lagunilla	LAG
Hangares	HAN
UAM Iztapalapa	UIZ
Tacuba	TAC
ENEP Acatlán	EAC
Benito Juárez	BJU
Taxqueña	TAX
San Agustín	SAG
Azcapotzalco	AZC
Tlalnepantla	TLA
Xalostoc	XAL
Merced	MER
Cuajimalpa	CUA
Pedregal	PED
Tlalpan	TPN
Cerro de la Estrella	CES
Plateros	PLA
Tláhuac	TAH

Chapter 4

Implementation of The Buildings Effects Parametrization in aLMo

Abstract

This study investigates the capacity of the weather forecast model aLMo (the operational numerical weather prediction model of MeteoSwiss) to reproduce the effect of a city on the Planetary Boundary Layer (PBL) atmospheric flow fields . For this purpose, the model was runned for the city of Basel and its surroundings where a large measurement campaign (BUBBLE) have been conducted in 2001 and 2002. With those measurements, we underline the presence of an Urban Heat Island (UHI) over Basel. However, the aLMo simulations were not able to reproduce the UHI even with increased horizontal and vertical resolution.

The Buildings Effects Parametrization (BEP) have been implemented into aLMo and adapted in order to study its ability to reproduce the effects induced by the presence of a city. The simulation with BEP shows a modification of the wind flow above and around the city of Basel. Using BEP allows aLMo to reproduce a UHI, however slightly weaker than the measurements. The UHI is not limited to the city but extends up to 20 km around it. Moreover, a two week simulation has been conducted in order to demonstrate the capacity of BEP to be used for long term computations.

This study shows that the traditional surface scheme used in the operational numerical weather prediction model of MeteoSwiss is not adapted for urban areas and that it can be improved by BEP. The BEP module is able to reproduce the main behavior of the urban boundary layer and hence offers a real enhancement potential for aLMo.

4.1 INTRODUCTION

Meteorological information has become more and more important in our society, as many activities and life being are largely influenced by the weather. For example, air and maritime transport security, air quality control, global change study, natural disaster forecast, water resources management or simply freetime activities require meteorological forecast and/or analysis. Our capacity to forecast the weather has hence became a great issue. Today half of the worlds' population lives in urban areas, where a wide variety of human activities takes place. Meteorological forecast needs are very important for urban area even if it represents only 0.05 % of the Earth's surface.

In order to answer at best to these needs, the numerical forecast models are used. The quality of the information delivered by such models are strongly dependent on their resolution. During the last decade, computers performances have strongly increased, making it possible to constantly improve the model resolution. Being able to take into account finer scale and hence smaller geomorphological features, we could expect an improvement of the model results accuracy. However, results are only improved when different parametrizations, which take into account subgrid effects and the Earth's surface representation (landuse), are regularly updated to fit with the increasing resolution.

Concerning the Earth's surface fluxes exchanged with the atmosphere, increase of the model resolution have led to the adaptation of surface exchange parametrizations to take into account urbanized areas reproduced in mesoscale models by high resolution landuse database.

Different solutions are available in order to parametrize the urban area in weather forecast models. The most common is based on the Monin-Obukhov Similarity Theory (MOST), which assumes that a stable surface layer develops above the ground and where turbulence is constant in time and space. A more sophisticated

solution is to use Urban Canopy Models (UCM), where the surface fluxes are solved by taking into account buildings, different surfaces of city (roof, road and wall) and their interactions with the atmosphere (Martilli et al., 2002; Masson, 2000).
In this study, we investigate the capacity of two parametrization (a MOST based scheme and an UCM) to reproduce the urban area effects in a Numerical Weather Prediction (NWP) model. We focus on the Urban Heat Island (UHI) which is a typically phenomenon for urban areas and relatively easy to measure and quantify. For this purpose, the model of the Swiss Federal Office of Meteorology and Climatology (MeteoSwiss) is used. This mesoscale model called Local Model (LM) uses a traditional urban area parametrization (dry soil and adapted surface roughness) based on MOST. It is used for operational numerical weather prediction since 2001 with a horizontal resolution of 7 km on a domain covering most of western Europe.
In order to see if LM is able to reproduce the urban effect, it is applied to the City of Basel, a mid-size city situated in Switzerland, where an extensive meteorological measurement campaign has been conducted in the city of Basel under the BUBBLE project (Basel UrBan Boundary Layer Experiment) (Rotach et al., 2005) from summer 2001 to summer 2002. This experiment investigates in detail the boundary layer structure over a city. Different modeling studies have been conducted in relation with this experiment (Roulet, 2004; Hamdi, 2005), but none of them with an operational model able to take into account numerous phenomenon, *i.e.* clouds, rain, snow, etc.
In this chapter, the ability of LM to reproduce urban effects, and more particularly the UHI, is evaluated using BUBBLE measurement data as reference, first with the operational configuration of the model, and then with a finer horizontal and vertical resolution.
In a second step, we focus on an urban canopy model developed by Martilli et al.

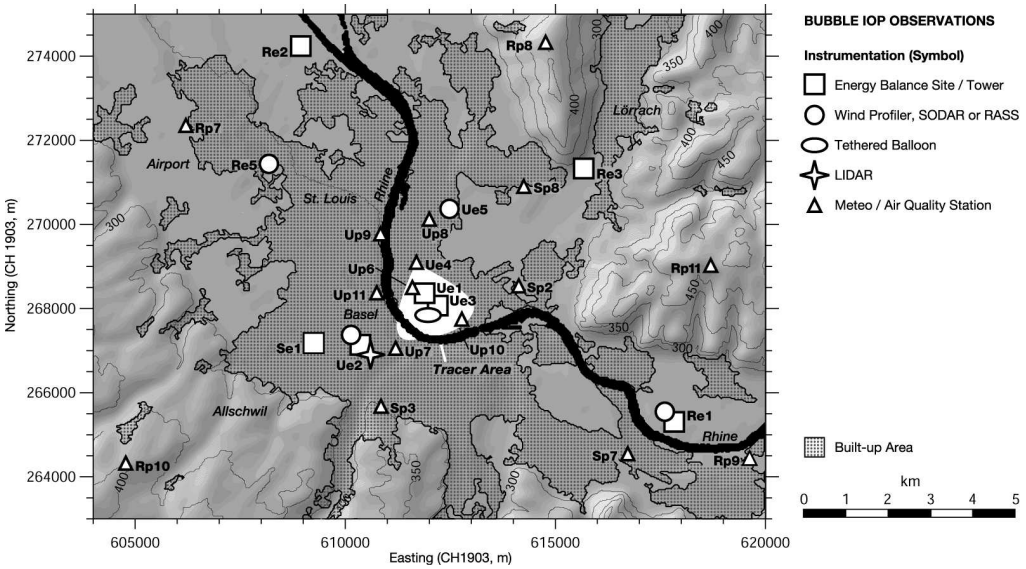

Figure 4.1: Map of the greater area of the city of Basel with an overview of all sites operated during the BUBBLE IOP in June/July 2002. The thick black line denotes the river Rhine. A complete list of the measuring stations can be found in Appendix .1

(2002). This Urban Effects Parametrization (BEP) is presented and implemented into LM. This implementation and its ability to reproduce the urban effects in LM for the case of Basel city are then evaluated and discussed.

4.2 BUBBLE

4.2.1 THE EXPERIMENT

The City of Basel is located in the North-Western part of Switzerland and borders both France and Germany. It is the Switzerland's third most populous city with 190,000 inhabitants. It is situated on the Rhine river, at an altitude of about 260 m and surrounded by gentle but non-negligible topography (750m).

The Basel UrBan Boundary Layer Experiment (BUBBLE) took place from Au-

gust 2001 to July 2002. Its main goal is to study boundary-layer and surface-exchange processes over different types of surfaces (*i.e.* urban, sub-urban and rural) and their role in the transport and diffusion of air pollution. A more complete description of BUBBLE can be found in Rotach et al. (2005) and on the BUBBLE website.

For that purpose, two meteorological towers for turbulence measurements, a Lidar and wind profiler were operated. An Intensive Observation Period (IOP) took place from 15 June and 12 July 2002, with additional surface towers, sodars and tethered balloons (Fig. 4.1).

4.2.2 MEASUREMENTS OF THE UHI

In contrast to rural area, a city represents a dry surface with obstacle (buildings) and a source of anthropogenic heat. The urban area modifies the energy budget, thus creating meteorological differences between urban and rural area. These dissimilarities can be formulated as the differences between urban and rural air temperatures, the first one being usually higher. This phenomenon is called the Urban Heat Island (UHI). As a UHI indicator, averaged and height corrected surface temperature observations within the city are compared with measurements from surroundings rural areas.

The BUBBLE campaign provide temperature measurements at 2 m height on several representative sites for urban or rural conditions. Averaging temperature in both areas (urban and rural) allow to obtain a temperature difference between the city and its surroundings, which can be assimilated to the UHI.

Figure 4.2 shows this averaged temperature difference between urban and rural area measured during the IOP. It is always positive and varies from 0.7 to 6.9 °C with an average of 2.8 °C. If we look at the weather bulletin (Appendix .2)

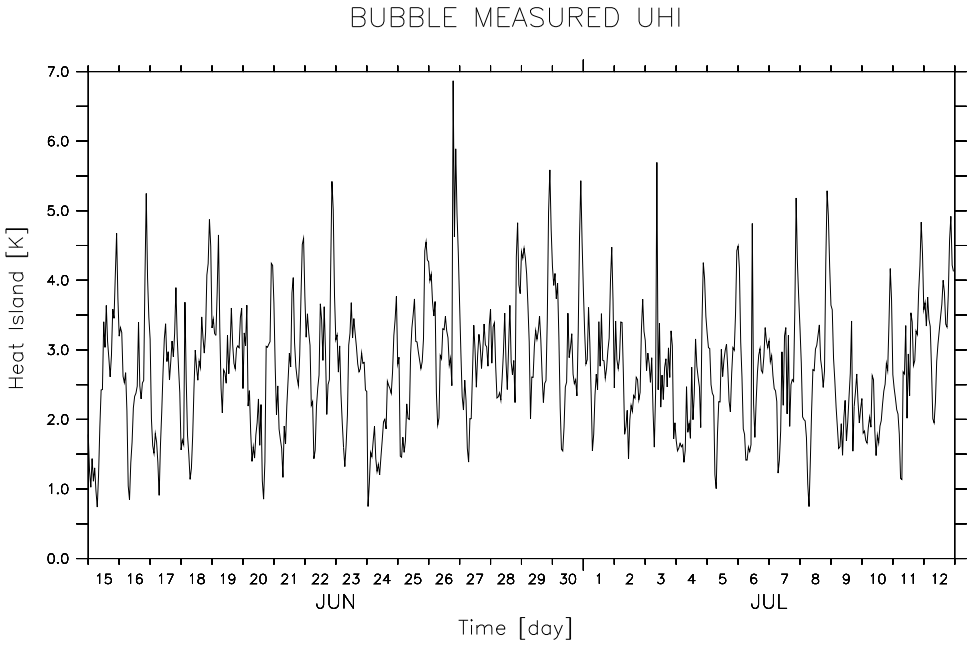

Figure 4.2: The UHI measured for the city of Basel at 2mAGL during the BUBBLE IOP in June/July 2002

during the IOP, the period from 25 to 27 June is characterized by a very constant meteorological situation and strong daily cycle. The mean UHI over this episode is representative for the IOP with an average of 3.0 °C. This episode is used to study UHI formation over Basel. Furthermore, it corresponds to the period studied by Roulet (2004).

In the following, an in-depth analysis of this UHI episode using measurements and numerical simulations is presented.

4.3 LM

4.3.1 MODEL DESCRIPTION

The LM (Lokal-Modell[1]) is developed within the framework of the COnsortium for Small-Scale MOdeling (COSMO) bringing together the National Weather Services from Switzerland, Italy, Poland and Greece under the lead of the National Weather Service of Germany (DWD). LM is a nonhydrostatic fully compressible limited-area atmospheric model. It has been designed for both operational Numerical Weather Prediction (NWP) and various scientific applications on the meso-β and meso-γ scales (scales from which the nonhydrostatic effects begin to play an important role on the behavior of the atmospheric fluxes (Orlanski, 1975). The LM prognostic variables are horizontal and vertical cartesian wind components, temperature, pressure perturbations, specific humidity, as well as different cloud water species and turbulence quantities according to the parametrizations chosen for the phenomena. The model is based on the primitive thermo-hydrodynamical equations describing a compressible flow in a moist atmosphere. The model equations are formulated horizontally in rotated geographical coordinates (λ, ϕ) and vertically in a generalized terrain following height coordinate (ζ). These equations are solved numerically using finite difference methods in an Arakawa-C/Lorenz grid (Figure 4.3 shows a grid box volume). Constant increments $\Delta\lambda, \Delta\phi, \Delta\zeta$ are used to set up the computational grid and the domain is represented by a finite number of grid points (i, j, k). Each of these points is the center of a rectangular grid box volume $\Delta V = \Delta\lambda\Delta\phi\Delta\zeta$.

[1] A more detailed description of the LM can be found on the COSMO website.

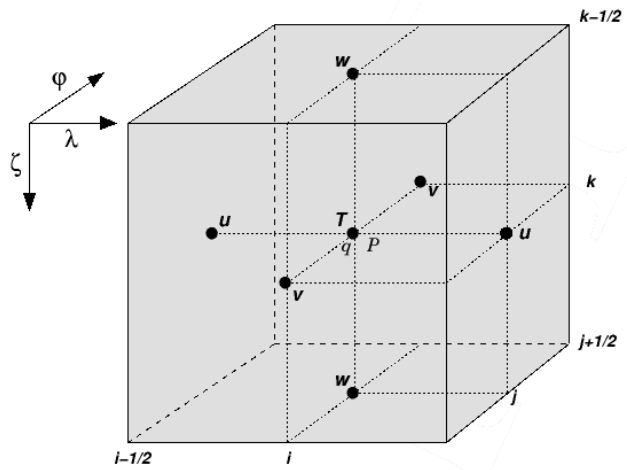

Figure 4.3: A grid box volume $\Delta V = \Delta\lambda\Delta\phi\Delta\zeta$ showing the *Arakawa-C/Lorenz* staggering of the dependent model variables. The scalar variables T, P and q are defined at the centre (i, j, k) of the box, whereas the normal velocity components are defined on the corresponding box faces $(i \pm 1/2, j \pm 1/2, k \pm 1/2)$.

NUMERICAL INTEGRATION

(a) THE TIME INTEGRATION SCHEME

To illustrate the integration used in LM, let consider the model equations in the generic form

$$\frac{\partial \psi}{\partial t} = s_\psi + f_\psi, \tag{4.1}$$

where ψ denotes a prognostic model variable (u, v, w, T, p' or q), f_ψ the forcing terms due to the slow modes and s_ψ the source terms related to the acoustic and gravity wave modes. Equation 4.1 is solved using a Kemp-Wilhelmson time-splitting algorithm, where terms related to the slow modes are solved using a large time step dt, whereas the acoustic and gravity waves modes are solved using a small time step $d\tau$. The slow-mode forcing f_ψ is evaluated only once every large time step and kept constant throughout the small time steps, whereas the fast-mode terms contained in s_ψ are calculated for each small time step.

We focus on the turbulent fluxes of heat and momentum which are contained in the slow mode term f_ψ. Horizontal advection is treated explicitly and evaluated at mid-time level n, whereas diffusion evaluated at time level n would be unstable with respect to explicit *Leapfrog* integration scheme. Thus, the computational mixing terms are formulated following a simple forward scheme, *i.e.* they are evaluated at the time level $n-1$. Vertical advection and vertical turbulent diffusion are treated implicitly using the *Crank-Nicolson* scheme involving the time levels $n-1$ and $n+1$. This results in a vertically coupled set of equations, abbreviated by

$$\frac{\psi^{n+1}-\psi^{n-1}}{2\Delta t} = f_\psi^n = f_\psi(\psi^{n-1}, \psi^n, \psi^{n+1}) \tag{4.2}$$

Finally for the slow mode tendency $\tilde{\psi}^{n+1}$, evaluating the finite difference equations for u, v, w, T, $p^{'}$ and q from (4.2) enables to obtain a linear tridiagonal equations system, which may be written in the general form

$$A_k\tilde{\psi}_{k-1}^{n+1} + B_k\tilde{\psi}_k^{n+1} + C_k\tilde{\psi}_{k+1}^{n+1} = D_k(\psi^n, ...), \tag{4.3}$$

for variables defined on main levels by k ($k = 1, ..., N_\zeta$). Boundary conditions are included in the inhomogeneous term D_k. Thus, we end up with a tridiagonal matrix of dimension $(N_\zeta)\times(N_\zeta)$, which can be solved by Gaussian elimination in LM.[2]

(b) LAND-SURFACE SCHEME

The turbulent mixing terms for temperature, moisture variables and horizontal momentum (in both directions u and v) are related respectively to the turbulent fluxes of sensible heat ($\hat{H}^3$), moisture (F_q^3) and momentum (τ^{13} and τ^{23}) respec-

[2]The matrix diagonal terms A_k, B_k and C_k, as well as the D_k-term are derived in Doms et al. (2002a).

tively. These fluxes are defined at model half levels and at the horizontal position corresponding to the transported quantity. The calculation of the mixing terms requires boundary conditions for turbulent fluxes at the top ($\zeta = 1/2$) and at the bottom ($\zeta = N_\zeta + 1/2$) half level of the model , where N_ζ is the number of vertical levels. At the upper boundary, zero flux conditions are specified:

$$\begin{aligned} (\tau^{13})_{\zeta=1/2} = (\tau^{23})_{\zeta=1/2} &= 0, \\ (\hat{H}^3)_{\zeta=1/2} = (F_q^3)_{\zeta=1/2} &= 0 \end{aligned} \tag{4.4}$$

At the lower boundary, the turbulent fluxes are specified which a standard bulk-transfer scheme using a drag-law formulation [3]:

$$\begin{aligned} (\tau^{13})_{\zeta=N_\zeta+1/2} &= \tau^{13}_{sfc} = -\rho C_m^d |\vec{v}_h| u, \\ (\tau^{23})_{\zeta=N_\zeta+1/2} &= \tau^{23}_{sfc} = -\rho C_m^d |\vec{v}_h| v, \\ (\hat{H}^3)_{\zeta=N_\zeta+1/2} &= \hat{H}^3_{sfc} = -\rho C_h^d |\vec{v}_h| (\theta \pi_{sfc} - T_{sfc}), \\ (F^3_{q^v})_{\zeta=N_\zeta+1/2} &= (F^3_{q^v})_{sfc} = -\rho C_h^d |\vec{v}_h| (q^v - q^v_{sfc}), \end{aligned} \tag{4.5}$$

where u, v, θ and q^v are the horizontal velocity components, the potential temperature and the specific humidity at the lowest grid level above the surface ($\zeta = N_\zeta$). $|\vec{v}_h|$ is the absolute horizontal wind speed at the same level. C_m^d denotes the drag coefficient for momentum exchanges at the ground and C_h^d is the bulk-aerodynamical transfer coefficient for turbulent heat. The transfer coefficient for moisture is assumed to be equal to the one for heat in LM. The air density ρ is evaluated from the surface values for temperature, pressure and humidity. Temperature and specific humidity at the ground are either provided by the soil model or externally specified, whereas the surface pressure is determined by hydrostatic

[3] As described in the Part II of the LM documentation (Doms et al., 2002b).

extrapolation of the total pressure $p = p_0 + p'$ at the first layer above the ground. The transfer coefficients C_m^d and C_h^d are calculated diagnostically and derived from the Monin-Obukhov Similarity Theory (MOST). Similarity theories are empirical relationships for variables of interest when our knowledge of the governing physics is insufficient to derive laws based on first principles (Stull, 1988). MOST is a first order approximation usually applied to the surface layer and assumes constant fluxes. Thus, in order to apply MOST for surface fluxes parametrization, the lowest grid layer of the model must be within the constant-flux layer. Usually, the top of the surface layer in rural areas is in the range of 10m to 30m.

THE SOIL AND VEGETATION MODEL

Surface fluxes represent the lower boundary conditions for the atmospheric part of the model. Their calculation requires temperature and specific humidity as input in the first soil layer predicted by the soil model.

For land surfaces, the multi-layer soil model TERRA_LM (Doms et al., 2002b) provides surface temperature and specific humidity at the ground to the LM model. Most parameters of the soil model (heat capacity, water storage capacity, volume of voids, etc.) strongly depend on soil texture. Five different types are distinguished: sand, sandy loam, loam, loamy clay and clay. Three special soil types are considered additionally: ice, rock and peat. The ground temperature is calculated by the equation of heat conduction which is solved in an optimized two-layer model, to which a third layer called the climatological layer, characterized by constant temperature, is added.

The urban and built-up land are described as a loam-clay soil with specific parameters described in Table 4.1

The temperature at 2 m Above Ground Level (AGL) is computed diagnostically

Table 4.1: Characteristic parameters for urban and built up areas in TERRA_LM: z_0 is the surface roughness.

Land use class	z_0 [m]	root depth [m]	plant cover		leaf area index	
			Max	Min	Max [-]	Min [-]
urban and built up land	1.00	0.60	10%	5%	4.70	0.10

from the ground surface temperature and the temperature in the first model layer according to the land-surface scheme *i.e.*, the Monin-Obukhov Similarity Theory.

4.3.2 aLMo : The *aLpine Model*

Since April 2001, a nonhydrostatic mesoscale model, the aLpine Model (aLMo), is used at MeteoSwiss for operational Numerical Weather Prediction (NWP). It is the Swiss configuration of the COSMO model, LM. The current (fall 2006) Swiss version of the model has a horizontal resolution of about 7 km. The domain covers most of western Europe. A terrain following vertical coordinate system is used, with 45 vertical layers and about 50 to 100 m vertical resolution in the lowest 2 km of the atmosphere, and an upper level at a geopotential height of 20 hPa. The 2 mAGL temperature is computed according to MOST using the temperature of the first layer and the surface temperature in the model.

The operational run of aLMo at MeteoSwiss is performed twice daily, at 1:30 am and 1:30 pm GMT. Calculations are performed on a NEC-SX/5 supercomputer at the Swiss National Supercomputing Center (CSCS) in Manno (TI). A 72 hour forecast takes roughly 70 minutes real-time. Accurate initial conditions are generated with an additional assimilation system, using observations within the model

domain (*e.g.* wind profiler). Boundary conditions are taken from the global model of the European Center for Medium-Range Weather Forecasts (ECMWF) in Reading (UK).

A new version, called aLMo2, is currently being developed and tested at MeteoSwiss. It will use a horizontal grid-size of roughly 2 km, a more accurate vertical resolution and is planned to become operational at the beginning of 2008.

4.3.3 MODEL SETUP

For this study, the operational aLMo configuration is used, with a domain size limited to the Basel area. The computed domain centered on the city of Basel is 13 by 13 grid point for a total surface of 8281 km^2 with a 7 km horizontal resolution. The vertical resolution is 60 m for the lowest model layer. Boundary conditions are taken from the hourly analysis of aLMo computed by MeteoSwiss and are interpolated to our domain. The run lasts 72 hours and covers the 3 days described above, *i.e.* 25 to 27 June, 2002. The main model configuration parameters are summarized in Table 4.2.

4.4 aLMo VS. MEASUREMENTS

A general overview of the model performance for the selected episode is presented in this section. In general, the model shows good agreement with the observed meteorological conditions. As the model is driven using analysis for boundary conditions, this is to be expected. In the following, the computed surface fields over the target area, *i.e.* the city of Basel and its immediate rural surroundings, are analyzed and compared to observations.

The computed temperature is generally in good agreement with the measurements

Table 4.2: The main model input parameters are: nx and ny the number of urban grid point in each horizontal direction, ny the number of layer on the grid, dx and dy the horizontal grid resolution, dz_{ground} the lowest layer depth and dt the slow modes time step

The main model input parameters	
nx	13
ny	13
nz	45
dx dy	7 km
dz_{groud}	60 m
dt	12 min
episode	25 to 27 June 2002 (72h)

in rural area. Figure 4.4 shows the measured temperature averaged over several rural measuring sites (cf. map in Fig. 4.1) and the computed temperature averaged over the corresponding grid points. The computed maximum temperature at 2 mAGL in rural area occurs one hour earlier and is 0.5°C lower compared to the measurements for the first two days. During nighttime the simulated temperature fits very well to the measurements.

However simulated temperature in urban area are too low by 1.5 to 3.0 °C (Fig. 4.5).

The difference between the urban and rural temperature corresponds to the UHI. Figure 4.6 shows the measured and computed UHI over the city. The averaged computed UHI is 0.14 °C, hence showing no significant temperature difference between urban and rural areas. The temperature in the city is even regularly lower than the temperature in the rural area, particularly during nighttime.

As a conclusion, aLMo with the operational configuration is not able to reproduce the UHI and underestimates the magnitude of the urban-rural temperature difference. One possible reason is a too low horizontal and vertical resolution:

- With a 7 km **horizontal resolution**, the city of Basel fills only one grid

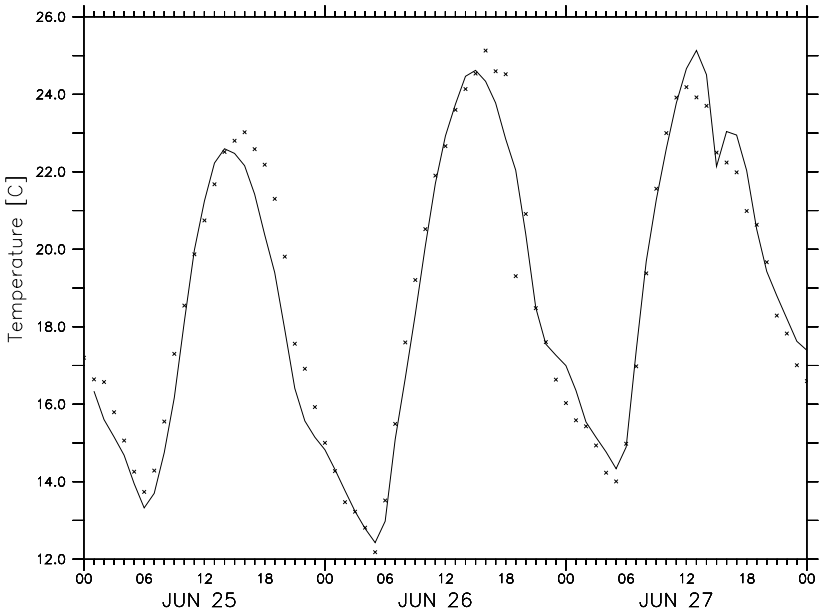

Figure 4.4: temperature at 2mAGL in rural areas for the period June 25 to 27, measured (crosses) and computed by aLMo (solid line) with the operational configuration.

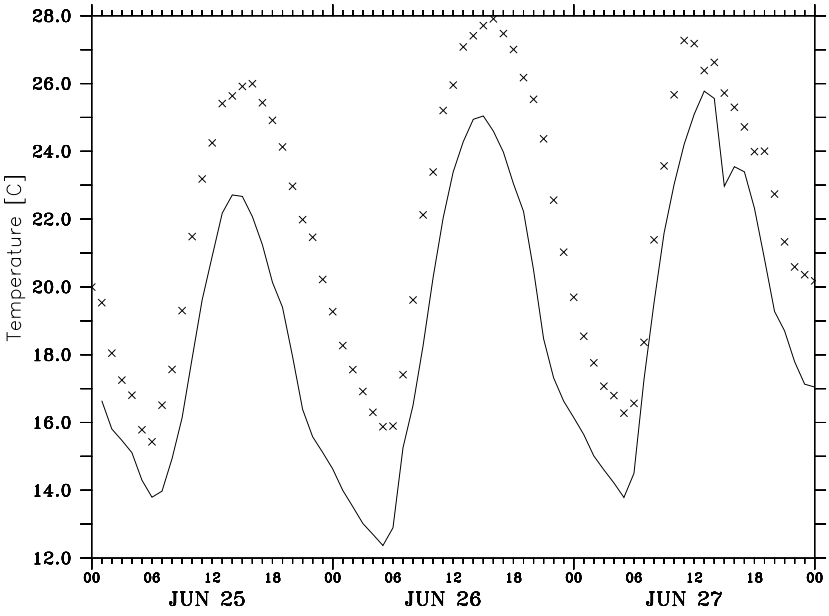

Figure 4.5: Temperature at 2mAGL in urban areas for a the period June 25 to 27, measured (crosses) and computed by aLMo (solid line) with the operational configuration.

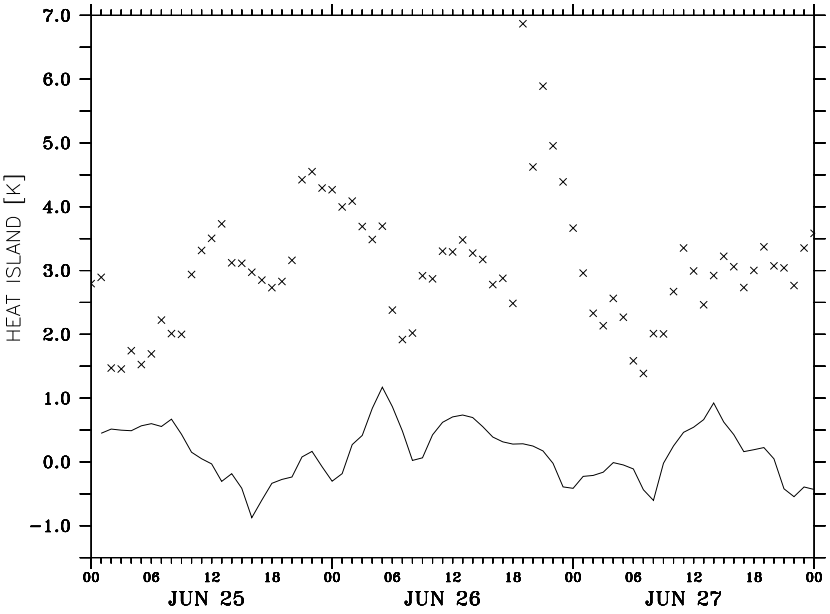

Figure 4.6: The Urban Heat Island (UHI) at 2mAGL for a three day period (June 25 to 27) measured (crosses) and computed by aLMo (solid line) with the operational configuration.

point; a finer horizontal resolution would allow to represent the city more accurately.

- The aLMo **vertical resolution** used is too low. An accurate representation of the boundary layer structure is of crucial importance in order to capture the physics leading to the UHI development.

4.4.1 INCREASING THE HORIZONTAL RESOLUTION

In order to investigate if the model is able to reproduce the UHI with an increased horizontal resolution, a simulation with the same model setup, and a finer horizontal grid spacing of 2.2 km is performed. This corresponds to the horizontal resolution of the aLMo2 configuration.

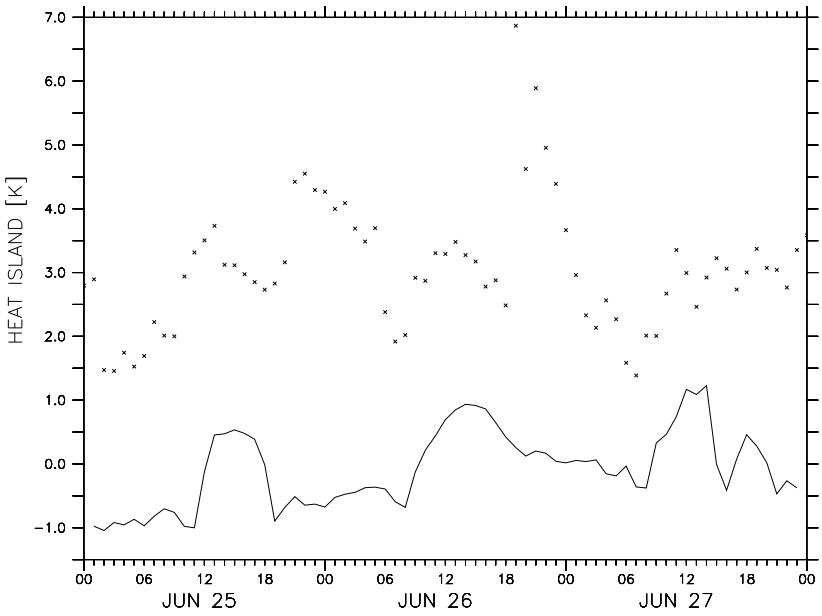

Figure 4.7: The Urban Heat Island (UHI) at 2m for a three day period (June 25 to 27) measured (crosses) and computed by aLMo (solid line) with an increasing horizontal resolution of 2.2 km.

As with the 7 km resolution, the 2 mAGL temperature in rural area is in good agreement with the measurements (not shown). For urban areas, the temperature is still too low and the UHI is not reproduced (Fig. 4.7). The average UHI is with 0.1 °C even lower than with a 7 km horizontal resolution.

In this case, increasing the horizontal resolution of aLMo has no positive influence on the UHI simulation.

4.4.2 INCREASING THE VERTICAL RESOLUTION

In this section, the vertical resolution is increased, applying heights of 20, 26 and 31 m respectively to the first three model layers. The horizontal resolution is kept at 2.2 km, this configuration corresponding to the model setups of aLMo2.

As for the simulations with a lower vertical and horizontal resolution, aLMo is not

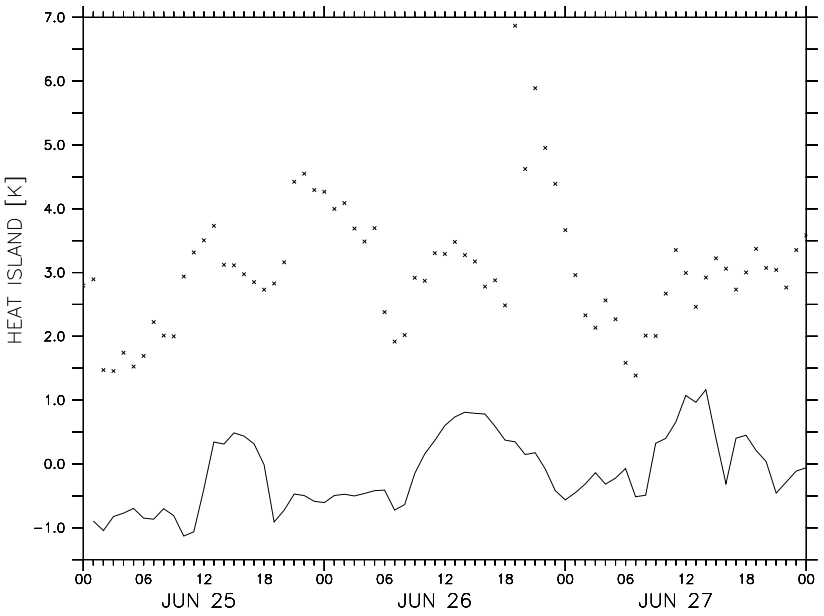

Figure 4.8: Urban Heat Island (UHI) at 2mAGL for 25 to 27 June, measured (crosses) and computed by aLMo (solid line) with the aLMo2 configuration.

able to reproduce an UHI (Fig. 4.8). As a conclusion, the ground surface temperature computed by the soil model TERRA_LM and use of the MOST land-surface scheme does not allow to take into account the modifications of the Planetary Boundary Layer (PBL) flow fields induced by the presence of a city. The street canyon geometry reduces sky view factor and wind speed and increases surface area and multiple reflection. Moreover, buildings characteristics modify the energy budget in the city. These factors affect the exchange surfaces-atmosphere from sensible heat and trapping radiation, and cannot be neglected (Oke, 1987). It is necessary to use an adapted parametrization in order to take into account the presence and the effect of a city in the model. For that purpose, the Building Effects Parametrization (BEP), developed by Martilli et al. (2002) is implemented into the aLMo model.

4.5 BEP : *Building Effects Parametrization*

Results from the last section indicate that there is a clear need to better represent the physical processes of typical urban environments in order to improve the representation of these regions in mesoscale models. In this study we will use the parametrization developed by Martilli (2001) called the Building Effects Parametrization (BEP). It has initially been developed for the mesoscale model FVM and tested extensively on several situation (Martilli, 2002; Roulet et al., 2005) and applied to different cities (Athens (Martilli et al., 2003), Basel (Roulet, 2004), Bogota (Zárate et al., 2006) and Mexico (present work)).

This section contains a description of BEP. The next two sections present the implementation of BEP in aLMo and the tests over the city of Basel.

BEP takes into account the main characteristics of the urban environment: *(i)* vertical and horizontal surfaces (wall, canyon floor and roofs), *(ii)* shadowing and radiative trapping effects of the buildings, *(iii)* anthropogenic heat fluxes through the buildings wall and roof. In this parametrization the city is represented as a combination of several urban classes. Each class is characterized by an array of buildings (Fig. 4.9) of the same width B located at the same distance from each other W (canyon width), but with different heights (with a probability $\gamma(z)$ to have a building with height z and a density function $\Gamma(z)$ of buildings with height z or higher). To simplify the formulation we assume that the length of the street canyons is equal to the horizontal grid size.

BEP computes urban effects on its own grid. The horizontal resolution is identical to the resolution of the mesoscale grid, while the vertical resolution is generally finer than the mesoscale resolution, and is usually set to 5 meters. Vertically the BEP grid extends up to one layer above the highest buildings.

In this parametrization, the fluxes contributions of every urban surface type (canyon floor, roofs and walls) on the momentum, heat and turbulent kinetic energy (E)

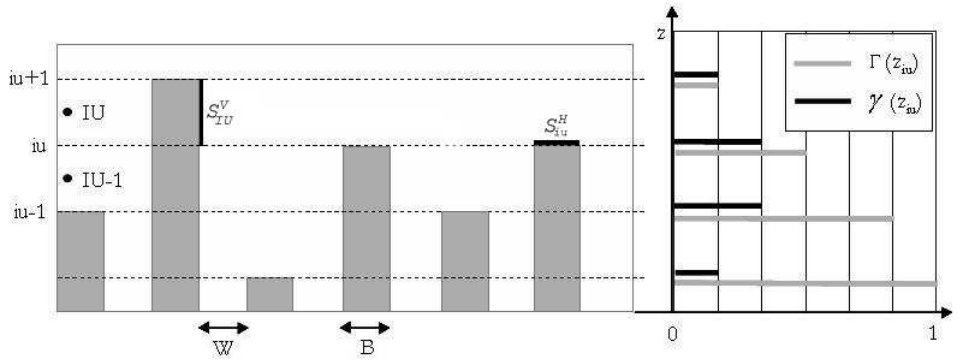

Figure 4.9: Schematic representation of the city in the urban grid of BEP and the buildings vertical distribution of density $\Gamma(z)$ and probability $\gamma(z)$ (Martilli, 2001).

equations are computed separately.

Firstly, the contributions of the horizontal surfaces (canyon floor and roofs) are calculated using the formulation of Louis (1979) based on MOST. The roughness lengths used for this calculation are representative for the local roughness of the specific surface types (roofs or canyon floor).

Secondly, the exchange of momentum and E on the vertical surfaces (walls) are parametrized as the effect of pressure and drag forces induced by the buildings. The temperature fluxes from the walls are a function of the difference between air and wall temperature. They are parametrized using the formulation of Clark (1985) proposed by Arnfield and Grimmond (1998) in their urban energy budget model. The energy budget is computed for every mentioned surface (canyon floor, roofs and walls). Firstly, the direct and infrared radiation at the surfaces are calculated to take into account the shadowing and radiative trapping effects of the buildings. Then, the surface temperatures for roofs, walls and canyon floor are solved by heat diffusion equation in several layers within the material (concrete or asphalt). After their calculation in the urban grid, the fluxes are vertically interpolated into the mesoscale grid.

We will now consider the input parameters that are needed by BEP for each urban class:

Thermal parameters The material thermal diffusivity K_s $[m^2 s^{-1}]$ and specific heat C_s $[Jm^{-3}K^{-1}]$ for each urban surface (roof, canyon floor and wall), as well as building inside temperature T_{int} $[K]$.

Radiation parameters The surface albedo α and emissivity ε for each urban surface (roof, canyon floor and wall).

Roughness parameter The roughness length z_0 $[m]$ for the horizontal surfaces (roof and canyon floor).

Geometrical parameters The street direction, length and width, the buildings height and width, as well as the probability $\gamma(h)$ to have buildings of height h.

Meteorological variables The wind components (u and v), temperature and solar radiation (angle and intensity) from the mesoscale models.

Urban fraction parameter $u_{fraction}(i, j, iurb) \in [0 : 1]$ gives the urban fraction in each cell covering the city.

BEP is then able to compute new surface temperature, momentum, heat and E fluxes for each layer of the mesoscale grid influenced by the city.

4.5.1 TEMPERATURE at 2 mAGL

The temperatures available for model validation are generally measured at 2 m above the ground. So the model needs to compute the temperature at this height. In aLMo, it is computed as a prognostic variable using MOST, which is based on

constant-flux layer approximation in the surface layer. Rotach (1993a,b) shows that the turbulent fluxes are not constant with height in the urban roughness sublayer (1-3 time mean building height) and that similarity theory cannot therefore be applied.

As BEP takes into account the presence of a city, its computed fluxes can be used to specify the temperature at 2 m height. For that purpose modifications are implemented in BEP, that will allow to compute diagnostic variables (typically 2 m temperature, 10 m wind) consistent with the land-surface scheme assumptions.

The temperature at 2 mAGL corresponds to the temperature simulated in the urban grid, in so far as the first layer near the ground remains thin enough for being considered as the temperature at 2 m. The energy budget equations for sensible heat, momentum and turbulent kinetic are hence solved in the urban grid.

With low horizontal resolution (here 2 km) compared to the high vertical resolution (5 m), vertical fluxes dominate the horizontal fluxes and represent the main source term in the energy budget equation. Therefore the horizontal fluxes can be neglected as shown by Masson et al. (2002) with measurements. The vertical turbulent exchanges balance the fluxes coming from the buildings and the ground, thus the equations for sensible heat, momentum and turbulent kinetic energy are parametrized for each layer in the urban grid as follows:

$$\frac{\partial}{\partial z}\left(K_z \frac{\partial \theta}{\partial z}\right) = a_\theta \theta + b_\theta \tag{4.6}$$

$$\frac{\partial}{\partial z}\left(K_z \frac{\partial U_i}{\partial z}\right) = a_{U_i} U_i + b_{U_i} \tag{4.7}$$

$$\frac{\partial}{\partial z}\left(K_z\frac{\partial E}{\partial z}\right) = a_E E + b_E + \rho K_z\left[\left(\frac{\partial U_x}{\partial z}\right)^2 + \left(\frac{\partial U_y}{\partial z}\right)^2\right] - \frac{g}{\theta_0}\rho K_z\frac{\partial \theta}{\partial z} - \rho C_\varepsilon\frac{E^{3/2}}{l_\varepsilon} \tag{4.8}$$

Equations 4.6 and 4.7 parametrize respectively the temperature θ and the wind speed U_i for each direction in accordance with Pielke (1984). a_ψ and b_ψ are the flux source terms computed by BEP and K_z $[\frac{m^2}{s}]$ are the vertical diffusion coefficients. Equation 4.8 is the prognostic equation for the turbulent kinetic energy E $[\frac{m^2}{s^2}]$ according to Bougeault and Lacarrere (1989) with a $k-l$ closure. In this equation, $\rho K_z\left[\left(\frac{\partial U_x}{\partial z}\right)^2 + \left(\frac{\partial U_y}{\partial z}\right)^2\right]$ and $\frac{g}{\theta_0}\rho K_z\frac{\partial \theta}{\partial z}$ are the production terms representing the shear and the buoyancy respectively. The $\rho C_\varepsilon\frac{E^{3/2}}{l_\varepsilon}$ term is the dissipation rate where l_ε is a characteristic length of the energy-containing eddies. l_k $[m]$ is a characteristic length for eddies determined as the minimum between street width and height where l_k is computed. C_ε is a numerical coefficient set to 0.71 (Bougeault and Lacarrere, 1989).

The system of 4 equations is characterized by 5 unknowns (θ ,U_x, U_y, E and K_z) for each layer of the urban grid. In order to close the system, K_z is defined as a function of E (Bougeault and Lacarrere, 1989) and is written:

$$K_z = C_k l_k E^{1/2}, \tag{4.9}$$

where C_k is a numerical coefficient set to 0.4 (Bougeault and Lacarrere, 1989).

In BEP, this system is solved by iteration once the flux source terms a_ψ and b_ψ are computed. Firstly E is estimated for computing K_z according to equation 4.9. Then temperature and wind speed are computed with equations 4.6 and 4.7, and E can be computed with (4.8). A new K_z is then calculated using the new E

value, and iterations are made until E converge. The energy profile in the urban grid is used to initialize K_z for the next time step.

It is necessary to determine the upper-boundary conditions in the urban grid. For wind, they are directly given by the mesoscale models at the height of the urban grid top.

For E and temperature at the top of the urban grid (above the buildings), it is assumed that a surface layer is developing above the roughness layer (Roth, 2000), which is virtually starting from the zero-plane displacement (Oke, 1987) situated in the roughness layer (Fig. 4.10). In the surface layer, the vertical turbulent fluxes of momentum and heat are assumed to remain constant (Seinfeld and Pandis, 1998). In this case, only the production (shear and buoyancy) and the dissipation terms remain in the prognostic equation for E, *i.e.*

$$\rho C_\varepsilon \frac{E^{3/2}}{l_\varepsilon} = \rho K_z \left[\left(\frac{\partial U_x}{\partial z} \right)^2 + \left(\frac{\partial_U y}{\partial z} \right)^2 \right] - \frac{g}{\theta_0} \rho K_z \frac{\partial \theta}{\partial z} \tag{4.10}$$

In accordance with the assumed surface layer properties, shear is defined as:

$$\rho \frac{U_*^3}{\kappa(z - z_d)} \phi, \tag{4.11}$$

Where κ is the von Karman constant set to 0.40, under neutral conditions and ϕ is equal to 1 (Businger et al., 1971). U_* is the friction velocity and z_d, the zero-plan displacement, is defined as $0.67 * \textit{building height}$ (Grimmond and Oke, 1999).

The buoyancy in the surface layer is defined as:

$$\frac{g}{\theta_0} \rho U_* \theta_* \tag{4.12}$$

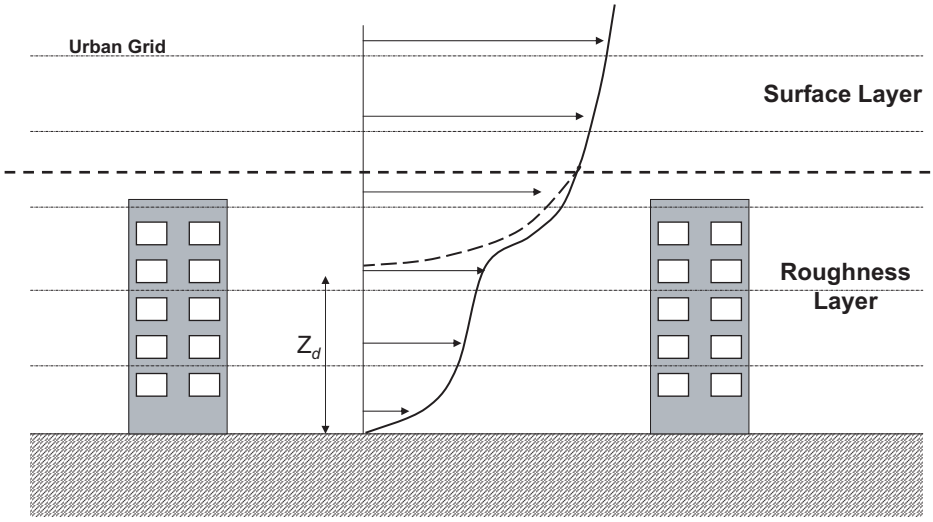

Figure 4.10: Schematic representation of a wind profile in the roughness layer and in the surface layer. It assumes that a surface layer has developed above the urban canopy and virtually starts at the zero plane displacement height Z_d.

Where θ_* is a potential temperature scale. U_*^2 is the total momentum flux and $U_*\theta_*$ the total heat flux:

$$U_*^2 = \sqrt{(A_{u_x}U_x + B_{u_x})^2 + (A_{u_y}U_y + B_{u_y})^2} \tag{4.13}$$

$$U_*\theta_* = A_\theta\theta + B_\theta \tag{4.14}$$

Where A_ψ and B_ψ represent the total source term in the urban grid.

Based on (4.10) and using equations 4.11 to 4.14, E at the top of the urban grid is estimated as:

$$E_{top} = \left[\frac{1}{C_\varepsilon}\left(\frac{U_*^3}{\kappa} - \frac{g(z-z_d)}{\theta_0}U_*\theta_*\right)\right]^{2/3} \tag{4.15}$$

The upper-boundary condition for temperature is parametrized with a logarithmic

profile (Pielke, 1984),

$$\theta_* = \frac{\kappa(\theta_z - \theta z_d)}{0.74[\ln(z/z_0) - \psi_H(z/L)]} \tag{4.16}$$

As explained before, the flux θ_* remains constant within the neutral surface layer. A further assumption is to neglect perturbation terms $\psi_H(z/L)$. Temperature $\theta_{z_{top}}$ at the top of the urban grid (z_{top}) can then be expressed as a function of the temperature at the first mesoscale model layer above the urban grid $\theta_{z_{meso}}$:

$$\theta_{z_{top}} = \theta_{z_{meso}} - 0.74\frac{\theta_*}{\kappa}\ln\left(\frac{z_{top} - z_d}{z_{meso} - z_d}\right) \tag{4.17}$$

The temperature at the urban grid top, $\theta_{z_{top}}$, is linked both to the mesoscale model, by the value above the urban grid $\theta_{z_{meso}}$ and to the urban parametrization, by the potential temperature scale θ_*.
This method also solves wind speed and turbulent kinetic energy in the urban grid.

4.6 IMPLEMENTATION OF BEP IN aLMo

BEP outputs consist of a ground surface temperature and of momentum and heat fluxes profiles calculated over the entire height of the urban grid. In the original version of aLMo, surfaces fluxes are implicitly calculated by the soil module, using the formulations given in equation 4.5. In the modified version, BEP is implemented in aLMo and runs after the soil module. In the following, two implementation methods are presented.

4.6.1 FIRST METHOD

The first method is based on the re-computation of the transfer coefficients C_m^d and C_h^d in order to impose surface variable tendencies corresponding to the ones computed in BEP. It is then necessary to find a formulation for the coefficients depending on the tendencies calculated by BEP, (*i.e.* u_{flux}, v_{flux} and t_{flux}). Beginning with the first two equations of system (4.5):

$$(\tau^{13})_{\zeta=N_\zeta+1/2} = \tau^{13}_{sfc} = -\rho C_m^d |\vec{v}_h| u = -\rho C_m^d \sqrt{u^2+v^2}\, u, \tag{4.18}$$

$$(\tau^{23})_{\zeta=N_\zeta+1/2} = \tau^{23}_{sfc} = -\rho C_m^d |\vec{v}_h| v = -\rho C_m^d \sqrt{u^2+v^2}\, v, \tag{4.19}$$

and introducing two new coefficients $C^d_{m,u}$ and $C^d_{m,v}$ to take into account both wind directions u and v:

$$\tau^{13}_{sfc} = -\rho C^d_{m,u} \sqrt{u^2+v^2}\, u, \tag{4.20}$$

$$\tau^{23}_{sfc} = -\rho C^d_{m,v} \sqrt{u^2+v^2}\, v, \tag{4.21}$$

with units $[\frac{kg}{ms^2}]$.

BEP module gives the tendencies u_{flux} and v_{flux} with units $[\frac{m}{s^2}]$, coming from wind speed temporal derivative, *i.e.* $\frac{\partial}{\partial t}[\frac{m}{s}]$. Thus, it is possible to find a relation between the tendencies of BEP and the surface fluxes of aLMo. In the following, this relation is derivated for the u-direction:

$$\tau^{13} = \Delta z \rho u_{flux}, \tag{4.22}$$

where Δz is the height of the first mesoscale layer and ρ is the density. Replacing τ^{13} by (4.20) and simplifying the density terms, we have:

$$-C^d_{m,u}\sqrt{u^2+v^2}u = \Delta z u_{flux}, \tag{4.23}$$

Finally, resolving for $C^d_{m,u}$ and similarly for the v-direction, we obtain the equations linking the momentum transfer coefficients with the fluxes within BEP:

$$C^d_{m,u,BEP} = -\Delta z \frac{u_{flux}}{u\sqrt{u^2+v^2}}, \tag{4.24}$$

$$C^d_{m,v,BEP} = -\Delta z \frac{v_{flux}}{v\sqrt{u^2+v^2}}, \tag{4.25}$$

Following a similar approach, we can find a relation between the transfer coefficient C^d_h and the heat flux tendency t_{flux}, with units $[\frac{K}{s}]$. The third equation of (4.5) becomes:

$$\begin{aligned}(\hat{H}^3)_{\zeta=N_\zeta+1/2} = \hat{H}^3_{sfc} &= -\rho C^d_h|\vec{v}_h|(\theta\pi_{sfc} - T_{sfc}) \\ &= \rho C^d_h\sqrt{u^2+v^2}(T_{sfc} - T_{\zeta=N_\zeta}),\end{aligned} \tag{4.26}$$

with units $[\frac{kgK}{sm^2}]$. We have then to divide $\hat{H}^3_{sfc}$ by a density term ρ and a length term Δz to obtain $[\frac{K}{s}]$. Thus:

$$t_{flux} = \frac{\hat{H}^3_{sfc}}{\rho\Delta z} = \frac{\rho C^d_h\sqrt{u^2+v^2}(T_{sfc} - T_{\zeta=N_\zeta})}{\rho\Delta z}, \tag{4.27}$$

Again, simplifying the density terms and resolving for C^d_h, lead to an expression

linking the transfer coefficient for sensible heat with the tendency given by BEP:

$$C^d_{h,BEP} = \Delta z \frac{t_{flux}}{\sqrt{u^2 + v^2}(T_{sfc} - T_{\zeta=N_\zeta})}, \tag{4.28}$$

These three coefficients calculated by BEP are then used to create the final coefficients for input into aLMo, following a linear combination between BEP's and aLMo's coefficients:

$$\begin{aligned} C^d_{m,i,final} &= u_{fraction} C^d_{m,i,BEP} + (1 - u_{fraction}) C^d_{m,LM}, \\ C^d_{h,sensible,final} &= u_{fraction} C^d_{h,BEP} + (1 - u_{fraction}) C^d_{h,LM}, \end{aligned} \tag{4.29}$$

where $i = u, v$ and $u_{fraction} \in [0 : 1]$ defines the urban fraction in a mesoscale cell and depends on the landuse type.

We have now to consider the fact that BEP consider urban areas as a set of totally dry surfaces. Thus, the module does not calculate any tendencies for latent heat fluxes. A final coefficient for the latent heat is nevertheless calculated, using the following combination:

$$C^d_{h,latent,final} = (1 - u_{fraction}) C^d_{h,LM}, \tag{4.30}$$

so that the moisture exchanges at the surface are characterized by the rural fraction $(1 - u_{fraction})$ affected to each urban cell.

As already mentioned, BEP also calculates a street surface temperature tgs_u. The module is defined with three soil layers, the deepest having a constant temperature. At time $t = t_0$, the constant temperature of aLMo is used to initialize the temperature in every soil layers of BEP. Then, the module calculate a thermal gradient over all layers at each time step and gives tgs_u. As for (4.29) and (4.30), the final ground surface temperature is calculated with a linear combination between tgs_u from BEP and t_s from aLMo:

$$t\_s_{final} = u_{fraction} tgs\_u + (1 - u_{fraction}) t\_s \tag{4.31}$$

This temperature finally replaces aLMo's ground surface temperature t_s at each time step.

The advantage of this implementation method of BEP into aLMo is that it requires no knowledge about the code solver and that the model code does not need to be modified. Nevertheless, it is not optimal for several reasons. With such an implementation, only the first mesoscale layer can be influenced by BEP. This means that it is not possible to consider buildings higher than the first mesoscale level. Moreover, terms 4.24, 4.25 and 4.28 show that for low wind speeds the recomputed exchange coefficient may numerically diverge. Thus, it is necessary to control and to limit the transfer coefficients for the low wind speed situations.
This implementation method has some limits. Therefore a second method to implement BEP and to take into account the source flux terms above the first layer of the mesoscale model is presented in the next section.

4.6.2 SECOND METHOD

The first method is more complex but does not modify the LM code. This second method is simpler and more powerful but modifications must be applied to the implicit LM solver.

To avoid the limitations of the first implementation method, a more direct method is presented that needs less modifications in BEP and LM code and acts on each vertical mesoscale layer influenced by urban areas. It relies on the use of tendencies ψ_{flux} and source terms a_ψ and b_ψ, where $\psi = u, v, t$.

BEP calculates the tendency u_{flux} using the source terms, as follows

$$u_{flux} = \rho\Delta z(a_u u + b_u), \tag{4.32}$$

This can be generalized by:

$$\psi_{flux} = \rho\Delta z(a_\psi \psi + b_\psi), \tag{4.33}$$

where a_ψ and b_ψ are the implicit and explicit source terms respectively and $\rho\Delta z$ a conversion factor from BEP's tendencies and aLMo's fluxes. Now, if we look at equation (4.33) in term of temporal derivative, we have:

$$\frac{\psi^{n+1} - \psi^n}{\Delta t} = \rho\Delta z(a_\psi \psi^{n+1} + b_\psi), \tag{4.34}$$

The step is now to implement the tendencies and the source terms in aLMo through equation (4.3) for k-level only, which means:

$$B_k \psi_k^{n+1} = D_k(\psi^n, ...), \tag{4.35}$$

Finally, if we take the implicit and explicit terms of (4.34) and (4.35), it is possible, by analogy, to connect BEP to aLMo through the source terms:

$$\begin{aligned} B_k &\longrightarrow B_k - a_\psi, \\ D_k &\longrightarrow D_k + b_\psi \end{aligned} \tag{4.36}$$

Two valuable methods to implement BEP in aLMo have been presented. The choice of the implementation method depends on the user's knowledge of the mesoscale code and on the possibility to modify it. With some adaptations, but keeping the same implementation philosophy, these two methods allow to implement BEP in numerous mesoscale models.
Having the possibility to change the implicit solver of LM, the second method is used in this study, which allows to take into account the urban source terms in each layer of the mesoscale grid influenced by the urban canopy.

4.7 SIMULATION OF THE BASEL UHI

4.7.1 MODEL SETUP

In this part, we keep the same simulation domain over Basel and its surroundings (cf. section 4.3.3) with the aLMo2 configuration *i.e.*, a 2.2 km horizontal resolution,

a first layer thickness of 20 m and a 3 day simulation period from June 25 to 27. The characteristics and the fraction of urban area in each cell is determined from the KABA data base (Fehrenbach, 1999). Two city categories are defined:

- *City center*: high density of buildings (15 m high), narrow street and 80% of urban area[4]. Represented by 7 grid points.

- *Sub-urban areas*: smaller density of small buildings (7 m high) and 60% of urban area. Represented by 17 grid points.

Figure 4.11 shows the simulated domain with cells considered as urban and sub-urban. The properties for both urban and sub-urban categories are determined according to KABA and Roulet (2004) and are presented in Appendix .3. For the cells containing urban area, the parameters of the rural part have been changed in order to represent park and green area. The main model input parameters are summarized in Table 4.3.

4.7.2 RESULTS

In this section, we compare results from the mesoscale model calculated both with and without BEP, and give a general overview of the model performance with BEP for the selected episode.

[4]It means that 80% of the area of the grid cell fluxes are computed by the urban parametrization (BEP) and the rest is handled by the traditional LM parametrization with values for rural area.

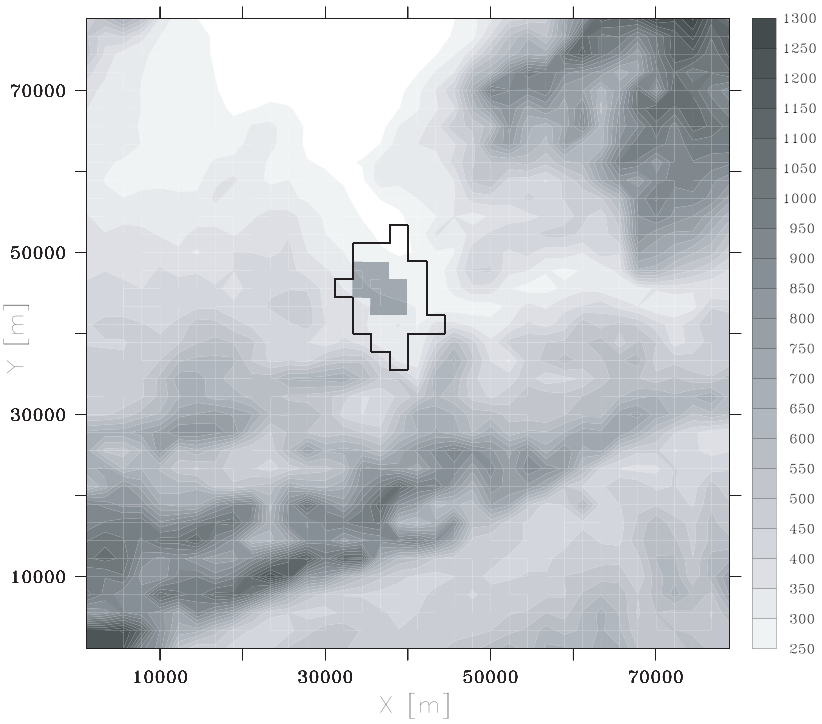

Figure 4.11: Topography [mASL] of the simulation domain (2.2 km horizontal resolution) over the city of Basel and the urban (gray squares) and sub-urban cells (black shape).

Table 4.3: The main model input parameters are: nx and ny the number of model grid points in each horizontal direction, nz the number of vertical layers, dx and dy the horizontal grid spacing, dz_{ground} the lowest layer depth and dt the slow modes time step

The main model input parameters	
nx	36
ny	36
nz	60
dx dy	2.2 km
dz_{groud}	20 m
dt	12 min
period	25 to 27 June 2002 (72h)

WIND

The wind pattern (Fig. 4.12 and Fig. 4.13) is very typical for Basel area with strong inflow from the Rhine valley in the North and going up along the slopes of the terrain. The comparison between simulations with and without BEP shows only slight differences in the wind fields. A small decrease of wind speed over the city is observed with BEP. The air flow simulated without BEP (Fig. 4.12) is not modified above the city. However, the simulation with BEP (Fig. 4.13) shows a divergence-convergence system around the city. The simulation shows a divergence and a decrease of the wind speed upstream the city due to drag effect of the buildings. The wind accelerates around the city. Wind speed decreases drastically downstream as a combined effects of drag force and buoyancy due to temperature increase in the city. A convergence is observed south of the city. BEP impacts the air flow up to 7 km upwind and downwind the urban area.
Looking hour by hour, we observe that the effect on wind flow increases with wind speed *i.e*, the impact of BEP increases with increasing wind speed.

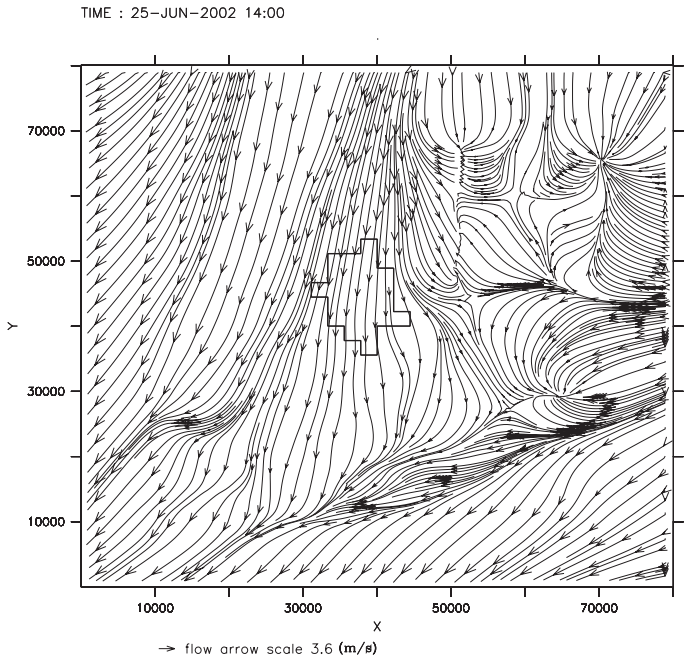

Figure 4.12: Simulated wind streamline (the size of the arrows indicates the wind speed strength) with aLMo, June 25 at 14LT in the first layer (20 meters height) above and around the city of Basel (black shape).

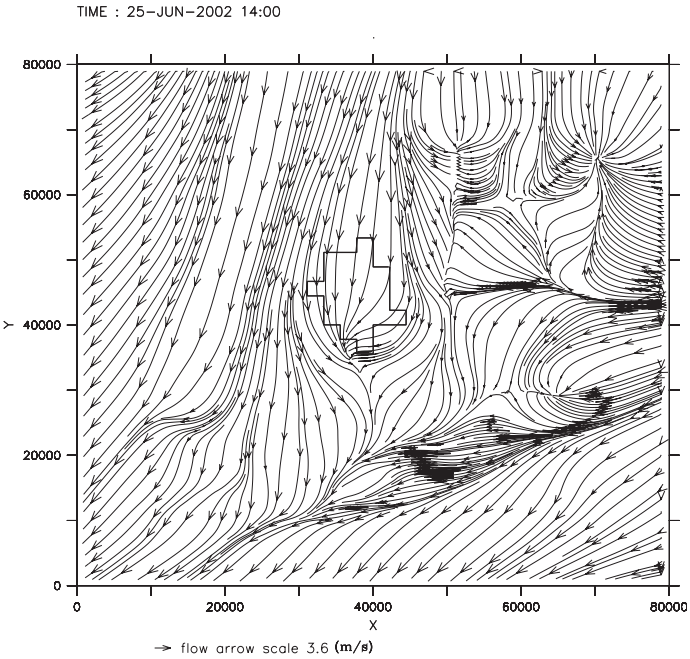

Figure 4.13: Simulated wind streamline with aLMo/BEP, June 25 at 14LT in the first layer (20 meters height) above and around the city of Basel (black shape).

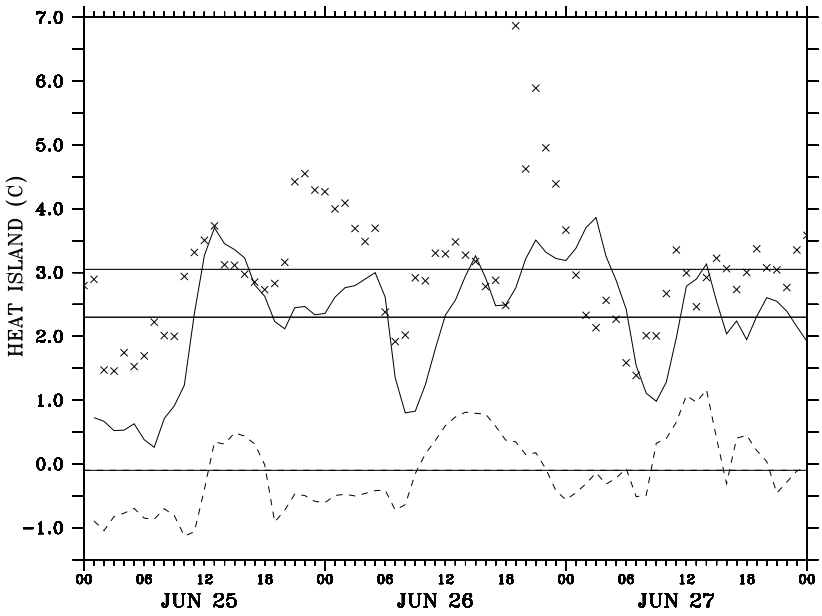

Figure 4.14: The Urban Heat Island (UHI) at 2m for a three day period (June 25 to 27) measured (crosses) and computed by aLMo with BEP (solid line) and without BEP (dashed line) with an horizontal resolution of 2.2 km

TEMPERATURE

The simulated temperature at 2 m shows warmer temperature in the urban area with BEP than without. The computed UHI (Fig. 4.14) is always stronger in the simulations with BEP by 0.7 to 4 °C.

The averaged UHI simulated with BEP reaches 2.3 °C, which is in agreement with the measurements (average UHI of 3 °C, Fig. 4.14). Furthermore, the simulated UHI is late by around 3 hours during the morning and too weak from 18LT to 00LT. We also observed a peak in the measurements at 18 LT on June 26 that the simulation is not able to reproduce. It is instructive to look at absolute temperature values and not differences in order to explain the observed inconsistencies.

Figure 4.15 shows that the city is warmer with BEP particularly during nighttime. The morning temperature increase simulated with BEP comes with a delay, which explains the phase shift of the UHI observed above. Even if the maximum

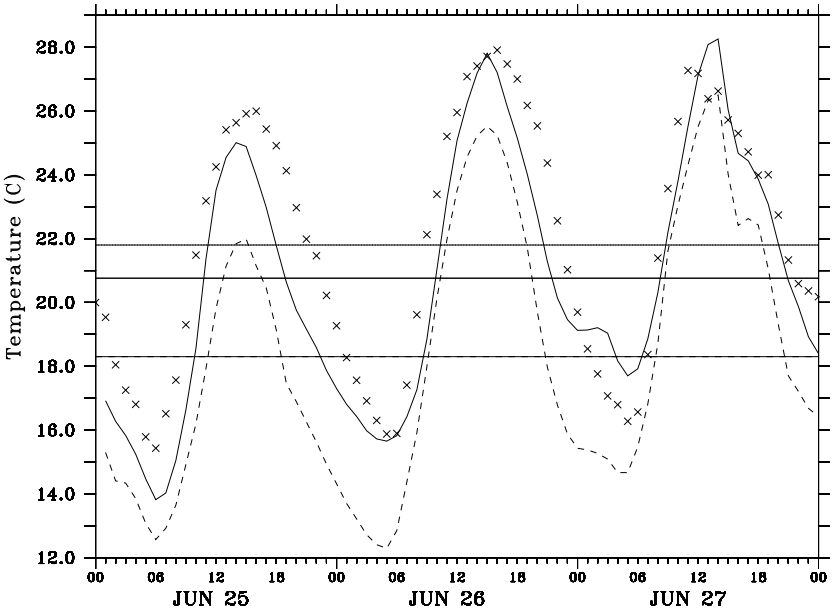

Figure 4.15: Average temperature at 2 m in the city of Basel, measured (crosses), simulated in aLMo without BEP (dashed line) and with BEP (solid line).

of temperature is too low the first day, it is generally well reproduced with the BEP simulation and the UHI during daytime is well reproduced. The temperature decrease in the afternoon and evening occurs earlier with BEP than in the measurements and a maximum difference between simulation and measurement is reached at sunset (20 LT). This explains the strong UHI anomaly at the end of the day and beginning of the night (cf. Fig. 4.14). The maximum of measured UHI reached at 18 LT on June 26 is not observed in the urban temperature. This maximum is due to a decrease of the temperature in the rural area (not shown).

Numerous tests have been conducted on the input parameters of BEP used to describe the city. Using typical values found in the literature (Oke, 1987; Masson et al., 2002; Dupont et al., 2004), the following parameters have been varied and sensitivity of the results studied:

- The *Thermal Parameters* of the materials, *i.e.* the thermal diffusivity and the specific heat for roof, wall and ground.
- The *Radiation Parameters* of the surfaces, *i.e.* the albedo and the emissivity of roof, wall and ground.
- The *Roughness Length* of horizontal surfaces (ground and roof).
- The *Geometrical Parameters* of the city, *i.e.* street direction and width, buildings height and width and their repartition.

An impact on the average and on the amplitude of the temperature curve is observed when these parameters are modified. However the shape of the curve is not modified, *i.e.* the morning increase temperature is always late and the temperature decreases too early in the afternoon. Furthermore, modifying the parameters in the range proposed by the literature produces weak impacts (not shown) on the temperature, of around 0.6 °C on the amplitude and 0.3 °C degrees on the average. The results presented above have been computed with the set of parameters that provide the best fit between simulation and measurements.
To summarize, the results show that a parametrization of heat and momentum fluxes over urban areas clearly improve mesoscale simulations using an horizontal resolution of 2.2 km. Results with BEP show a much better representation of the UHI as well as the general temperature evolution over an urban area such as Basel. Remaining differences between measured and simulated urban temperatures are dominated by a phase shift in the morning increase and evening decrease. This effect does not show any sensitivity to changes in BEP's input parameters. If measurements are considered representative of the urban environment, this gives an indication that the processes considered in BEP are not complete and some physical mechanisms determining the temperature are not well represented.

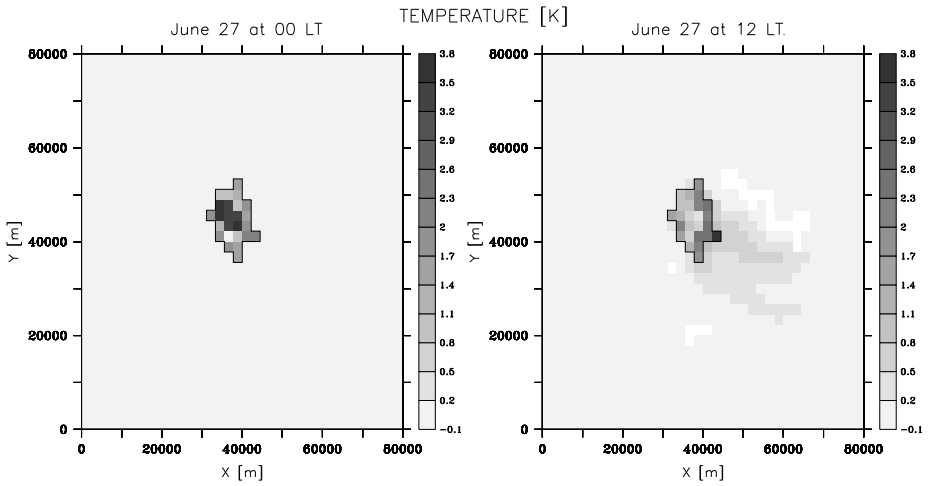

Figure 4.16: Temperature differences at 2 mAGL [°C] between an aLMo simulation with BEP and without BEP over the city of Basel (black shape) for 27 June, 2002 at midnight (left) and 27 June, 2002 at noon (right)

UHI DISPERSION

Figure 4.16 shows the difference of temperature at 2 mAGL between a simulation with and without BEP.

Two behaviors are observed:

- During nighttime (left panel of Figure 4.16), the simulation using BEP is clearly warmer above the city by 3.0 to 3.8 °C for the city center and by 1.5 to 2.0 °C for the sub-urban area. During this period, the wind is weak and temperature increase is observed only in the urban cells.

- During daytime (right panel of Figure 4.16), temperature increase above the city with BEP is weaker than during nighttime (1.5 to 2.5 °C in the city center), however a maximum of 3.4 °C is reached in the east- and southeast-part of the sub-urban area. The wind is stronger during daytime and blows to south east. It creates a displacement of the maximum and a temperature "plume" which is observed south-east of the city and reaches 0.5 to 1.0 °C.

In both situations BEP increases the temperature in the city. The intensity and diffusion of this temperature increase are strongly dependent on the wind speed, so that BEP modifies not only the urban area but also the nearby area, up to 20 km downwind in the presented case.

4.7.3 14 DAYS SIMULATION

Up to now, BEP has only been tested on 2 to 4 day episodes. The implementation of BEP in an operational forecast model gives the opportunity to test it for longer periods (weeks or months) and different kinds of meteorological situations (days with strong cloudiness and/or precipitation). In this section we present a 14 days simulation during the BUBBLE IOP from June 21 to July 4 2002.

Figure 4.17 shows the temperature simulated with aLMo/BEP in the urban area. No tendency being observed, BEP does not accumulate or lose heat during this 14 days period. Thus, BEP is able to compute the urban heat and momentum fluxes for longer period than 3 days.

The mean temperature reaches 21.1 °C for measurements, 20.3 °C for the simulation with BEP and 18.3 °C for the simulation without BEP (not shown). The mean temperature is well reproduced with BEP as well as the general temperature behavior. The same tendencies are observed than during the 3 day simulations, which showed a warmer city by 2.4 °C with BEP. During nighttime of 23, 27 and 30 June, BEP slightly overestimates the temperature. The average of the computed UHI (Fig. 4.18) is 1.6 °C whereas it is around 2.8 °C in the measurements. The difference between measurements and simulation for the UHI is larger than the difference in the urban area temperature because, in the average, aLMo overestimates the temperature in rural area by 0.4 °C.

If we focus on the temperature at 2 mAGL on June 24 when an important rainfall episode occurs form 01LT to 12 LT (Appendix .2), we observe that the simula-

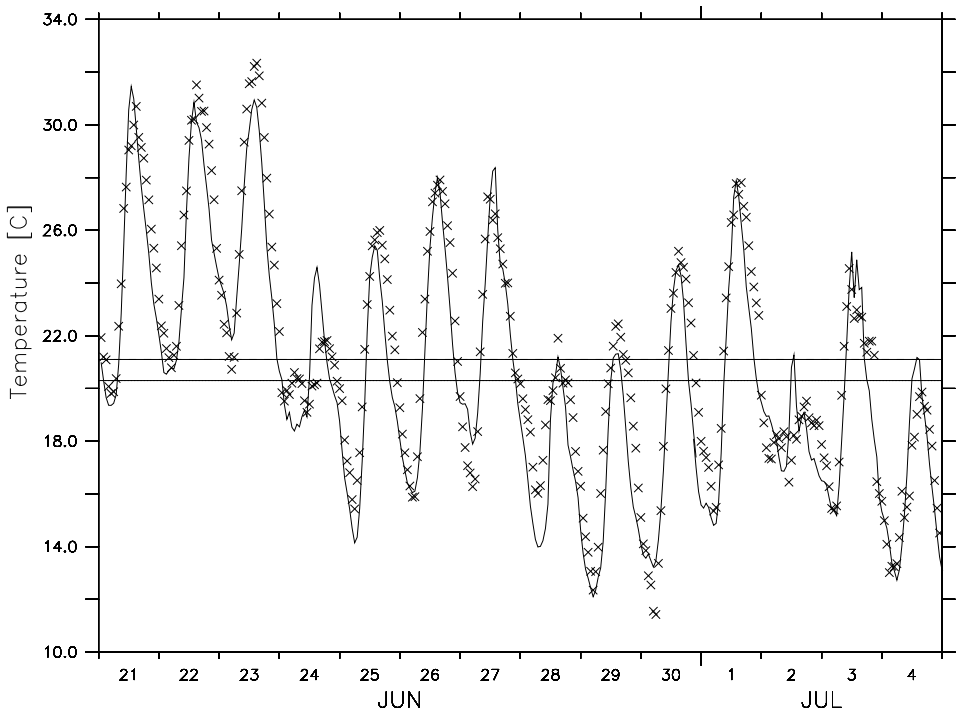

Figure 4.17: Urban temperature at 2m for a 14 days period (June 21 to July 4, 2002) measured (crosses) and simulated by aLMo with BEP (solid line) with a horizontal resolution of 2.2 km. The horizontal lines are the average of the measured temperature (21.1 °C) and the average of the computed temperature (20.3 °C).

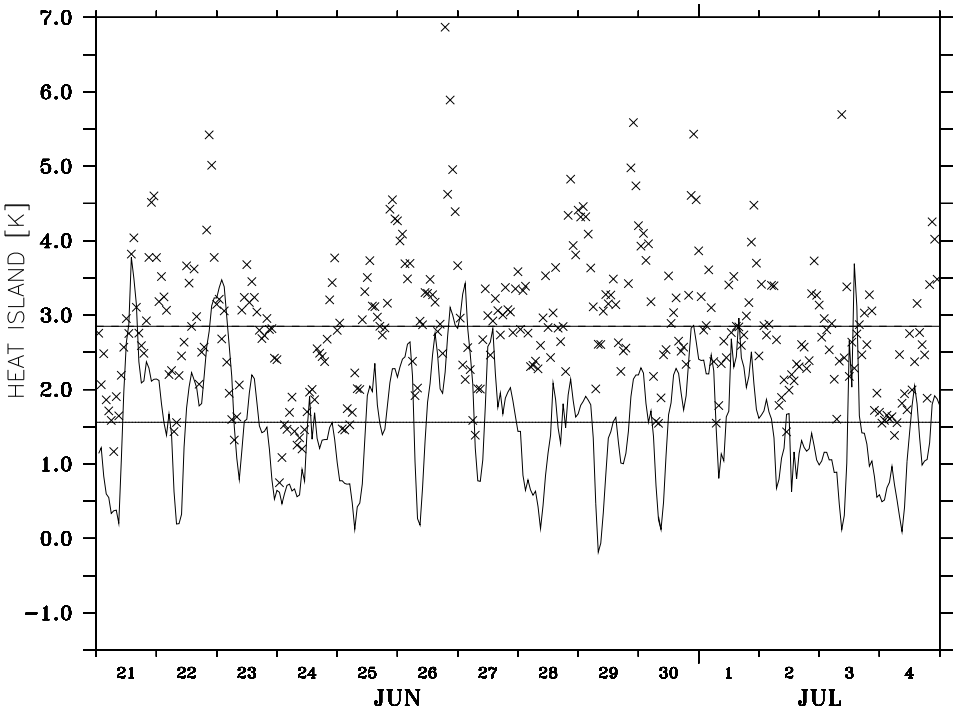

Figure 4.18: Urban Heat Island (UHI) at 2m for a 14 days period (June 21 to July 4, 2002) measured (crosses) and computed by aLMo with BEP (solid line) with a horizontal resolution of 2.2 km. The horizontal line are the average of the measured and of the computed UHI.

tion underestimates the temperature during nighttime and overestimates it during daytime. This phenomenon is also observed in the simulation without BEP (not shown), and is probably due to a too weak cloud cover in the simulation. The ground loses too much energy during nighttime by radiative effects and receives too much energy due to incoming solar radiation during daytime. The same phenomenon is observed on July 2 while very weak rainfall is observed during nighttime. However important rainfalls are observed during nighttime from 3 to 4 July and the simulation during this period fits very well to the measurement (Fig. 4.17). Even if BEP does not take into account latent heat flux, water storage or urban rainfall runoff, the rainfall episode does not deteriorate the results of temperature simulation. Nevertheless, taking into account water budget and latent heat flux in BEP could improve the urban energy balance and the temperature simulation which have shown a too fast cooling at the end of the day (section 4.7.2).

4.8 CONCLUSION

The presence of a city modifies the fluxes between the atmosphere and the Earth's surface. From August 2001 to July 2002, a year-long measurement campaign (BUBBLE) has been conducted in the city of Basel (Switzerland) and its surroundings with the aim of investigating in details the boundary layer structure in an urban area. During the intensive observation period (IOP), form June 15 to July 12 2002, an Urban Heat Island (UHI) has been underlined by temperature measurements at 2 mAGL inside and outside the city (Table 4.4).

In order to investigate the ability of mesoscale models to take into account the effect of urban areas on atmospheric flow fields and to reproduce the UHI, we have selected a three day episode during the IOP for simulation with the aLMo

Table 4.4: Average Urban Heat Island (UHI) in °C for the period of June 25 at 00 LT to June 27 at 23LT, for the BUBBLE measurements (left column), an aLMo simulation with 2.2 km horizontal resolution and 20 m vertical resolution for the first layer (center column) and an aLMo simulation and the urban parametrization BEP with the same configuration (right column).

UHI average for June 25 to 27 2002		
Measurement	aLMo	aLMo - BEP
3.0 °C	-0.1 °C	2.3 °C

mesoscale model.

aLMo is the operational numerical weather prediction model of MeteoSwiss. It is used on a domain covering most of western Europe with a horizontal resolution of 7 km and a vertical resolution with a 60 m depth for the first layer above the ground.

The results obtained with aLMo over the city of Basel and its surroundings shows no UHI. With a 7 km horizontal resolution and a 60 m vertical resolution, the city of Basel and the urban boundary layer are not represented with enough accuracy. In order to investigate if a better resolution allows aLMo to reproduce the measured UHI over Basel, the horizontal resolution has been increased to 2.2 km and the vertical resolution to 20 m for the first layer. The results show that a finer resolution has no impact on the UHI simulation by aLMo (Table 4.4).

As a conclusion, the surface scheme in aLMo based on the similarity theory is not adapted to the urban areas.

In order to take into account the presence of a city with a more accurate surface scheme, the Buildings Effects Parametrization (BEP) has been implemented in aLMo. BEP has been modified in order to compute the temperature at 2 mAGL inside the urban canopy.

Results show that the implementation is successful and works as expected. The

results obtained with BEP show that the urban parametrization modifies the wind flow above and around the city. The wind speed decreases above the city and a system of divergence-convergence is observed around it. As it is shown in the previous chapter for Mexico City, wind divergence-convergence systems are particularly important in air pollution study as they generally lead to a pollution maximum.
The temperature is reproduced with a good accuracy in the urban area. Thus, aLMo with BEP is able to reproduce an UHI in the city of Basel (Tab. 4.4). We have underlined that the temperature increase does not stay confined in the urban area, but extends around the city up to 15 to 20 km.
Nevertheless, the UHI computed with BEP is generally too weak (Tab. 4.4) and even with tuning the urban parameters, BEP is not able to reach the measured values. Sometime, a phase shift is also observed between the measured and simulated temperature. BEP is based on a simplified representation of the urban area and several phenomenon are neglected. The urban parametrization could be adapted in order to take into account different phenomenon, which should modify the urban energy balance:

- The vertical surfaces in BEP are uniform and opaque. Take into account the **windows** will modifying the radiative budget at wall surfaces and in the buildings.

- The **temperature inside the buildings** is maintained constant during the simulation. It will be necessary to take into account its variations in order to represent the buildings energy budget more realistically.

- The **natural ventilation** is the air exchange between inside and outside the buildings (windows opened, ventilation, ...). Koutrakis et al. (1992) estimated that more than 50% of the buildings volume of air can directly be exchanged with the outdoor each hour.

- The **air conditioning** cools down the air inside and rejects heat in the urban atmosphere. It modifies the balance between inside and outside buildings, and is an important source of heat due to its energy consumption.
- No **urban water budget** is computed in BEP. It doesn't take into account precipitation, pipped water supply of the city and water vapor released due to anthropogenic activities, such as combustion.

A 14 days period has been simulated with aLMo/BEP. It is the first time that BEP is applied for a such long period. That allows to verify that BEP does not accumulate or lose energy and that it can be used for long term simulations. Rainfall episodes are included in these 14 days. BEP does not take into account latent heat flux, water storage and urban rainfall runoff. Nevertheless, the simulation with BEP are in good agreement with the measurements.
The results show the importance to have an adapted parametrization for urban areas in order to take into account the modification of the atmospheric flow fields induced by the presence of a city. The increase of horizontal and vertical resolution in aLMo2 is not sufficient to take into account the presence of a city, the use of an adapted parametrization is necessary.
BEP implementation in aLMo is a distinct enhancement for the simulation above urbanized region. We have focused our study on the 2 m observations for temperature, 10 m observations for the wind and the horizontal dispersion of the UHI. The urban effects are also present in the vertical direction. It is important to investigate the impact of BEP on the vertical structure of the atmosphere and its capacity to be used with a low resolution mesoscale model for operational forecast purposes.

Bibliography

Arnfield, A. J. and Grimmond, C. S. B.: 1998, 'An Urban Canyon Energy Budget Model and its Application to Urban Storage Heat Flux Modelling', *Energ. Buildings*, **27**, 61-68.

Bougeault, P. and Lacarrere, P.: 1989, 'Parameterisation of Orography-Induced Turbulence in a Mesobeta-Scale Model', *Mon. Wea. Rev.*, **117**, 1872-1890.

BUBBLE. *http://pages.unibas.ch/geo/mcr/Projects/BUBBLE.*

Businger, J. A., Wyngaard, J. C., Izumi, Y., Bradley, E. F.: 1971, 'Flux-Profile Relationships in the Atmospheric Surface Layer', *J. Atmos. Sci.*, **28**, 181-189.

Clarke, J. A.: 1985, *Energy Simulation in Building Design*, Adam Hilger, Bristol, 362 pp.

COSMO. *http://www.cosmo-model.org/public/documentation.htm.*

Doms, G., Fäurstner, J.,Heise, E.,Herzog, H.-J.,Raschendorfer, M., Schrodin, R.,Reinhardt, T., Vogel, G.: 2002, 'A Description of the Nonhydrostatic Regional Model LM, Part I: Dynamics and Numerics', *Documentation of the LM Package*, 2nd version.

Doms, G., Fäurstner, J.,Heise, E.,Herzog, H.-J.,Raschendorfer, M., Schrodin, R.,Reinhardt, T., Vogel, G.: 2002, 'A Description of the Nonhydrostatic Re-

gional Model LM, Part II: Physical Parameterization', *Documentation of the LM Package*, 2nd version.

Dupont, S., Otte, T.L. and Ching, J.K.S.: 2004, 'Simulation of meteorological fields within and above urban and rural canopies with a mesoscale model', *Boundary-Layer Meteorol.*, **113** (1), 11-158.

Fehrenbach, U.: 1999, 'Analyse und Bewertung lokal- und regional-klimatisch wirksamer Faktoren in der Region Basel, Diss. Phil.-Nat. Fak., Univ. Basel, ISBN 3-85977-245-7

Grimmond, C. S. B., Oke, T. R.: 1999, 'Aerodynamic Properties of Urban Areas Derived from Analysis of Surface Form', *J. Appl. Meteorol.*, **38**, 1262-1292.

Koutrakis, P., Briggs, S.L.K., Leaderer, B. P.: 1992, 'Source Apportionment of Indoor Aerosols in Suffolk and Onondag Counties, New York', *Environ. Sci. Technol.*, **26**, 521-527.

Hamdi, R.: 2005, 'Validation for the cities of Basel and Marseilles', *PhD Thesis*. Université catholique de Louvain, Belgium.

Louis, J.-F.: 1979, 'A parametric model of vertical eddy fluxes in the atmosphere',*Bound.-Layer Meteor.*, **17**, 187-202.

Martilli, A.: 2001, 'Development of an urban turbulence parameterisation for mesoscale atmospheric models', *PhD Thesis N^o* **2445**. Federal Institute of Technology (EPFL), Lausanne, Switzerland.

Martilli, A., Clappier, A., Rotach, M. W.: 2002, 'An urban surfaces exchange parameterisation for mesoscale models', *Bound.-Layer Meteor.*, **104**, 261-304.

Martilli, A., 2002: 'Numerical study of urban impact on the boundary layer structure: sensitivity to wind speed and urban morphology, and rural soil moisture', *J. Appl. Meteorol.*, **41**, 1247-1267.

Martilli, A., Roulet, Y.-A., Junier, J., Kirchner, F., Rotach, M. W., Clappier, A. 2003: 'On the impact of urban surface exchange parameterisations on air quality simulations: the Athens case', *Atmos. Environ.*, **37**, 4217-4231.

Masson, V.: 2000, 'A Physically-Based Scheme For The Urban Energy Budget In Atmospheric Models', *Bound.-Layer Meteor*, **94**, 357-397.

Masson, V., Grimmond, C.S.B, Oke, T.R.: 2002, 'Evaluation of the Town Energy Balance (TEB) scheme with direct measurements from dry districts in two cities', *J. Applied Meteorol.*, **41**, 1011-1026.

Oke, T.R: 1987, 'Boundary Layer Climates', 2nd edn. London: Methuen, 435 pp.

Orlanski, L.: 1975, 'A rational subdivision of scales for atmospheric processes', *Bull. Amer. Meteor. Soc.*, **56**, 527-534.

Pielke, R.: 1984, '*Mesoscale Meteorological Modeling*, Academic Press, San Diego, pp 612.

Rotach, M. W.: 1993, 'Turbulence close to a rough urban surface. Part I: Reynolds stress', *Bound.-Layer Meteor.*, **65**, 1-28.

Rotach, M. W.: 1993, 'Turbulence close to a rough urban surface Part II: variances and gradients', *Bound.-Layer Meteor.*, **66**, 75-92.

Rotach, M. W., Vogt, R., Bernhofer, C., Batchvarova, E., Christen, A., Clappier, A., Feddersen, B., Gryning, S.-E., Martucci, G., Mayer, H., Mitev, V., Oke, T. R., Parlow, E., Richner, H., Roth, M., Roulet, Y.-A., Ruffieux, D., Salmond, J.

A., Schatzmann M., Voogt, J. A.: 2005, 'BUBBLE - an Urban Boundary Layer Meteorology Project', *Theor. Appl. Climatol.*, **81**, 231-261.

Roth, M.: 2000, 'Review of atmospheric turbulence over cities', *Q. J. R. Meteorol. Soc.*, **126**, 941-990.

Roulet, Y.-A.: 2004, 'Validation and Application of an urban turbulence parameterisation scheme for mesoscale atmospheric models', *PhD Thesis N^o.* **3032**, Swiss Federal Institute of Technology, Lausanne.

Roulet, Y.-A., Martilli, A., Rotach, M. W., Clappier, A. 2005: 'Validation of an urban surface exchange parameterization for mesoscale models - 1D case in a street canyon', *J. of App. Meteorol.*, **44**, 1484-1498

Seinfeld, J. H., Pandis, S. N.: 1998,'Atmospheric Chemistry and Physics', *Wiley Interscience publication*, New-York, pp 1326.

Stull, R.B.: 1988, 'An Introduction to Boundary Layer Meteorology', Kluwer Academic Publisher, Dordrecht, pp 670.

Zárate, E., Clappier, A., Belalcázar, L. C.: 2006, 'A study of the photochemical plume formed in Bogota (Colombia) using numerical simulations', *submitted to J. Environ. Manage.*

Appendices

.1 BUBBLE MEASURING STATIONS

List of the measuring stations available during the BUBBLE IOP. The first letter of the station code correspond to the situation of the station (U for Urban area, S for Sub-Urban area and R for Rural area).

Code on map (Fig. 4.1)	Station Name	Height [mASL]
Rp6	Aesch Schlatthof	353
Se1	Allschwil	277
Rp7	Airport Basel-Mulhouse	
Sp2	Basel - Bäumlihof	289
Sp3	Basel - Binningen (ANETZ, NABEL)	316
Up6	Basel - Feldbergstrasse	255
Ue4	Basel - Horburg	254
Re3	Basel - Lange Erlen	275
Up7	Basel - Leonhard	273
Ue5	Basel - Kleinhüningen	265
Up8	Basel - Novartis Klybeck	255
Ue3	Basel - Messe	255
Up9	Basel - Novartis St.Johann	257
Up10	Basel - Roche	255
Ue2	Basel - Spalenring	278
Ue1	Basel- Sperrstrasse	255
Up11	Basel- St. Johann	260
Rp11	St. Chrischonaturm	490
Sp4	Dornach	325
Re4	Gempen	710
Re1	Grenzach	265
Sp5	Liestal LHA	320
Rp8	Oetlingen	450
Rp9	Pratteln Hardwasser	272
Sp6	Rheinfelden	285
Rp10	Schönenbuch	400
Sp7	Schweizerhalle	270
Re5	St. Louis	250
Re2	Village Neuf	240
Sp8	Weil am Rhein	250

.2 Meteorological situation during the IOP

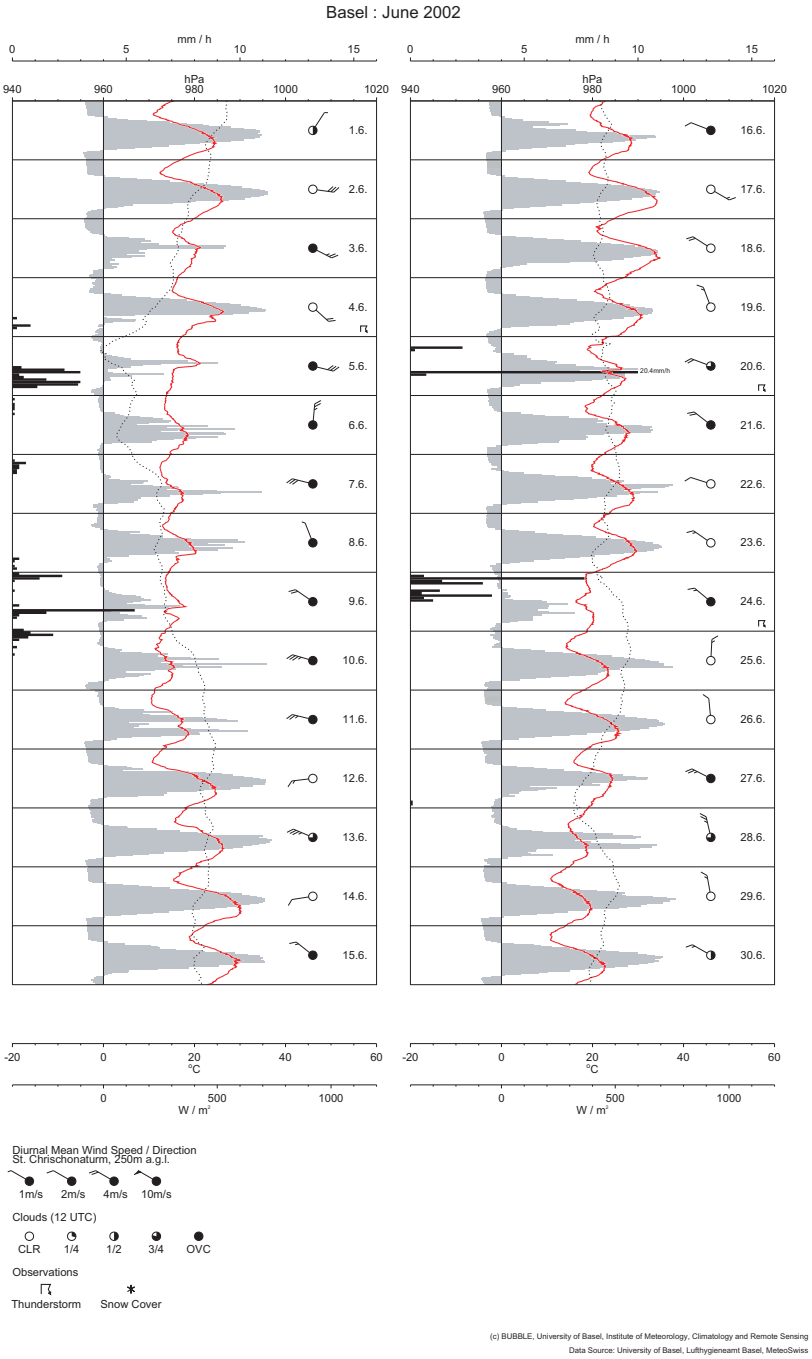

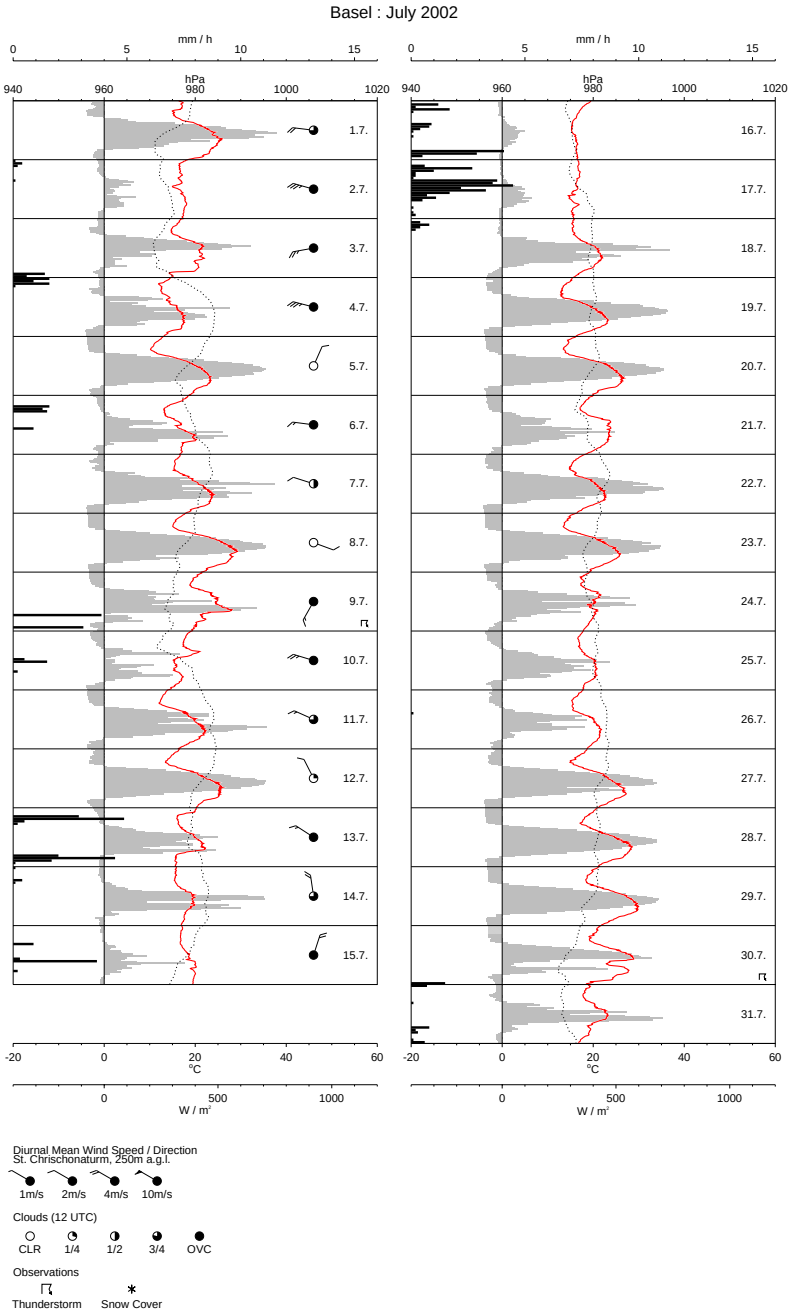
Basel : July 2002
mm / h
hPa
1.7.
2.7.
3.7.
4.7.
5.7.
6.7.
7.7.
8.7.
9.7.
10.7.
11.7.
12.7.
13.7.
14.7.
15.7.
16.7.
17.7.
18.7.
19.7.
20.7.
21.7.
22.7.
23.7.
24.7.
25.7.
26.7.
27.7.
28.7.
29.7.
30.7.
31.7.
°C
W / m²
Diurnal Mean Wind Speed / Direction
St. Chrischonaturm, 250m a.g.l.
1m/s
2m/s
4m/s
10m/s
Clouds (12 UTC)
CLR
1/4
1/2
3/4
OVC
Observations
Thunderstorm
Snow Cover
(c) BUBBLE, University of Basel, Institute of Meteorology, Climatology and Remote Sensing
Data Source: University of Basel, Lufthygieneamt Basel, MeteoSwiss

.3 The definition of urban categories for BEP

The urban properties as they are described in aLMo for the city of Basel

```
URBAN CATEGORY


!     Building parameters
! Ground thermal diffusivity [m^[m^2 s^-1]
      alag_u(1)=0.3e-06,
! Wall thermal diffusivity [m^2 s^-1]
      alaw_u(1)=0.2e-06,
! Roof thermal diffusivity [m^2 s^-1]
      alar_u(1)=0.2e-06,
! Specific heat of the ground material [J m^3 K^-1]
      csg_u(1)=1.4e+6,
! Specific heat of the wall material [J m^3 K^-1]
      csw_u(1)=0.2e+6,
! Specific heat of the roof material [J m^3 K^-1]
      csr_u(1)=0.2e+6,
! Temperature inside the buildings behind the wall [K]
      twini_u(1)=295.,
! Temperature inside the buildings behind the roof [K]
      trini_u(1)=295.,
!     Radiation parameters
! Albedo of the ground
      albg_u(1)=0.2,
! Albedo of the wall
      albw_u(1)=0.2,
```

```
! Albedo of the roof
      albr_u(1)=0.2,
! Emissivity of ground
      emg_u(1)=0.95,
! Emissivity of wall
      emw_u(1)=0.9,
! Emissivity of roof
      emr_u(1)=0.9,
!     Roughness parameters
! The ground's roughness length
      z0g_u(1)=0.0005,
! The roof's roughness length
      z0r_u(1)=0.0005,
!     Street configuration parameters
! Number of street direction
for each urban class
      nd_u(1)=2,
! Street direction [radian]
      drst_u(1,1)=0.7854, !45.*pi/180.
      drst_u(2,1)=2.3562, !135.*pi/180.
! Street width [m]
      ws_u(1,1)=15.,
      ws_u(2,1)=15.,
! Building width [m]
      bs_u(1,1)=22.,
      bs_u(2,1)=22.,
! Bulding's heights [m]
```

```
      h_b(1,1)=10.,
      h_b(2,1)=15.,
      h_b(3,1)=17.,
! The probability that a building has an height h_b
      d_b(1,1)=20.,
      d_b(2,1)=55.,
      d_b(3,1)=25.,

------------------------------------------------------------------------------
------------------------------------------------------------------------------

SUB-URBAN CATEGORY

!     Building parameters
! Ground thermal diffusivity [m^2 s^-1]
      alag_u(2)=0.47e-6,
! Wall thermal diffusivity [m^2 s^-1]
      alaw_u(2)=0.37e-06,
! Roof thermal diffusivity [m^2 s^-1]
      alar_u(2)=0.42e-06,
! Specific heat of the ground material [J m^3 K^-1]
      csg_u(2)=1.75e+6,
! Specific heat of the wall material [J m^3 K^-1]
      csw_u(2)=0.5e+6,
! Specific heat of the roof material [J m^3 K^-1]
      csr_u(2)=0.5e+6,
! Temperature inside the buildings behind the wall [K]
```

```
      twini_u(2)=293.,
! Temperature inside the buildings behind the roof [K]
      trini_u(2)=293.,
!     Radiation parameters
! Albedo of the ground
      albg_u(2)=0.2,
! Albedo of the wall
      albw_u(2)=0.2,
! Albedo of the roof
      albr_u(2)=0.2,
! Emissivity of ground
      emg_u(2)=0.95,
! Emissivity of wall
      emw_u(2)=0.9,
! Emissivity of roof
      emr_u(2)=0.9,
!     Roughness parameters
! The ground's roughness length
      z0g_u(2)=0.005,
! The roof's roughness length
      z0r_u(2)=0.005,
!     Street configuration parameters
! Number of street direction
for each urban class
      nd_u(2)=2,
! Street direction [radian]
      drst_u(1,2)=0.7854, !.45.*pi/180.
```

```
      drst_u(2,2)=2.3562, !135.*pi/180.
! Street width [m]
      ws_u(1,2)=25.,
      ws_u(2,2)=25.,
! Building width [m]
      bs_u(1,2)=17.,
      bs_u(2,2)=17.,
! Building's heights [m]
      h_b(2,2)=6.,
      h_b(3,2)=9.,
! The probability that a building has an height h_b
      d_b(1,2)=75.,
      d_b(2,2)=25.,
```

Chapter 5

The Buildings Effects Parametrization and the mesoscale grid resolution

Abstract

The goals of this study are to test the urban parametrization BEP (Martilli et al., 2002) in a mesoscale model with a low resolution and to investigate the impact on the vertical structure of the urban boundary layer.

Implemented in aLMo, the operational weather forecast model of MeteoSwiss, BEP have proven to be able to reproduce an Urban Heat Island (UHI), as well as an unstable layer above the city of Basel during nighttime. However, aLMo has shown a great dependency on the vertical resolution. Errors induced by the use of a low vertical resolution in aLMo are in the same order of magnitude than the improvements brought by the urban parametrization.

BEP is modified in order to improve results at low vertical resolution. The mesoscale model furnishes the upper boundary conditions for the inner calculation of BEP. That is, BEP recalculates independently the vertical profiles of wind, temperature and energy based on the surface fluxes of momentum, heat and turbulent kinetic energy. Results obtained with the modified version of BEP are very close for both low and high vertical resolution. Moreover, the temperature profile computed in the urban grid (BEP grid with a 5 m vertical resolution) shows good agreement with street-canyon measurements in Basel. Thus, wind, temperature and turbulent kinetic energy computed in the urban grid can be used as input for dispersion models using a high vertical resolution.

Finally, BEP is tested with the aLMo operational configuration (low horizontal and vertical resolution). In this configuration, aLMo with BEP is able to simulate the formation of an UHI. Thus, it is not necessary to have a high resolution to take into account the impact of a city.

5.1 INTRODUCTION

Urbanization causes drastic changes in the radiative, thermal, moisture and aerodynamics properties of the land surface (Oke, 1987), leading to an important modification of the near surface atmospheric flow. As Frehlich et al. (2006) show with measurements, the urban and sub-urban areas impact not only the land surface but also the atmosphere over those regions. It is the entire Planetary Boundary Layer (PBL) structure that is affected by the presence of a city. According to Stull (1988) and Rotach et al. (2005), the Urban Boundary Layer (UBL) can be divided in 2 distinct layers, the surface layer containing the roughness layer and the mixed layer (Fig. 5.1). The roughness layer height depends on the height and density of roughness elements. In this layer, the effects of each roughness elements can be discerned. The roughness layer can be divided into two parts, the urban canopy that ranges from the ground up to roughly the average height of the buildings, and the wake layer situated above the urban canopy. Above the roughness layer, the surface layer feels the average effect of the urban area and we can assume that the Monin-Obukhov Similarity Theory (MOST) is valid. Then, the mixed layer, also known as the convective boundary layer, is situated above the surface layer.

A modeling study of Makar et al. (2006) shows that the urban effects on the vertical structure of the boundary layer can not be neglected and that it is necessary to take into account anthropogenic heat sources and the modification of the energy budget induced by a city in a numerical forecast model. They have hence incorporated a constant flux of anthropogenic heat and modified the land surface parametrization with adapted surface roughness and radiative properties. The results show an improvement on the simulated temperature and on the mixing layer heights. According to Makar et al. (2006), a more advanced and detailed parametrization for the urban boundary layer is necessary for higher resolution simulations.

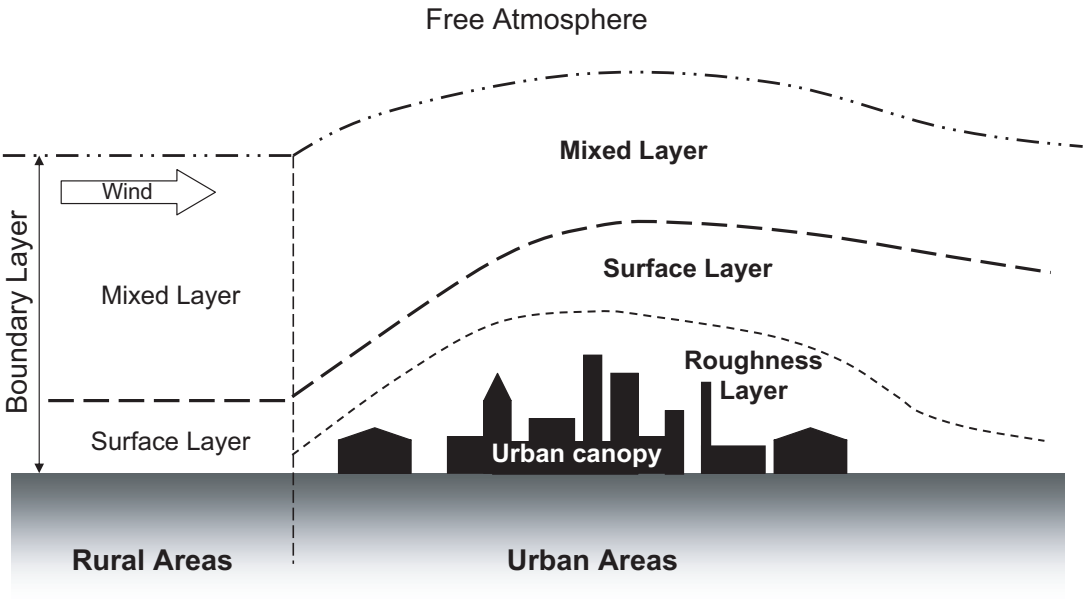

Figure 5.1: Schematic representation of the planetary boundary layer over rural and urban areas during daytime. According to Stull (1988) and Rotach et al. (2005), the Urban Boundary Layer (UBL) is divided into 3 different layers with, from the ground to the free atmosphere, the roughness layer including the urban canopy sub-layer and the wake sub-layer, the surface layer and the mixed layer.

In the previous chapter, we have used the operational forecast model of MeteoSwiss, aLMo, in order to simulate the Urban Heat Island (UHI) over the city of Basel. The operational configuration, *i.e.* a 7 km horizontal resolution and a first layer thickness of 60 m, did not reproduce a UHI. The horizontal and vertical resolutions have been increased in the aLMo2 configuration in order to have a better representation of the urban area. Nevertheless, an increased resolution did not improve the results significantly. As proposed by (Makar et al., 2006), a detailed urban parametrization, the Buildings Effects Parametrization (BEP, Martilli et al. (2002)), is implemented in order to take into account the urban effects. With the aLMo2 configuration, *i.e.* a 2.2 km horizontal resolution and 20 m thickness for the first layer above ground, BEP improves the results for the Basel case study and reproduces the UHI. We have focused our study on the impact of BEP for a

city represented with a high vertical and horizontal resolution.

In this chapter, the goal is to test BEP with different resolutions. After the increase of the horizontal and vertical resolution in the previous chapter, we now use BEP in aLMo with a lower resolution. We focus on BEP impacts on the vertical structure of the urban boundary layer.

The impact of BEP on mesoscale simulations is tested with both high and low vertical resolution. The aim is to evaluate the sensitivity of the urban scheme to the mesoscale vertical resolution.

In a next step, BEP is modified to better suit operational forecast models. We will not only focus on the impact of BEP in the mesoscale model, but also on the temperature profiles calculated by BEP in the urban grid, which are compared to the measurements from a 32 m high tower placed in a street canyon in the city of Basel.

Finally, the horizontal resolution is decreased in order to investigate the capacity of BEP to be used in the operational configuration of aLMo.

5.2 MODEL DESCRIPTION

5.2.1 aLMo

The aLpine Model (aLMo) is used for operational Numerical Weather Prediction (NWP) at MeteoSwiss. It is a mesoscale non-hydrostatic fully compressible limited-area atmospheric model, it is based on the primitive thermo-hydrodynamical equations describing a compressible flow in a moist atmosphere (Doms et al., 2002a,b).

Two configurations of aLMo are used in this chapter. The first one, denotated aLMo, uses a traditional land-surface scheme where the turbulent fluxes of sensible

heat, moisture and momentum are computed with the Monin-Obukhov Similarity Theory (MOST). The second one, denoted aLMo/BEP, which uses the Building Effects Parametrization (BEP, Martilli et al. (2002)) for computing the turbulent fluxes of sensible heat and momentum in urban areas.

5.2.2 BEP : *Building Effects Parametrizations*

A parametrization adapted to urban areas, developed by Martilli (2001) and called the Building Effects Parametrization (BEP) is used in this study.
BEP takes into account the properties of the vertical and horizontal surfaces (wall, canyon floor and roofs), shadowing and radiative trapping effects of the buildings, as well as the anthropogenic heat fluxes through the buildings walls and roofs. The fluxes contributions (a_i, b_i) of every urban surface type (canyon floor, roofs and walls) on momentum, heat and Turbulent Kinetic Energy (E) budgets are computed separately in the BEP's grid (hereafter the urban grid). In the previous chapter, BEP has been modified in order to compute the temperature θ, the wind speed U_i and the turbulent kinetic energy E in the urban grid, and which are parametrized respectively with:

$$\frac{\partial}{\partial z}\left(K_z \frac{\partial \theta}{\partial z}\right) = a_\theta \theta + b_\theta \tag{5.1}$$

$$\frac{\partial}{\partial z}\left(K_z \frac{\partial U_i}{\partial z}\right) = a_{U_i} U_i + b_{U_i} \tag{5.2}$$

$$\frac{\partial}{\partial z}\left(K_z\frac{\partial E}{\partial z}\right) = a_E E + b_E + \rho K_z\left[\left(\frac{\partial U_x}{\partial z}\right)^2 + \left(\frac{\partial U_y}{\partial z}\right)^2\right] - \frac{g}{\theta_0}\rho K_z\frac{\partial \theta}{\partial z} - \rho C_\varepsilon\frac{E^{3/2}}{l_\varepsilon} \tag{5.3}$$

The upper-boundary conditions used to solve this equation set are determined with the assumption that a neutral sublayer is developed above the canopy layer.

5.2.3 MODEL SETUP

As in the previous chapter, aLMo with a high vertical resolution (aLMo/BEP 20) is applied over the city of Basel and its surroundings with a 2.2 km horizontal resolution. The vertical resolution is set to 20 m for the lowest layer depth.
A 3 days period from June 25 to June 27 is simulated. This episode take place during the Intensive Observation Period (IOP) of the Basel UrBan Boundary Layer Experiment (BUBBLE, Rotach et al. (2005)).
For the simulation with BEP, the urban area is represented by 24 grid cells, with two different urban types, one for the city center (7 grid points) and another one for the sub-urban area (17 grid points).

5.3 IMPACTS OF VERTICAL RESOLUTION

In this section, the vertical structure of the boundary layer above the city of Basel is investigated using high vertical resolution simulations with and without BEP (section 5.3.1).
In a second step, simulations with a lower vertical resolution are conducted in

order to study the impact of the vertical resolution on the atmospheric flow fields obtained with aLMo and with aLMo/BEP (section 5.3.2).

5.3.1 VERTICAL TEMPERATURE, STABILITY AND MIXING HEIGHT

Here, the potential temperature profiles simulated with aLMo 20 and with aLMo/BEP 20 are compared over an urbanized grid point situated in Basel's city center. The aim is to evaluate the impact of BEP on the vertical structure of the urban boundary layer in terms of stability and mixing height. Both simulations use the aLMo2 configuration, *i.e.* a high vertical resolution with a lowest layer of 20 m height.

Figure 5.2 shows a potential temperature vertical profile during daytime above the city of Basel obtained with aLMo 20 and aLMo/BEP 20 respectively. The simulation with BEP shows that the temperature increases near the ground with the formation of an UHI (as shown previously) and also in the first 1000 m above the ground. The mixing height[1] with aLMo/BEP 20 is situated at around 1000 m Above Ground Level (mAGL) while it is at around 700 mAGL in aLMo 20. An increase of the mixing height with BEP during daytime is hence observed.

The greatest differences between model and measurements are observed during nighttime (Fig. 5.3): aLMo 20 shows a stable profile above the city while measurements (not shown) from a tower in a street canyon show an unstable layer (Christen, 2005).

aLMo/BEP 20 shows a warmer profile for the first 200 m above the ground and hence creates an unstable layer near the ground that aLMo 20 is not able to reproduce. With aLMo/BEP 20, the mixing height reaches around 150 mAGL.

[1]The mixing height is defined here as the height where the profile slope of potential temperature becomes positive after an unstable layer

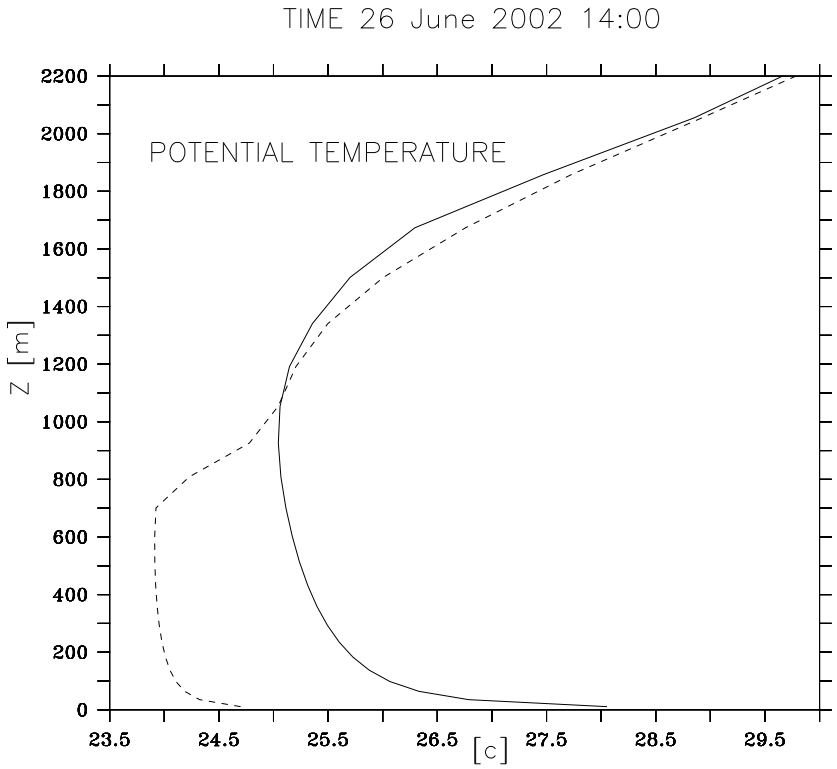

Figure 5.2: Simulated potential temperature profile above the city of Basel, June 26 2002 at 14LT. The dashed line corresponds to the aLMo 20 simulation and the solid line to the aLMo/BEP 20 simulation. Both results have been obtained with a high vertical resolution.

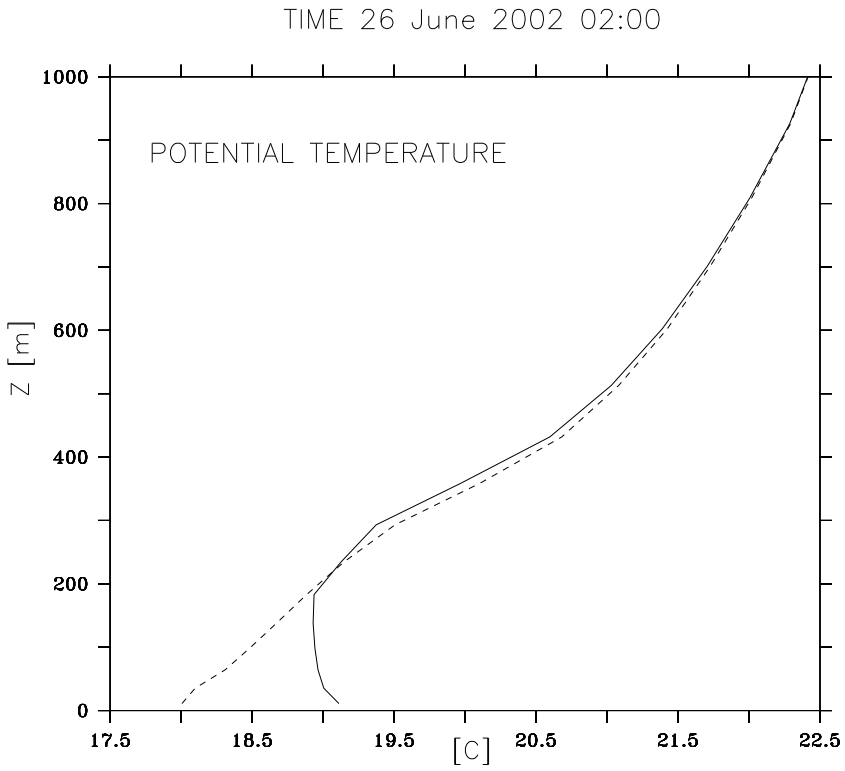

Figure 5.3: Simulated potential temperature profile above the city of Basel, June 26 2002 at 02LT. The dashed line correspond to the aLMo 20 simulation and the solid line to the aLMo/BEP 20 simulation. Both results have been obtained with a high vertical resolution.

BEP impacts not only the first layer of the model (the urban canopy layer), but deeply modifies the full boundary layer in term of mixing height and stability. It increases the turbulence which in turn creates more instability above the city and increases the mixing height.

5.3.2 DECREASING THE VERTICAL RESOLUTION

Up to now, BEP has always been tested with a vertical resolution of the mesoscale model corresponding to the urban canopy height. In this section, the vertical resolution of the mesoscale grid is decreased in order to evaluate the sensitivity of

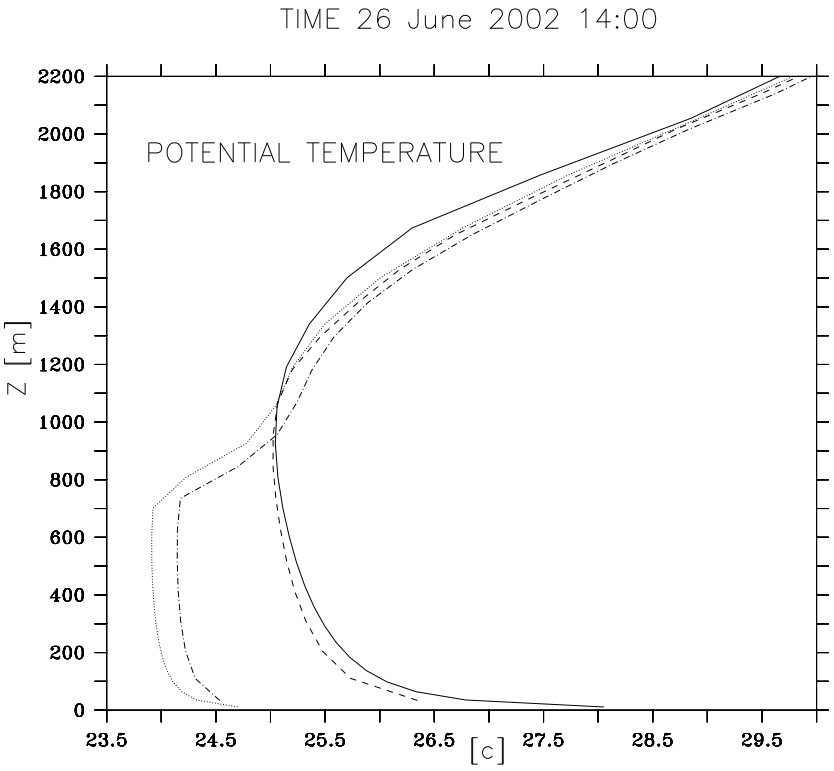

Figure 5.4: Simulated potential temperature profiles above the city of Basel, June 26 2002 at 14LT. The dashed line corresponds to the aLMo/BEP 60 simulation and the alternately dashed to the aLMo 60 simulation. Both results have been obtained with a low vertical resolution. The dotted line show the results of aLMo 20 and the solid line those of aLMo/BEP 20, both simulations have a high vertical resolution.

the model outputs to its vertical resolution and to test the BEP impact when used at low vertical resolutions. Two simulations have been conducted with the same grid resolution, *i.e.* 60 m for the lowest layer: one without BEP (aLMo 60), and one with BEP (aLMo/BEP 60). Both simulations are compared and also evaluated against the 20 m vertical resolution simulations (aLMo 20 and aLMo/BEP 20).

Figures 5.4 and 5.5 show the potential temperature vertical profiles during daytime and nighttime respectively. Firstly, the comparison of aLMo results (without BEP) with different resolutions indicates a dependence of the model results on the

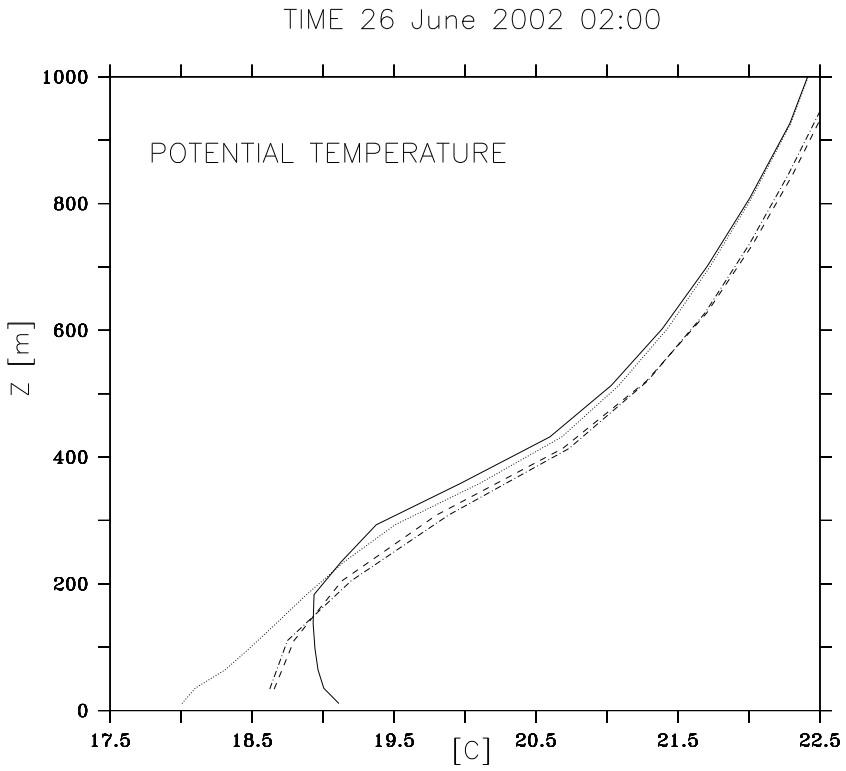

Figure 5.5: Simulated potential temperature profiles above the city of Basel, June 26 2002 at 02LT. The dashed line corresponds to the aLMo/BEP 60 simulation and the alternately dashed to the aLMo 60 simulation. Both results have been obtained with a low vertical resolution. The dotted line show the results of aLMo 20 and the solid line those of aLMo/BEP 20, both simulations have a high vertical resolution.

vertical resolution. During daytime (Fig. 5.4), the differences between aLMo 20 and aLMo 60 are very small within the mixing layer, which is slightly thicker for a low resolution simulation, respectively 690 m with aLMo 20 and 730 with aLMo 60. During nighttime, under stable conditions, differences are larger (Fig. 5.5). As a conclusion for this case study, the low resolution simulation (aLMo 60) shows warmer and less stable air than aLMo 20. aLMo is sensitive to the vertical resolution and more particularly under stable situations.

If we take a look to the two simulations conducted with BEP (aLMo/BEP

20 and aLMo/BEP 60), important differences according to the vertical resolution can also be observed. During daytime (Fig. 5.4), both simulations indicate the same mixing height. However, potential temperature at 30 mAGL (first layer in the low resolution and second layer in the high resolution configuration) is 0.5 °C lower with aLMo/BEP 60. During nighttime (Fig. 5.5), the differences remains at around 0.5 °C near the ground. Furthermore, with a high resolution, an unstable layer is observed above the city (as measurements indicate, see section 5.3.1 and Christen (2005)), while the atmosphere is stable with a low resolution. The results of aLMo/BEP are influenced by the mesoscale vertical resolution, as in the case of aLMo. According to the results obtained in the previous chapter, we can consider that the results with aLMo/BEP 20 are the most accurate. A decrease of the vertical resolution is therefore associated with a decrease of the results accuracy.

The comparison of both simulations with a 60 m vertical resolution (aLMo 60 and aLMo/BEP 60) shows that the use of BEP increases the mixing height during daytime (Fig. 5.4) and that the atmosphere is warmer in the first 900 m above ground. However, the results obtained with aLMo/BEP 60 during nighttime are very close to aLMo 60 (Fig. 5.5). Using a low vertical resolution does not allow BEP to reproduce the unstable layer above the city during nighttime which is measured and correctly reproduced by aLMo/BEP 20.

As a conclusion, BEP does not reproduce the same boundary layer structure for various vertical resolutions of the mesoscale model and its impacts are different. In other words, results obtained with aLMo/BEP are dependent on the mesoscale model vertical resolution. The error induced by a decrease of the vertical resolution (simulations aLMo/BEP 20 and aLMo/BEP 60) is approximately in the same order of magnitude than the temperature modification between aLMo/BEP 20 and

aLMo 20. In this case, the improvements due to BEP with a high resolution are lost when the vertical resolution is decreased. Results indicate, that the current implementation of BEP in the aLMo mesoscale model is not suitable for simulations at the current grid resolutions used in the operational forecast configuration of MeteoSwiss. Some adaptations of the parametrization are therefore necessary in order to use it with the model at a low vertical resolution.

5.4 ADAPTATION OF BEP

In this section, we present the modifications provided to the urban parametrization BEP in order to use it in mesoscale models with low vertical resolution.
In the traditional implementation of BEP (Fig. 5.6), wind and temperature profiles are linearly interpolated from the mesoscale to the urban grid at each time step (Martilli, 2001). The flux source terms a_ψ and b_ψ, computed by BEP, are hence solved from the mesoscale value. This method is justified if the mesoscale grid resolution is close enough to the urban canopy height in order to follow the energy budget evolution occurring in the urban area. If the first layer of the mesoscale model grid is 2 to 3 times thicker than the urban canopy, the verticale profiles of wind and temperature on BEP urban grid will be initialized with constant values each time step. This cannot be justified and is not representative for the urban canopy.

As it has been presented in the previous chapter, BEP calculates profiles for temperature, wind and turbulent kinetic energy in the urban grid. In order to follow the evolution of wind, air temperature and surfaces temperature (roof, wall, ground), the profiles computed in the urban grid at time step N are conserved and will initialize the BEP urban grid at the next time step $N + 1$ (Fig. 5.7).

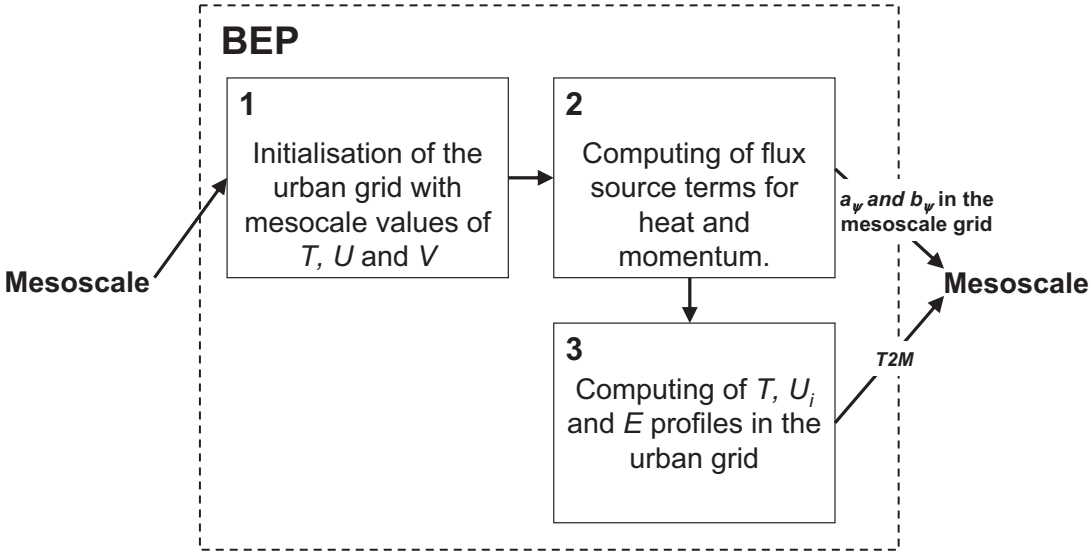

Figure 5.6: Schematic representation of the BEP structure used until now, where the urban grid is initialized with the mesoscale values (T2M=Temperature at 2 mAGL).

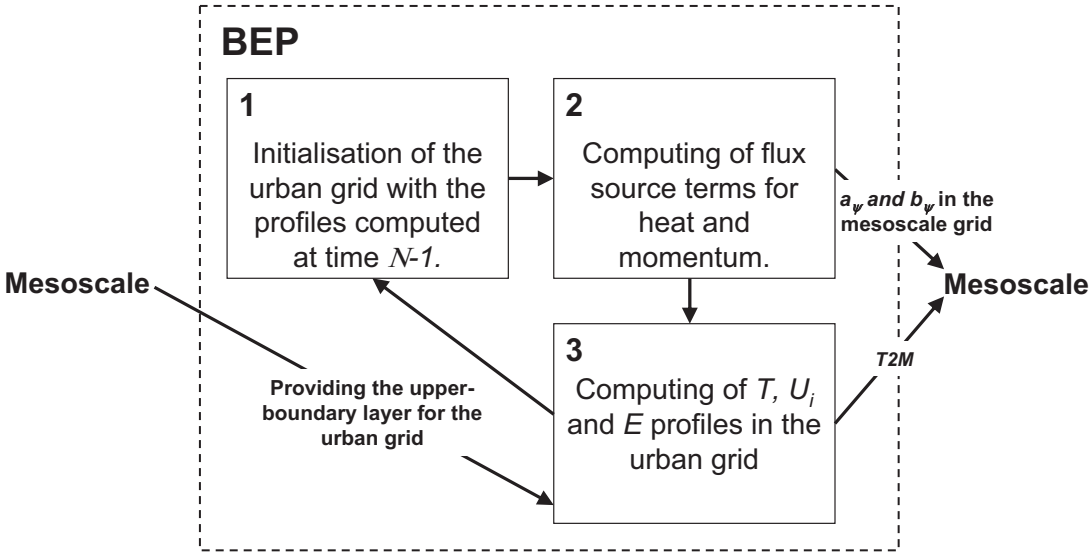

Figure 5.7: Schematic representation of the BEP structure where the urban grid is initialized with temperature and wind speed computed in the urban grid at the previous time step $N-1$. In this case, BEP is linked with the mesoscale model by the upper-boundary (T2M=Temperature at 2 mAGL).

With this method, temperature, wind and energy profiles calculated by BEP in a previous time step ($N-1$), are used as input for BEP in the present time step (N). Hence, the urban flux source terms and the urban surface temperature in the urban grid are computed from temperature, wind and energy profiles calculated by BEP and linked to the mesoscale model only by the upper-boundary condition. The time-lag induced by the use of the urban profiles computed at the previous time step, $N-1$, is neglected. We also neglect all direct horizontal contributions (pressure, advection) to compute the profile evolution in the urban grid.

The capacity of this new version, denoted BEP2, to be used in the operational configuration of aLMo, *i.e* with a low vertical and horizontal resolution, is investigated in the next section.

We will also verify the agreement between the temperature computed in the urban grid and in the mesoscale grid. Finally, we will compare the results obtained in the urban grid with street canyon measurements obtained during the BUBBLE campaign.

5.5 RESULTS

5.5.1 IMPACT OF THE VERTICAL RESOLUTION

In a first step, the results obtained with the former version of BEP are compared with the new version. The same simulations as in previous chapter have been conducted with the two versions of BEP (aLMo/BEP 20 and aLMo/BEP2 20). In this situation, the first mesoscale grid layer (20 m) is close to the urban canopy height (25 m). The results obtained (not shown) with both version of BEP are similar, *i.e.* the temperature differences are never larger than 0.8 % and the wind differences are always lower than 5 % over the entire simulation domain. Conse-

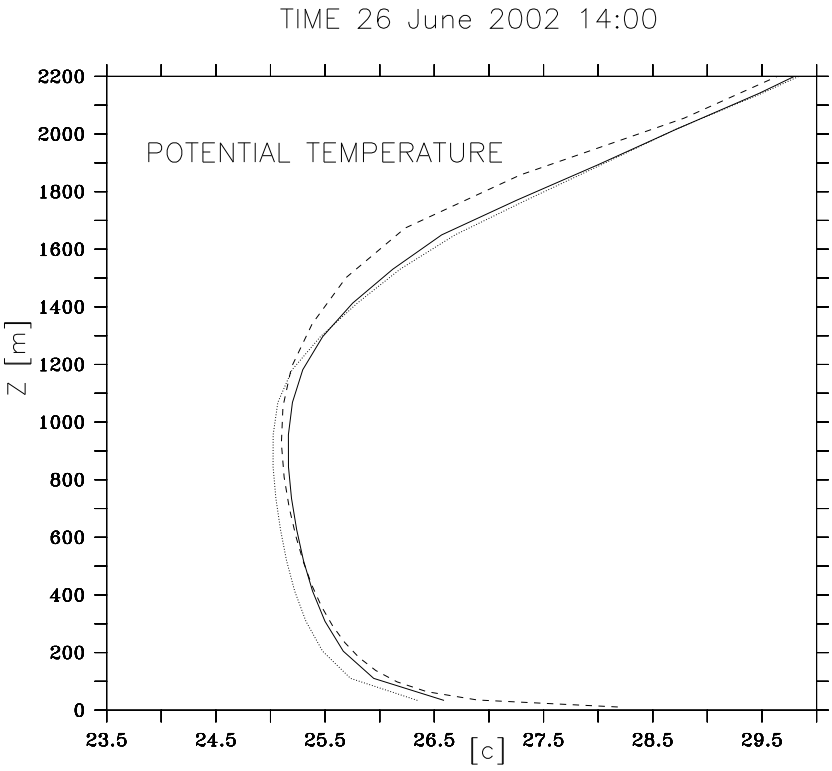

Figure 5.8: Simulated potential temperature profiles above the city of Basel, June 26 2002 at 14LT. The results with the aLMo/BEP2 60 configuration are plotted with the solid line, the dotted line represents the aLMo/BEP 60 configuration and the dashed line represents the aLMo/BEP2 20 configuration.

quently, the BEP modifications do not modify in a significant manner the results obtained with the former method (aLMo/BEP 20) for vertical resolutions close to the urban canopy thickness.

In a second step, a simulation (aLMo/BEP2 60) with BEP2 and a low vertical resolution (60m) is performed over the city of Basel during 3 days (horizontal resolution remains 2.2 km).

Figures 5.8 and 5.9 show potential temperature vertical profiles during daytime and nighttime. With BEP2, the results obtained using a low vertical resolution (aLMo/BEP2 60) are very close to the results with a high vertical resolution

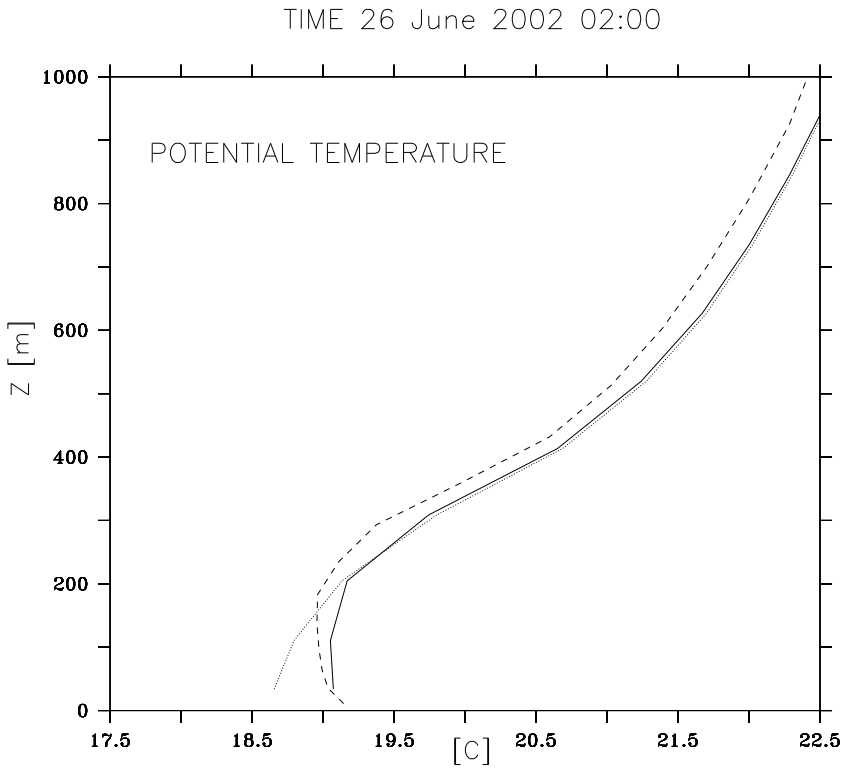

Figure 5.9: Simulated potential temperature profiles above the city of Basel, June 26 2002 at 02LT. The results with the aLMo/BEP2 60 configuration are plotted with the solid line, the dotted line represents the aLMo/BEP 60 configuration and the dashed line represents the aLMo/BEP2 20 configuration.

(aLMo/BEP2 20).

Whereas the former version of BEP was not able to reproduce an unstable layer above urban areas during nighttime, BEP2 simulates a mixing height at around 110 m above the ground in the city center. The use of BEP2 allows to obtain a more accurate temperature simulation for lower vertical resolutions, despite of aLMo dependency on the vertical resolution (cf. Fig. 5.4 and 5.5).

The modifications made in the parametrization allow a better reproduction of the urban boundary layer. Furthermore, BEP2 results are less dependant on the mesoscale model vertical resolution.

5.5.2 ANALYSIS OF URBAN AND MESOSCALE RESULTS

We have shown that the modified version of BEP (BEP2) improves the results of the mesoscale model. Furthermore, the parametrization provides additional data, *i.e.* estimation of the temperature, wind and turbulent kinetic energy profiles in the urban grid. The modifications made in order to obtain BEP2, link the mesoscale model and BEP itself only through the upper-boundary of the urban grid used for BEP. It implies that the advection is neglected. In this section, it is verified that this partial disconnection does not deteriorate results obtained for the urban grid simulation. For this purpose, the temperature generated at the first layer of the mesoscale model is compared to the temperature obtained in the urban grid. This comparison is made for both high and low vertical resolution.

In the case of high vertical resolution, a simulation has been conducted over the city of Basel, with a first layer thickness of 20 m (the urban grid is 25 m height) and 100% of urban fraction in order to compare the evolution of the temperature in the urban grid and in the first level of the mesoscale model.

Figure 5.10 shows the relative difference between the mean temperature over the first 20 meters of the urban grid and the temperature in the first layer of the mesoscale grid. The results show a difference lower than 2.4 % and a significant positive correlation between the temperature difference and the wind speed (cf. Fig. 5.10), which is due to the fact that advection in BEP2 is neglected. However, these differences remain low, as wind speed in urban areas are generally decreased by the buildings.

In the case of low resolution, the temperature computed in the urban grid is also compared to the temperature computed in the mesoscale grid with a first layer

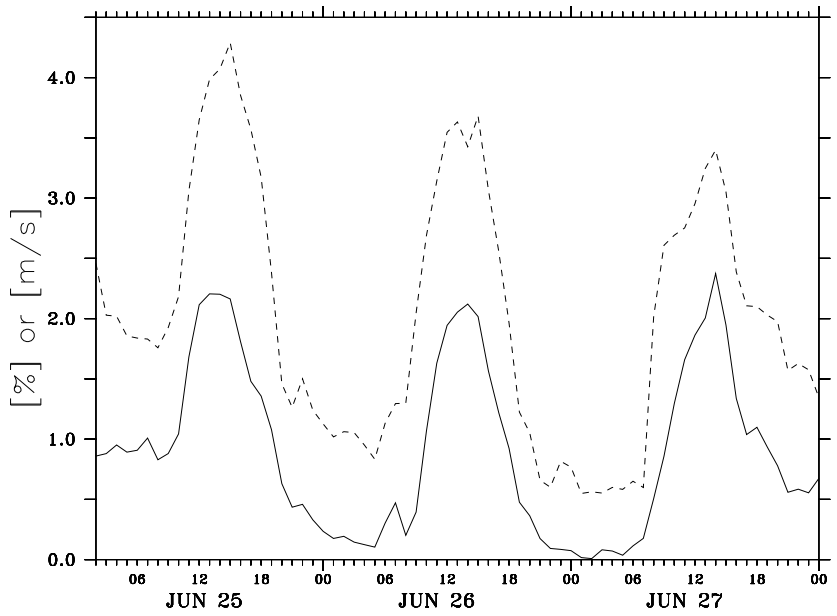

Figure 5.10: Relative difference $\left(\frac{T_{urb}-T_{meso}}{T_{urb}}\right)$ between the mean temperature in urban grid T_{urb}, and the temperature in the first layer of the mesoscale model T_{meso} (solid line). The dashed line shows the wind speed in mesoscale model first layer at the same urban grid point. Results obtained with aLMo/BEP2 20

thickness of 60 m and 100% of urban fraction.

Figures 5.11 and 5.12 show potential temperature profiles simulated by aLMo with BEP2 (aLMo/BEP2 60 configuration). The mesoscale profile stops at 30 mAGL as the depth of the first layer in the mesoscale model is 60m. The profile computed by BEP2 in the urban grid, from 2.5 to 22.5 mAGL is shown in the same figures. For both a very unstable situation (daytime) or a less unstable situation (nightime) is observed. The temperature computed by BEP2 is in good agreement with the mesoscale profile. A continuity is observed between both profiles (mesoscale and urban). Despite the fact that BEP2 is only linked to the mesoscale model by the upper-boundary, the profiles from the urban grid are in good agreement with the profiles from the mesoscale model.

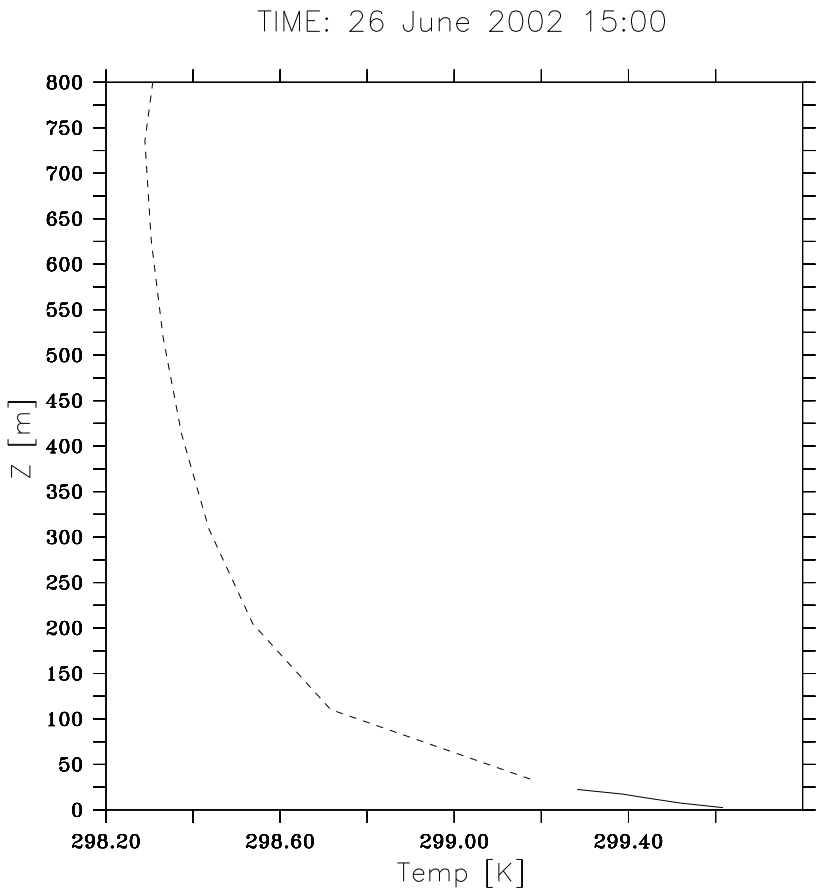

Figure 5.11: Simulated potential temperature profile above the city of Basel, June 26 2002 at 15LT. The dashed line shows the potential temperature in the mesoscale grid as calculated by aLMo/BEP2 60 and the solid line is the potential temperature computed by BEP2 in the urban grid at the same horizontal grid point and time step.

5.5.3 URBAN GRID VS. MEASUREMENTS

In the previous sections, we have shown that BEP2 is able to compute reasonable potential temperature profiles in the urban grid even if the mesoscale model uses a low vertical resolution. It was also shown that these profiles are in good agreement with the mesoscale profiles. In this section, a validation of urban simulation profiles against the measurements is performed in order to evaluate the possibility to use the simulated profiles as input for dispersion models.

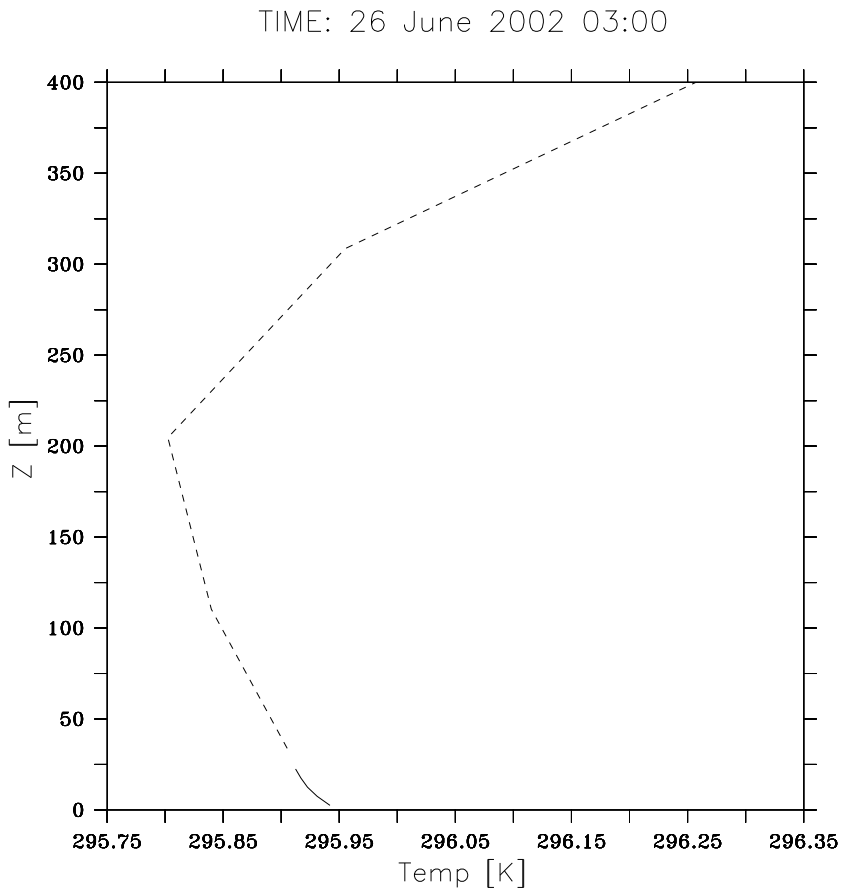

Figure 5.12: Simulated potential temperature profile above the city of Basel, June 26 2002 at 03LT. The dashed line shows the potential temperature in the mesoscale grid as calculated by aLMo/BEP2 60 and the solid line is the potential temperature computed by BEP2 in the urban grid at the same horizontal grid point and time step.

During the BUBBLE IOP, the main urban experimental site was located in a heavily built-up part (Sperrstrasse). This site is representative for Basel city center. The instrumentation was mounted on a 32 m high tower, installed inside a 13 m wide street canyon and surrounded by buildings of 15 m height. This measurements set was used by Roulet et al. (2005) to validate BEP in a 1D case.

Figure 5.13 shows both simulated (aLMo/BEP2 60) and measured potential temperature in the Sperrstrasse. The difference between the simulation and mea-

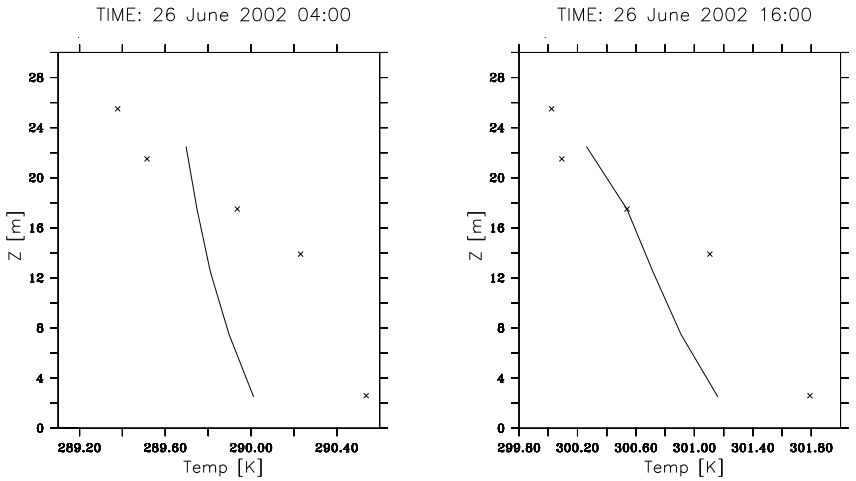

Figure 5.13: Potential temperature profile in the urban grid (solid line) simulated with aLMo/BEP2 60 and measured potential temperature (crosses) on the tower at Sperrstrasse, June 26 2002 at 04LT (left) and June 26 2002 at 16LT (right).

surements never exceeds 1 °C over the entire profile. The simulated profiles are more stable than observed and no change in the simulated curve slope at roof height (15 m) occurs during nighttime. However during daytime, the shape of the simulated profile is close to the measurement with a slightly unstable layer in the street canyon and increasing instability at roof height.

5.5.4 IMPACT OF THE HORIZONTAL RESOLUTION

In this section, we use the operational aLMo configuration with a 7 km horizontal resolution in order to investigate if aLMo/BEP2 is able to take into account the effect of a city with a low horizontal and vertical resolution. With this resolution, the city of Basel is represented by one grid point only. The urban fraction and the urban parameters are set according to KABA (Fehrenbach, 1999).

Figure 5.14 shows the potential temperature profile above the urban grid point during nighttime. Whereas aLMo was not able to simulate a mixing layer (cf.

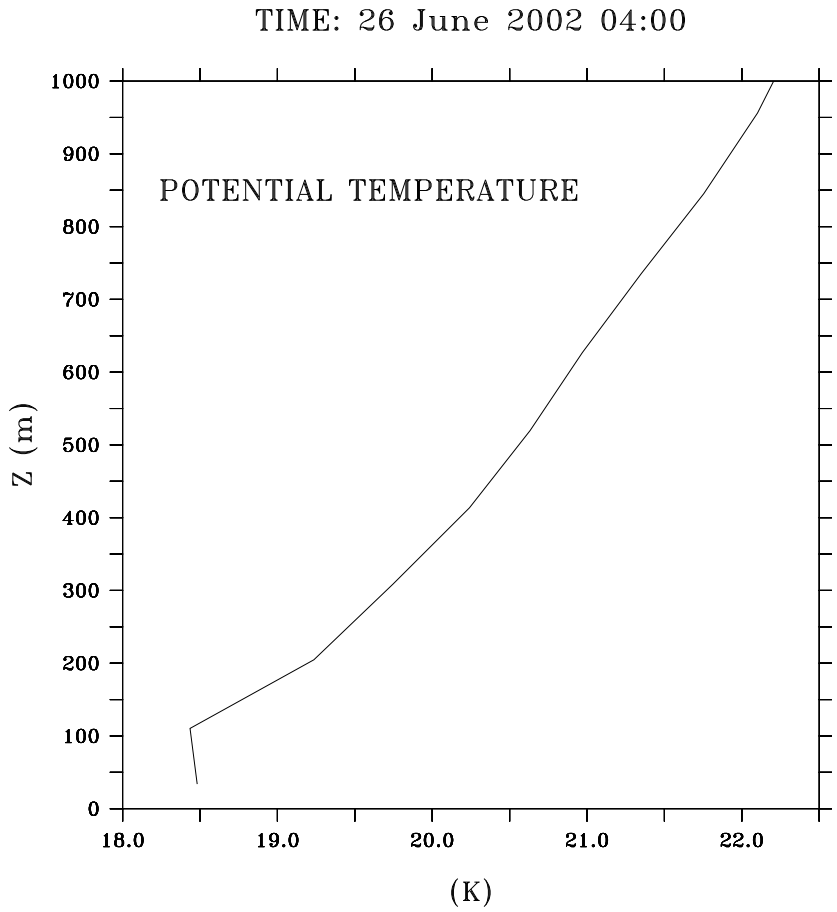

Figure 5.14: Simulated potential temperature profile above the city of Basel, June 26 2002 at 02LT. Results with the aLMo/BEP2 60 and a 7 km horizontal resolution (operational configuration) are plotted with the solid line.

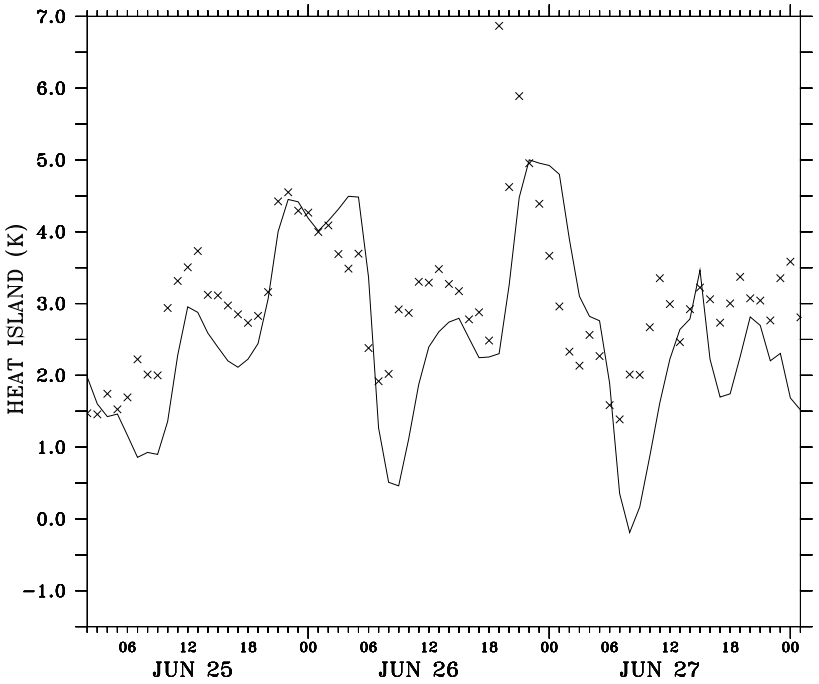

Figure 5.15: Urban Heat Island (UHI) at 2mAGL for a 3 day period (June 25 to June 27) measured (crosses) and computed by aLMo with BEP2 (solid line) with the aLMo configuration, *i.e.* 7 km horizontal resolution and 60 m thickness for the first layer.

Fig. 5.5), aLMo/BEP2 produces a mixing height at around 120 mAGL, as it is the case with a high horizontal and vertical resolution (aLMo/BEP2 20 with a 2 km horizontal resolution, not shown).

Figure 5.15 shows the simulated UHI (see Chapter 4 for definition of UHI calculation). We observe a UHI with a 2.4 °C intensity. The results of aLMo/BEP2 60 is similar to the UHI obtained with aLMo/BEP 20, whereas we have shown in the previous chapter that aLMo without BEP was not able to reproduced an UHI.

5.6 DISCUSSION

Table 5.1 summarizes the configuration used for aLMo, as well as results obtained in this chapter and in the previous chapter (Chapter 4). aLMo with the traditional surface scheme based on MOST is not able to reproduce the UHI, while the BEP implementation allows to take into account the urban areas impact, which is discussed in this section.

In section 5.5.1, we have shown that the modification of BEP (named BEP2) does not change the mesoscale model results when the vertical resolution is high and close to the urban canopy height. Thus, the results obtained in the previous chapter (Chapter 4) are still valid even if BEP has been modified. Nevertheless, we have shown that BEP2 allows to improve the mesoscale simulation results with a low vertical resolution and to decrease the sensitivity of aLMo to the vertical resolution, whereas aLMo without the urban parametrization is highly sensitive to the vertical resolution. This contribution makes aLMo more flexible since now it can take into account the effects of the city independently from the vertical resolution used.

Also, vertical resolution of current operational weather forecasting models are far from resolving process in the urban canopy and will profit considerably from the computed profiles in the urban grid. Temperatures simulated in the urban grid have shown good agreement with measurements. This is particularly interesting in order to use the simulated profiles as input for dispersion models with high vertical resolution.

In section 5.5.4, an UHI has been simulated using the aLMo operational configuration. Even with a low horizontal resolution and a coarse representation of the urban area, aLMo with BEP is able to take into account the presence of the city and to reproduce the urban effects on the PBL. With the new parametrization approach, it is not necessary to have a high resolution for taking into account

Table 5.1: Summary of aLMo configurations and capacity to reproduce an Urban Heat Island (UHI). The averaged UHI measured reaches 3.0 °C.

	Urban Para.	hor. resol.	vert. resol.	UHI
aLMo	MOST[1]	7 km	60 m	0.1 °C
aLMo 60	MOST	2 km	60 m	0.1 °C
aLMo 20	MOST	2 km	20 m	-0.1°C
aLMo/BEP 20	BEP	2 km	20 m	2.3 °C
aLMo/BEP 60	BEP	2 km	60 m	1.5 °C
aLMo/BEP2 20	BEP2[2]	2 km	20 m	2.3 °C
aLMo/BEP2 60	BEP2	2 km	60 m	2.4 °C
aLMo/BEP2	BEP2	7 km	60 m	2.4 °C

[1] Traditional soil parametrization based on MOST
[2] Modified version of BEP

modifications of the atmospheric flow fields induced by a city.

5.7 CONCLUSION

In this study, the Buildings Effect Parametrization (BEP) have been modified in order to limit the sensitivity of aLMo to the grid resolution. The results obtained have shown a better agreement with the measurements and the capacity of the model to reproduce an unstable layer above urban areas during nighttime, which is usually observed by measurements in and above the street canyon.

Furthermore, the modified version of BEP gives additional meteorological fields (temperature, wind and E) in the urban canopy. The computed temperature in the urban canopy has been compared to measurements in a street canyon in Basel and has shown a good agreement. The results obtained in the urban grid can potentially be used as boundary conditions for a high resolution meteorological model or for a dispersion model.

Finally, the urban effects with the operational aLMo configuration has been sim-

ulated. It was shown that aLMo with the modified version of BEP is able to take into account the presence of a middle size city[2] as Basel. At the scale used in the operational weather prediction model of MeteoSwiss, this represents an important number of grid points influenced by BEP, and thus, probably modifying the meteorological fields simulated with aLMo.
In order to implement BEP in an operational version of aLMo, some adaptations to BEP should be done;

- Include **water** in the urban parametrization. BEP does not take into account water storage, rainfall runoff, latent heat flux, snow cover as well as freezing and melting processes. All this parameters modify the energy budget and it is important to include them in the parametrization.

- Improve the **computing time**. 2 % of urban grid points in the domain costs 4 % of the total CPU time of a model simulation. With a large domain and several daily simulations, computing time is an important issue for an operational forecast system.

- A systematic **definition of the urban area and its parameters** is necessary. Urban areas are very diversified and in continuous change. Satellite data seems to be a good solution for providing information about shape of the city, height of the buildings, etc. Dell'Acqua and Gamba (2006) or Zoran (2006) have presented automatic urban mapping methods (surface properties, building height, street width,...) using satellite data and Lafarge et al. (2005) has developed a parametric model based on satellite data able to automatically reconstruct a three dimensional urban area. These methods could be adapted to BEP's needs in order to provide it with the necessary data for describing urban areas.

[2]51 % of all urban population in the wolrd lives in cities with a population of fewer than 500,000 people (UN, 2004).

Acknowledgements

This study (the two chapters with aLMo) would not have been possible without the participation of Oliver Fuhrer from the Air and Soil Pollution Laboratory at the EPFL.

I also would like to thank Gil Fontannaz from the Air and Soil Pollution Laboratory at the EPFL, Daniel Leuenberger and Matteo Buzzi from MeteoSwiss in Zurich and Marco Consoli from the Swiss National Supercomputing Center (CSCS) in Manno.

Bibliography

BUBBLE. *http://pages.unibas.ch/geo/mcr/Projects/BUBBLE.*

Christen, A.: 2005, *Atmospheric Turbulence and Surface Energy Exchange in Urban Environments. Results from the Basel Urban Layer Experiment (BUBBLE)*, Stratus, Basel, 140 pp.

COSMO. *http://www.cosmo-model.org/public/documentation.htm.*

Dell'Acqua, F., Gamba, P.: 2006, 'Discriminating urban environments using multiscale texture and multiple SAR', *Int. J. Remote Sensing*, **27**, 3797-3812.

Doms, G., Fäurstner, J.,Heise, E.,Herzog, H.-J.,Raschendorfer, M., Schrodin, R.,Reinhardt, T., Vogel, G.: 2002, 'A Description of the Nonhydrostatic Regional Model LM, Part I: Dynamics and Numerics', *Documentation of the LM Package*, 2nd version.

Doms, G., Fäurstner, J.,Heise, E.,Herzog, H.-J.,Raschendorfer, M., Schrodin, R.,Reinhardt, T., Vogel, G.: 2002, 'A Description of the Nonhydrostatic Regional Model LM, Part I: Physical Parameterization', *Documentation of the LM Package*, 2nd version.

Fehrenbach, U.: 1999, 'Analyse und Bewertung lokal- und regional-klimatisch wirksamer Faktoren in der Region Basel, Diss. Phil.-Nat. Fak., Univ. Basel, ISBN 3-85977-245-7

Frehlich, R., Meillier, Y., Jensen, M.J., Balsley, B., Sharman, R.: 2006, 'Measurment of Boundary Layer Profiles in an Urban Environment', *J. Appl. Meteorol.*, **45**, 821-837.

Lafarge, F., Descombes, X., Zerubia, J., Pierrot-Deseilligny, M.: 2005, 'Parametric model for the automatic reconstruction in three dimensions of dense urban zones starting with highly resolved satellite images', *Rev. Fr. Photogrammetrie*, **180**, 4-12.

Makar, P.A., Gravel, S., Chirkov, V., Strawbridge, K.B., Froude, F., Arnold, J., Brook, J.: 2006, 'Heat flux, urban properties, and regional weather', *Atmos. Environ.*, **40**, 2750-2766.

Martilli, A.: 2001, 'Development of an urban turbulence parameterisation for mesoscale atmospheric models', *PhD Thesis N^o* **2445**. Federal Institute of Technology (EPFL), Lausanne, Switzerland.

Martilli, A., Clappier, A., Rotach, M. W.: 2002, 'An urban surfaces exchange parameterisation for mesoscale models', *Bound.-Layer Meteor.*, **104**, 261-304.

Oke, T.R: 1987, 'Boundary Layer Climates', 2nd edn. London: Methuen, 435 pp.

Stull, R.B.: 1988, 'An Introduction to Boundary Layer Meteorology', Kluwer Academic Publisher, Dordrecht, pp 670.

Rotach, M. W., Vogt, R., Bernhofer, C., Batchvarova, E., Christen, A., Clappier, A., Feddersen, B., Gryning, S.-E., Martucci, G., Mayer, H., Mitev, V., Oke, T. R., Parlow, E., Richner, H., Roth, M., Roulet, Y.-A., Ruffieux, D., Salmond, J. A., Schatzmann M., Voogt, J. A.: 2005, 'BUBBLE - an Urban Boundary Layer Meteorology Project', *Theor. Appl. Climatol.*, **81**, 231-261.

Roulet, Y.-A., Martilli, A., Rotach, M. W., Clappier, A. 2005: 'Validation of an urban surface exchange parameterization for mesoscale models - 1D case in a street canyon', *J. of App. Meteorol.*, **44**, 1484-1498

United Nations: 2006, 'World Urbanization Prospects. The 2005 Revision', *Departement of Economic and Social Affairs, Population Division*, New York.

Zoran, M. A.: 2006, 'Analysis of urban surface biophysical parameters from remote sensing imagery', *Proceedings of SPIE - The International Society for Optical Engineering*, **6366**.

Chapter 6

Conclusion and Outlook

Nowadays, half of the World's population is living in cities which puts the urban environment under a great stress. An air quality is one of the issues linked to human health and environment protection. Each year, more and more fossil fuels are burned in cities, increasing pollutant emissions and hence degrading urban air quality. Policy makers need decision-support tools for improving urban sustainability and decreasing the human health risks.

Air quality modeling is one of these decision-support tools. Given the complexity of the combined physico-chemical phenomena leading to air pollution episodes, air quality models represent the best approach currently available to understand the response of the atmosphere to the reduction strategies. The present thesis focuses on urban meteorology and air quality modeling. The aim of this work is to improve our understanding and our knowledge of the urban air pollution phenomena and hence to improve the modeling tools for urban areas. This study is divided in two distinct parts, *(i)* a first part on the applied case of Mexico City in order to illustrate the complexity of the air quality problem, and *(ii)* a second part which focuses on the urban parametrization BEP in order to improve mesoscale meteorological simulations in urban areas. The main results and conclusions of the work are presented here and some future research and perspectives are also pointed out.

In the first part of this research, a case study over the Mexico City area has been conducted. Mexico City is the World's second largest city with 20 million inhabitants, and one of the most polluted. The city is located in a high basin (around 2000 mASL) surrounded by a complex topography.

In a large number of ozone pollution cases, the maximum concentrations are observed far from the primary pollutant (NO_x, CO and $VOCs$) sources, downwind of the city. But in the case of Mexico City, the topographical situation and the size of the city lead to a maximum concentration of ozone in the urban area. An

original method used to classify measuring sites allows to follow and to understand the ozone plume development over Mexico City.

The meteorological simulations show that the synoptic and regional scale and the city extent play an important role over Mexico City basin. Despite the fact that these phenomena comprise several kilometers, it is very important to keep a fine resolution in the mesoscale simulations. A good reproduction of the local scale complex topography is crucial in order to simulate the meteorological situation with enough accuracy.

The air quality simulations show that the VOCs emission inventory is underestimated. For this specific case study, the emission inventory is not accurate enough to be used for the evaluation of abatement strategies. The ozone production behavior is highly dependant on precursor's concentrations and repartitions (NO_x and VOC), hence an accurate emission inventory, validated with measurements, is necessary in order to be used as a planning tool.

This study describes the case of a specific atmospheric flow pattern. For a more complete study and aiming to develop emission abatement strategies, information on a larger set of days is required in order to have a representative sample of the different meteorological situations characterizing Mexico City. For future studies, it will be of great interest to study many episodes with different flow patterns.

Furthermore, measurements in the surroundings of Mexico City are required for a validation of background concentrations which characterize the air swept into the Mexico City basin.

The second part of this research is focused on the meteorological simulation of urban areas.

The mesoscale urban air quality modeling can be used in two different ways:

- *Diagnostically* in order to reproduce pollution episodes and to identify the principal pollutant sources, to evaluate the reduction strategies or to plan the land settlement.
- For *forecasting* pollutant concentrations, in the short term in case of acute pollution or in the long term to evaluate pollutants trends.

In both cases, meteorological models are necessary. The operational meteorological models are able to answer to these needs. In this part of the work, the Swiss operational forecast model, aLMo, has been tested in order to evaluate its capacity to take into account the modifications in the atmospheric flow fields induced by urban areas.

Temperature measurements from the BUBBLE campaign have shown the presence of an Urban Heat Island (UHI) over the city of Basel (Switzerland). The UHI effect is typical of urban areas and easy to emphasize. The aLMo model has been applied to the city of Basel and its surroundings, in order to simulate this effect. With the low vertical and horizontal resolution of the operational configuration, as well as with finer resolutions, aLMo does not reproduce the UHI. The traditional surface parametrization used in the operational numerical weather prediction model of MeteoSwiss, based on Monin-Obukhov Similarity Theory (MOST), is not adapted to urban areas.

Therefore, the Buildings Effects Parametrization (BEP) has been adapted and implemented into aLMo in order to take into account the atmospheric flow field modifications induced by urban areas. Two implementations methods were presented. The first method needs no modification of the code solver and allow BEP to be implemented in several models without additional knowledge. This method influences only the first layer of the mesoscale grid. The second method computes the urban heat and momentum flux for all the mesoscale grid layers influenced by the city. This method needs adaptations within the mesoscale code. This second

method was used in this study, as it allows to take into account the urban area impacts over several layers of the mesoscale model.

With a fine resolution, aLMo with BEP is able to reproduce the UHI and to modify the wind pattern in and around the city of Basel. The results show that the city effects are not limited to the urban areas but extend to several kilometers in the rural area downwind the city. Furthermore, the mixing height and the air stability are modified with BEP, which is able to reproduce the main behavior of the urban boundary layer and has hence a real enhancement potential for aLMo.

However, it is shown that aLMo with or without BEP is sensitive to the vertical resolution and that the improvements induced by BEP become very weak when the resolution decreases. BEP is modified in order to limit the sensitivity of aLMo to the grid resolution. The results obtained after the modifications show a better agreement with the measurements, regardless of the mesoscale model resolution. Therefore, a version of aLMo which is less sensitive to a modification in the resolution and which is able to simulate the UHI is generated. That is, the modified version of BEP provides meteorological fields (wind speed and temperature) in the urban canopy even with a low vertical resolution in the mesoscale model. The temperature simulated in the urban canopy is in good agrement with the street canyon measurements. Results from BEP can be used as input for dispersion models.

The implementation and modification of BEP has improved the meteorological simulation in Basel's urban area. BEP impacts on meteorological fields over the city and its surroundings as well. In the vertical, we observe an increase of the mixing height and a decrease of the stability above the city.

This study shows the importance of taking into account urban areas in air quality studies and in meteorological simulations. Based on the foregoing results, a

series of perspectives emerge. Future research should be addressed to the following aspects:

- Some adaptations are necessary in order to improve BEP. The building energy budget parametrization could be improved by taking into account ventilation, air-conditioning systems, anthropogenic heat sources, windows and temperature variations in buildings. Furthermore, BEP could also be used for evaluating the energy budget of buildings, hence linking energy consumption in buildings, cities geometric characteristics, urban heat island and meteorological conditions together.

- Most of the data from urban measuring campaigns are representative of large homogenous urban structure (sub-urban area). Heterogeneous urban areas such as city centers require more detailed information which is difficult to obtain. In such situations, the three dimensional Computational Fluid Dynamics (CFD) model (Large Eddy Simulations (LES) or Reynolds-Averaged Navier-Stokes (RANS) simulation) with a high resolution (1 m) could be used for validating heat and momentum fluxes computed by BEP.

- An improved energy budget for buildings and the comparison with CFD models should allow to identify the most significant processes in BEP. The parametrization could hence be simplified in order to improve its computing time for operational use.

Those modifications will allow to plan the "ideal" city in terms of energy consumption in buildings. Nevertheless, this optimal case should not be considered isolated from other factors namely the optimization of the energy use in the transport, the minimization of pollutant emissions, the mitigation of the UHI or the control of air quality. As example, the table 6.1 points out some advantages and drawbacks of building highly dense city in comparison with a geographically extended city.

Table 6.1: Advantages and drawbacks in terms of environmental impacts of highly packed city.

Advantage	**Drawback**
• Low energy consumption for heating during wintertime.	• High energy consumption for air conditioning during summertime.
• Decrease of distance travel by cars ⇒ Decrease of traffic emission.	• Concentration of emissions ⇒ Increase people exposure.
• Decrease of car number	• Increase the UHI

The number of advantages is the same than the number of drawbacks and can be contradictory. Planning cities requires to take into account numerous phenomena.

Urban areas should be considered as a system with strong and complex interactions from the local to the regional scale and with many social, economic and environmental issues. Furthermore, the "urban system" cannot be considered individually, as interactions between the urban regional scale and the global scale are very important. A large part of the pollutants emitted in cities are greenhouse gases. Urban areas have hence a global effect, but action plans controlling the pollutant emission and energy consumption have to be implemented at the local and regional scale.

The urban air quality problem encompasses complex parameters with strong interactions at different scales. The study of each of these parameters and scales have to be improved. It is hoped that the present work will contribute towards the improvement of urban meteorological and air quality modeling.

Curriculum Vitae

Clive Muller

Ingénieur en sciences de l'environnement
Docteur en modélisation numérique

Rte d'Eclépens, CH-1307 Lussery-Villars
Tél. prof. 021 693 5701 Tél. privé 079 759 82 00
Email : clive.muller@a3.epfl.ch
Célibataire, 30 ans, Suisse

Expérience professionnelle

2002-2007 **Assistant de recherche** au *laboratoire de Pollution de l'Air et des Sols, EPFL.*
Chercheur en **modélisation atmosphérique et de la qualité l'air**, développement et application de modèles 3D. Rédaction de publications et participation à des conférences internationales. Charges d'enseignement aux étudiants du cycle Master et postgrade de l'EPFL et encadrement de diplômants.

2004-2006 **Administrateur informatique** du *laboratoire de Pollution de l'Air et des Sols, Ecole Polytechnique Fédérale de Lausanne (EPFL).*
Responsable de l'**installation** et de la **gestion du parc informatique** (Windows, Linux). Support aux utilisateurs. **Webmaster** du groupe de modélisation numérique.

2002 **Collaborateur** de *Agencement Ledermann SA, Romanel-sur-Lausanne*.
Elaboration et rédaction des éléments pour la **certification ISO9001** (entreprise d'une quarantaine d'employés).

2001-2002 **Diplômant** au ***Massachusetts Institute of Technology*** *(MIT), Cambridge, USA.*
Travail de recherche dans un contexte international dans le groupe du professeur M. J. Molina (lauréat du prix Nobel de chimie en 1995).

1999-2001 **Assistant-Etudiant** au *laboratoire Hydrologie et Aménagement, EPFL.*
Travail sur l'**influence des changements climatiques sur les ressources en eau** en Europe, analyse statistique de données et assistanat pour les étudiants du cycle Bachelor.

Formation

2002 à 2007 **Doctorant en science environnementale**, spécialiste en physique et chimie de l'atmosphère, *Ecole Polytechnique Fédérale de Lausanne*

1996-2002 **Master en sciences et ingénierie de l'environnement**, EPFL

1995 **Maturité Fédérale** type C (scientifique), Gymnase de Chamblandes, Pully

Langues

Français	Langue maternelle
Anglais	Bonne maîtrise orale et écrite (Publications, conférences)
Allemand	Connaissances scolaires, rapidement perfectibles

Informatique

Très bonnes connaissances des systèmes **Linux**, **Unix** et **Windows**
Très bonne maîtrise de la **programmation** en Fortran 77 et 90, shell-scripts, html, php

Loisirs

La **montagne** sous toutes ses formes : Ski, randonnée, vélo tout-terrain, escalade.
Basket-Ball : Champion Suisse espoirs en 1995 et entraîneur d'équipes junior et senior.